ACOUSTIC PROPAGATION IN NONUNIFORM CIRCULAR DUCTS CARRYING NEAR SONIC MEAN FLOWS

by

Jeffrey J. Kelly

Dissertation submitted to the Graduate Faculty of the

Virginia Polytechnic Institute and State University

in partial fulfillment of the requirements for the degree of

DOCTOR OF PHILOSOPHY

in

Engineering Mechanics

APPROVED:

Ali H. Nayfeh

Dr. A. H. Nayfeh, Chairman

Dean T. Mook

Dr. D. T. Mook

Edmund G. Henneke, II

Dr. E. G. Henneke, II

Layne T. Watson

Dr. L. T. Watson

Werner E. Kohler

Dr. W. E. Kohler

January, 1981

Blacksburg, Virginia

ACKNOWLEDGMENTS

The author would like to express his appreciation to Professors Nayfeh and Watson for their continuous guidance and assistance in the pursuance of this dissertation and their contribution to his education. Sincere appreciation is also extended to Professors Henneke, Kohler and Mook for serving as members of my examining committee and for their review of this dissertation.

Further, the author would like to thank his parents, Jesse and Katherine, for their encouragement and support. Finally, the author would like to express his appreciation to his wife for her support and excellent typing job.

This research was supported by NASA-Langley Research Center under Grant No. 314973-1.

TABLE OF CONTENTS

LIST OF FIGURES

Page

Page

CHAPTER ONE

Introduction

The use of high bypass turbofan engines has resulted in the reduction of noise associated with the jet exhaust and has enhanced the fuel economy of the engine. But noise emissions from the inlet nacelles produced by the fan are of such a level as to raise objections from communities near airports. Hence much attention has been devoted to reducing the inlet noise. Reduction of upstream noise can be accomplished with the use of a choked inlet[1,2] although such designs can have a negative effect on compressor efficiency. Therefore using a near sonic inlet, or partially-choked inlet, along with an acoustic duct liner is one method that has received considerable attention in the reduction of inlet noise.

In order to develop an appropriate mathematical model for the analysis of sound propagation in near sonic flows two problems must be considered: 1) acoustic theory is well developed for the study of sound propagation in parallel ducts but it is not fully developed for nonuniform ducts that carry mean flows with strong axial and transverse gradients, and 2) linear acoustic equations will not provide an accurate solution for near sonic mean flows. In this study an analysis of the first problem is performed using the wave-envelope technique[3,4] based on the method of variation of parameters. A nonlinear model is developed for the second problem.

A survey of the methods used for the analysis of acoustic propagation in uniform and nonuniform ducts was made by Nayfeh, Kaiser, and Telionis[5], Nayfeh[6], Vaidya and Dean[7], and Nayfeh, Kaiser, and Shaker[3]. A review of numerical techniques employed in linear duct acoustics was performed by Baumeister[8].

For nonuniform ducts with mean flows the methods employed include quasi-one-dimensional approximations, multiple-scales solutions, solutions for weak wall undulations, weighted residual methods, and direct numerical integration. Only the lowest mode is studied in the quasi-one-dimensional method[9-13] which assumes a slowly varying cross section and ignores the effects of transverse mean flow gradients or large liner admittances. The multiple-scales analysis[14-16] can determine the transmission and attenuation for all modes without ignoring transverse and axial gradients but it is limited to slow variations of the duct cross section. Also, the expansion needs to be carried out to second order to obtain reflections of the acoustic signal and intermodal coupling in transmission. A perturbation solution is determined in the weak-wall-undulation method[17] for ducts whose walls deviate only slightly from the uniform case.

For uniform source inputs in nonuniform ducts, finite-difference schemes[18,19] have been employed. At high frequencies a large number of grid points are needed to resolve the smallest wavelength which leads to large computational requirements. Also, in order to obtain transmission and reflection characteristics of the duct modes requires a transverse step size to be small enough to resolve the highest mode. To reduce the computational requirements, Baumeister[20] used an estimate of the wavelength of the fundamental mode to explicitly express the fast axial variation and solved only for the envelope of the acoustic disturbance.

Eversman[21] used the method of weighted residuals, or Galerkin method, which represents the acoustic signal as a linear superposition of basis functions. This approach can determine reflection and transmission coefficients but the short axial wavelengths at high frequencies will demand a small step size in the axial direction which increases the computational time.

Several finite-element models have been developed for the analysis of acoustic propagation in nonuniform ducts with compressible mean flows. Sigman, Majjigi and Zinn[22] applied a finite-element approach to the governing equations which were expressed in terms of a velocity-potential; thus their analysis is limited to irrotational mean flows. Majjigi, Sigman, and Zinn[23] expanded their method so that soft-wall ducts can be analyzed. Tag and Lumsdaine[24] also developed a finite-element scheme for irrotational flow.

Since the introduction of these finite-element models several finite-element approaches were employed which consider rotational mean flows. Quinn[25] investigated the use of various interpolation functions and finite-element methods on some relatively simple cases to check the theory. A general compressible mean flow is considered in the finite-element model of Abrahamson[26] but the results presented are for an incompressible case. Results from the wave-envelope method were compared with this finite element scheme for cases of low speed mean flows[3,4]. Acoustic pressure profiles were compared and the agreement is very good. Abrahamson[27] studied the possibility of reducing the computational effort associated with the finite-element analysis.

A comparison of the transmission and reflection coefficients evaluated using a finite-element scheme with those from the method of weighted residuals was performed by Eversman, Astley, and Thanh[28] in which good agreement was observed. Astley and Eversman[29] extended their original finite-element procedure. Also, Astley, Walkington, and Eversman[30] applied a finite-element analysis to ducts with a peripherally varying liner. In these studies the mean flow model is rotational but it appears that the refractive effect of a finite boundary-layer thickness at the duct walls was ignored.

The wave-envelope technique was developed for the analysis of sound transmission and attenuation in an infinite, hard-walled or lined circular duct carrying a compressible, sheared mean flow and having a variable-area cross section. The evaluation of transmission and reflection coefficients is aided by expressing the acoustic disturbance as a superposition of the quasiparallel duct modes. An explicit description of the fast axial variation of the acoustic disturbance is given and only the slower variations of the mode amplitudes and phases are calculated. The method is valid for large as well as small axial variations as long as the mean flow does not separate. Previously, Nayfeh[31] used the wave-envelope technique to analyze acoustic propagation in partially choked converging ducts for the case of axisymmetric flow. Several changes have been made to the original numerical procedure in the present study. These changes facilitate the computational efficiency of the wave-envelope model and also enhance the accuracy of the solution.

The significance of the nonlinear terms was presented in a number of studies. Numerical investigations of linear acoustic theory by Eisenberg and Kao[13] and Hersh and Liu[32] show it to be not valid for near sonic flow. An analysis by Callegari and Myers[33] using matched asymptotic expansions to examine the region where $1 - |M| = O(\varepsilon)$ explicitly confirms the singular behavior of the linear theory. From matching considerations the nonlinear effects are inferred to be important when the strength of the acoustic disturbance is the order of $(1-|M|)^2$, but no nonlinear results are reported. Several investigations incorporating nonlinear effects into a study of sound propagation through a near sonic flow region have been developed to date. One such attempt[32] treats the nonlinear terms as a source disturbance to the basic linear propagation process. Such an approach cannot succeed since it does not remove the mathematical singularity from the differential operator in the governing physical equations.

Callegari and Myers[34] applied matched asymptotic expansions to the nonlinear problem for upstream propagation of an acoustic source located at the throat of a converging-diverging duct. This theory was extended by Myers and Callegari[35] for a source located downstream of the throat. The results of these studies indicate the generation of superharmonics by a single frequency acoustic source and the formation of shocks if the source strengths or frequencies are sufficiently high. This analysis was extended for a source upstream of the throat[36] and for shock fitting in a flow containing a shock[37].

In this study the behavior of numerical solutions of the nonlinear, one-dimensional equations of motion are examined to gain insight into the mechanisms that operate in the near sonic region and to determine the mathematical techniques required to analyze these mechanisms. The one-dimensional model contains all the essential elements of the linear singularity and of the nonlinear harmonic interactions without the purely computational difficulties of the full two-dimensional problem. The acoustic disturbance is represented as a sum of a basic frequency and a finite number of higher harmonics, and the nonlinear interaction among the harmonics and their complex conjugates are calculated. A preliminary version of the above model was reported by Nayfeh et al[38].

In Chapter 2 a linear analysis is developed using the wave-envelope method. Results are presented for a converging duct and then for a converging-diverging duct. The nonlinear model is described and its results are shown in Chapter 3.

CHAPTER TWO

The Linear Problem

2.1 Axisymmetric and Spinning Mode Linear Propagation

The analysis of the transmission and attenuation of sound in hard and lined nonuniform circular ducts carrying viscous or inviscid compressible mean flows is presented in this section. The mean Mach number in the throat is subsonic and the axial and radial gradients of the mean flow are not necessarily small. The cross section of the duct is an arbitrary function of the axial distance.

The nondimensional form of the governing equations for the unsteady viscous flow in a duct are[39]:

Conservation of Mass

$$\frac{\partial \rho}{\partial t} + \nabla \cdot (\rho \bar{v}) = 0 \tag{2.1}$$

Conservation of Momentum

$$\rho\left(\frac{\partial \bar{v}}{\partial t} + \bar{v} \cdot \nabla \bar{v}\right) = -\nabla p + \frac{1}{R_e} \nabla \cdot \underline{\underline{\tau}} \tag{2.2}$$

Conservation of Energy

$$\rho\left(\frac{\partial T}{\partial t} + \bar{v} \cdot \nabla T\right) - (\gamma-1)\left(\frac{\partial p}{\partial t} + \bar{v} \cdot \nabla p\right) = \frac{1}{Re}\left[\frac{1}{Pr} \nabla \cdot (\kappa \nabla T) + (\gamma-1)\Phi\right] \tag{2.3}$$

Equation of State (perfect gas)

$$\gamma p = \rho T \tag{2.4}$$

Here, $\bar{v}$ is the velocity vector, t is the time, γ is the ratio of the gas specific heats, $Pr = \mu_w c_p/\kappa_w$ is the Prandtl number, c_p is the gas specific heat at constant pressure, and $Re = \rho_a c_a R_o/\mu_w$. Conditions at the duct wall are denoted by the subscript w, $\underline{\underline{\tau}}$ is the viscous stress tensor and Φ is the dissipation function. The reference quantities for these equations are: for velocity, the speed of sound c_a from some convenient reference point; for length, the duct radius in the uniform section R_o (Fig. 1); for time, R_o/c_a. The reference pressure is $\rho_a c^2{}_a$ and the reference density and temperature are again evaluated at a convenient reference point. Reference values for the viscosity μ and thermal conductivity κ are their wall values in the uniform section.

In the linear analysis considered in this section the duct carries a steady, sheared, subsonic mean flow that satisfies Eqs. (2.1)-(2.4). The presence of sound in the duct creates a perturbation of the flow variables so that

$$q(\bar{r},t) = q_o(\bar{r}) + q_1(\bar{r},t) \tag{2.5}$$

where q is any flow variable, $\bar{r}$ is the position vector, q_o is the mean flow, and q_1 is the acoustic disturbance. The substitution of Eq. (2.5) into Eqs. (2.1)-(2.4) results in the following acoustic equations after the mean-flow terms are eliminated:

$$\frac{\partial \rho_1}{\partial t} + \nabla \cdot (\rho_0 \vec{v}_1 + \rho_1 \vec{v}_0) = NL \tag{2.6}$$

$$\rho_0 (\frac{\partial \vec{v}_1}{\partial t} + \vec{v}_0 \cdot \nabla \vec{v}_1 + \vec{v}_1 \cdot \nabla \vec{v}_0) + \rho_1 \vec{v}_0 \cdot \nabla \vec{v}_0 =$$

$$= \nabla p_1 + \frac{1}{Re} \nabla \cdot \underline{\underline{\tau}}_1 + NL \tag{2.7}$$

$$\rho_0 (\frac{\partial T_1}{\partial t} + \vec{v}_0 \cdot \nabla T_1 + \vec{v}_1 \cdot \nabla T_0) + \rho_1 \vec{v}_0 \cdot \nabla T_0 - (\gamma-1)(\frac{\partial p_1}{\partial t}$$

$$+ \vec{v}_0 \cdot \nabla p_1 + \vec{v}_1 \cdot \nabla p_0) = \frac{1}{Re} [\frac{1}{Pr} \nabla \cdot (\kappa_0 \nabla T_1 + \kappa_1 \nabla T_0)$$

$$+ (\gamma-1)\Phi_1] + NL \tag{2.8}$$

$$\frac{p_1}{p_0} = \frac{\rho_1}{\rho_0} + \frac{T_1}{T_0} \tag{2.9}$$

where $\underline{\underline{\tau}}_1$ and Φ_1 are linear in the acoustic quantities and NL stands for the nonlinear terms in the acoustic quantities.

The solution of the problem described by Eqs. (2.6)-(2.9) subject to general initial and boundary conditions has not been determined to date. Therefore simplifying assumptions are made in order to obtain reasonable solutions for the propagation of sound in ducts. The acoustic disturbance is assumed to be inviscid and the nonlinear terms are neglected. Again one must emphasize the importance of the nonlinear terms when the mean flow is transonic (i.e., near the throat). Also the assumption that the mean flow is a function of the axial and radial coordinates only is made so that the possibility of swirling mean flows is eliminated. The cylindrical coordinate system (r,θ,x) shown in Fig. 1 is the appropriate reference frame to use. Assuming no swirling flow and that the time variation is sinusoidal implies that each flow variable $q_1(r,x,\theta,t)$ can be expressed as

$$q_1(r,x,\theta,t) = \sum_{m=o}^{\infty} q_{1m}(r,x)e^{-i(\omega t-m\theta)} \tag{2.10}$$

where ω is the dimensionless frequency. With the assumptions that are stated above Eqs. (2.6)-(2.9) can be expressed in cylindrical coordinates as

$$-i\omega\rho_1 + \frac{\partial}{\partial x}(\rho_0 u_1 + u_0\rho_1) + \frac{i\rho_0 m}{r} w_1 + \frac{1}{r}\frac{\partial}{\partial r}(r\rho_0 v_1 + rv_0\rho_1) = 0 \tag{2.11}$$

$$\rho_0[-i\omega u_1 + \frac{\partial}{\partial x}(u_0 u_1) + v_0\frac{\partial u_1}{\partial r} + v_1\frac{\partial u_0}{\partial r}] + \rho_1[u_0\frac{\partial u_0}{\partial x} + v_0\frac{\partial u_0}{\partial r}] = -\frac{\partial p_1}{\partial x} \tag{2.12}$$

$$\rho_0[-i\omega v_1 + \frac{\partial}{\partial r}(v_0 v_1) + u_0 \frac{\partial v_1}{\partial x} + u_1 \frac{\partial v_0}{\partial x}] + \rho_1[v_0 \frac{\partial v_0}{\partial r} + u_0 \frac{\partial v_0}{\partial x}] =$$

$$- \frac{\partial p_1}{\partial r} \tag{2.13}$$

$$\rho_0[-i\omega w_1 + v_0 \frac{\partial w_1}{\partial r} + \frac{v_0 w_1}{r} + u_0 \frac{\partial w_1}{\partial x}] = - \frac{im}{r} p_1 \tag{2.14}$$

$$\rho_0[-i\omega T_1 + v_0 \frac{\partial T_1}{\partial r} + u_0 \frac{\partial T_1}{\partial x} + v_1 \frac{\partial T_0}{\partial r} + u_1 \frac{\partial T_0}{\partial x}] + \rho_1[v_0 \frac{\partial T_0}{\partial r}$$

$$+ u_0 \frac{\partial T_0}{\partial x}] - (\gamma-1)[-i\omega p_1 + u_0 \frac{\partial p_1}{\partial x} + v_0 \frac{\partial p_1}{\partial r} + u_1 \frac{\partial p_0}{\partial x}$$

$$+ v_1 \frac{\partial p_0}{\partial r}] = 0 \tag{2.15}$$

$$\frac{p_1}{p_0} = \frac{\rho_1}{\rho_0} + \frac{T_1}{T_0} \tag{2.16}$$

where u_1, v_1, and w_1 are the velocities in the axial, radial, and azimuthal directions, respectively, and the subscript m has been suppressed.

The initial and boundary conditions must be specified in order to determine the solution to this problem. The duct wall is assumed to be lined with a point-reacting acoustic material whose specific acoustic admittance β may vary along the duct. This implies that for no-slip mean flows the particle displacements at the interface of the wall-fluid boundary must be continuous. Mathematically this boundary condition can be written as

$$v_1 - R'u_1 = \frac{\beta}{\rho_w c_w} p_1 \sqrt{1 + (R')^2} \text{ at } r = R \tag{2.17}$$

where R' is the slope of the wall and the subscript w refers to values at the wall. For a given duct section we want to calculate transmission and reflection matrices. Therefore the initial conditions consist of the successive input of each acoustic mode at the duct entrance.

An approximate solution to Eqs. (2.11)-(2.17), based on the method of variation of parameters, is sought in the form

$$p_1 \simeq \sum_{n=1}^{N} \{A_n(x)\psi_n^p(r,x)\exp(i\int k_n dx) + \tilde{A}_n(x)\tilde{\psi}_n^p(r,x)\exp(i\int \tilde{k}_n(x)dx)\} \quad (2.18)$$

$$u_1 \simeq \sum_{n=1}^{N} \{A_n(x)\psi_n^u(r,x)\exp(i\int k_n dx) + \tilde{A}_n(x)\tilde{\psi}_n^u(r,x)\exp(i\int \tilde{k}_n(x)dx)\} \quad (2.19)$$

with analogous expressions for v_1, w_1, T_1, and ρ_1. The tilde denotes upstream propagation, the $\psi_n(r,x)$ functions are the quasiparallel mode shapes corresponding to the quasiparallel wavenumbers $k_n(x)$, and the $A_n(x)$ are complex functions whose moduli and arguments represent, in some sense, the amplitudes and phases of the (m,n) modes. The circumferential (spinning) mode number is specified and the corresponding subscript on A, ψ, and k is not explicitly stated. Each acoustic variable consists of a summation over a finite number of radial modes N, with n = 1 referring to the fundamental radial mode rather than the conventional n = 0. Since k_n is complex, the quasiparallel wavenumber represents an estimate of the attenuation of the (m,n) mode and also the axial oscillations of the acoustic modes.

The ψ_n, being the quasiparallel mode shapes, satisfy the following problem:

$$-i\hat{\omega}\psi^\rho + ik\rho_o\psi^u + \frac{i\rho_0 m}{r}\psi^w + \frac{1}{r}\frac{\partial}{\partial r}(r\rho_o\psi^v) = 0 \quad (2.20)$$

$$-i\rho_0\hat{\omega}\psi^u + \rho_0\frac{\partial u_0}{\partial r}\psi^v + ik\psi^p = 0 \quad (2.21)$$

$$-i\rho_0\hat{\omega}\psi^v + \frac{\partial\psi^p}{\partial r} = 0 \quad (2.22)$$

$$-i\rho_0\hat{\omega}\psi^w + \frac{im}{r}\psi^p = 0 \quad (2.23)$$

$$- i\rho_0\hat{\omega}\psi^T + \rho_0 \frac{\partial T_0}{\partial r} \psi^v + i(\gamma-1)\hat{\omega}\psi^p = 0 \tag{2.24}$$

$$\frac{\psi^p}{p_0} = \frac{\psi^\rho}{\rho_0} + \frac{\psi^T}{T_0} \tag{2.25}$$

$$\psi^v - \frac{\beta}{\rho_w c_w} \psi^p = 0 \text{ at } r = R \tag{2.26}$$

where

$$\hat{\omega} = \omega - ku_0 \tag{2.27}$$

A well known problem for parallel duct eigenfunctions can be derived from Eqs. (2.20)-(2.27) in the form

$$\frac{\partial^2\psi^p}{\partial r^2} + [\frac{1}{r} + \frac{T_0'}{T_0} + \frac{2ku_0'}{\hat{\omega}}] \frac{\partial\psi^p}{\partial r} + [\frac{\hat{\omega}^2}{T_0} - k^2 - \frac{m^2}{r^2}]\psi^p = 0 \tag{2.28}$$

$$\frac{\partial\psi^p}{\partial r} - i \frac{\omega\beta}{T_w^{\frac{1}{2}}} \psi^p = 0 \text{ at } r = R \tag{2.29}$$

Solving Eqs. (2.28) and (2.29) will determine $\psi_n^p(r,x)$ at each axial location and its corresponding wavenumber $k_n(x)$. Because the basis functions vary in the axial direction they must be normalized to provide significance to the axial variations of the mode amplitudes. For the model implemented in this study the normalization procedure is the same as that defined by Zorumski[40]; that is,

$$\int_0^R r[\psi_n^p(r,x)]^2 dr = 1 \tag{2.30}$$

The quasiparallel eigenfunctions of the other acoustic variables can be expressed in terms of ψ_n^p and k_n with the use of Eqs. (2.20)-(2.25).

Since the transverse dependence in the assumed solutions, Eqs. (2.18) and (2.19), is chosen a priori, it cannot satisfy Eqs. (2.11)-(2.17) or a solvability condition exactly. Thus, the assumed solution is constrained by the solvability condition. Instead of using the usual method of weighted residuals which constrains the residuals in each of the Eqs. (2.11)-(2.17) to be orthogonal to some a priori chosen functions, the approach taken in this study is to require the deviations from the quasiparallel solution to be orthogonal to every solution of the adjoint quasiparallel problem[41].

The problem adjoint to the quasiparallel problem must be defined in order to enforce the constraints. This is determined by multiplying each of Eqs. (2.20)-(2.25) by the functions ϕ_1, ϕ_2, ϕ_3, ϕ_4, ϕ_5, and ϕ_6, respectively, which are the solutions of the adjoint problem, and adding the resulting equations. Integration of this equation by parts from $r = 0$ to $r = R$ transfers the r derivatives from the ψ's to the ϕ's with the result being

$$\int_0^R \psi^\rho[-i\hat{\omega}\phi_1 - \phi_6/\rho_0]dr + \int_0^R i\rho_0\psi^u[-\hat{\omega}\phi_2 + k\phi_1]dr + \int_0^R \rho_0\psi^v[-i\hat{\omega}\phi_3$$
$$+ \frac{\partial u_0}{\partial r}\phi_2 - r\frac{\partial}{\partial r}(\frac{\phi_1}{r}) + \frac{\partial T_0}{\partial r}\phi_5]dr + \int_0^R i\rho_0\psi^w[-\hat{\omega}\phi_4$$
$$+ \frac{m}{r}\phi_1]dr + \int_0^R \psi^p[ik\phi_2 - \frac{\partial\phi_3}{\partial r} + \frac{im}{r}\phi_4 + i(\gamma-1)\hat{\omega}\phi_5 + \phi_6/p_0]dr$$
$$+ \int_0^R \psi^T[-i\rho_0\hat{\omega}\phi_5 - \phi_6/T_0]dr + [\rho_0\psi^v\phi_1 + \psi^p\phi_3]_0^R = 0 \qquad (2.31)$$

Equating each of the brackets in the integrands of Eq. (2.31) to zero determines the adjoint equations. The adjoint equations permit each of the ϕ_n to be expressed as a function of ϕ_1 according to

$$\phi_2 = (k/\hat{\omega})\phi_1 \qquad (2.32)$$

$$\phi_3 = \frac{irT_0}{\hat{\omega}^2}\frac{\partial}{\partial r}\left(\frac{\hat{\omega}\phi_1}{rT_0}\right) \tag{2.33}$$

$$\phi_4 = \frac{m\phi_1}{r\hat{\omega}} \tag{2.34}$$

$$\phi_5 = \frac{\phi_1}{T_0} \tag{2.35}$$

$$\phi_6 = -i\rho_0\hat{\omega}\phi_1 \tag{2.36}$$

Equations (2.32)-(2.36) can be substituted into the remaining adjoint equation to obtain the following governing equation for ϕ_1:

$$\frac{1}{r}\frac{\partial}{\partial r}\left[\frac{rT_0}{\hat{\omega}^2}\frac{\partial \eta}{\partial r}\right] + \left[1 - \frac{T_0 k^2}{\hat{\omega}^2} - \frac{T_0 m^2}{r^2\hat{\omega}^2}\right]\eta = 0 \tag{2.37}$$

where

$$\eta = \phi_1\hat{\omega}/rT_0 \tag{2.38}$$

Equation (2.37) will reduce to the same equation ψ^p satisfies, i.e., Eq. (2.28). Dropping the adjoint equations in Eq. (2.31) and using Eqs. (2.22), (2.33), and (2.38) in the boundary terms results in

$$\frac{\partial \eta}{\partial r} - \frac{i\omega\beta}{T_w^{1/2}}\eta = 0 \text{ at } r = R \tag{2.39}$$

This is the same boundary condition (2.29); thus the conclusion is that $\eta = \psi^p$. Therefore solving the quasiparallel problem for ψ_n^p will also determine ϕ_{1n} from

$$\phi_{1n} = \frac{rT_0\psi_n^p}{\hat{\omega}} \tag{2.40}$$

and the remaining ϕ's are evaluated from Eqs. (2.32)-(2.36).

After the adjoint functions have been determined, the constraint conditions then are found. By multiplying Eqs. (2.11)-(2.16) by ϕ_{1n}, ϕ_{2n}, ..., ϕ_{6n}, respectively, adding the resulting equations, integrating this equation by parts from r = 0 to r = R to transfer the r derivatives to the ϕ's, and using the adjoint equations and Eq. (2.17) produces the following constraint:

$$\int_0^R \Big\{\phi_{1n}[-iu_0k_n\rho_1 - ik_n\rho_0u_1 + \frac{\partial}{\partial x}(\rho_0u_1 + u_0\rho_1)] - rv_0\rho_1 \frac{\partial}{\partial r}(\frac{\phi_{1n}}{r})$$

$$+ \phi_{2n}[- iu_0k_n\rho_0u_1 - ik_np_1 + \rho_0 \frac{\partial(u_0u_1)}{\partial x} + \rho_1(u_0 \frac{\partial u_0}{\partial x} + v_0 \frac{\partial u_0}{\partial r})$$

$$+ \frac{\partial p_1}{\partial x}] - u_1 \frac{\partial}{\partial r}(\rho_0v_0\phi_{2n}) + \phi_{3n}[- iu_0k_n\rho_0v_1 + \rho_0u_0 \frac{\partial v_1}{\partial x}$$

$$+ \rho_0u_1 \frac{\partial v_0}{\partial x} + \rho_1(v_0 \frac{\partial v_0}{\partial r} + u_0 \frac{\partial v_0}{\partial x})] - v_0v_1 \frac{\partial}{\partial r}(\rho_0\phi_{3n})$$

$$+ \phi_{4n}[-ik_n\rho_0u_0w_1 + \frac{\rho_0v_0w_1}{r} + \rho_0u_0 \frac{\partial w_1}{\partial x}] - w_1 \frac{\partial}{\partial r}(\rho_0v_0\phi_{4n})$$

$$+ \phi_{5n}[-iu_0k_n\rho_0T_1 + (\gamma-1)iu_0k_np_1 + \rho_0u_0 \frac{\partial T_1}{\partial x} + \rho_0u_1 \frac{\partial T_0}{\partial x}$$

$$+ \rho_1(v_0 \frac{\partial T_0}{\partial r} + u_0 \frac{\partial T_0}{\partial x}) - (\gamma-1)(u_0 \frac{\partial p_1}{\partial x} + u_1 \frac{\partial p_0}{\partial x} + v_1 \frac{\partial p_0}{\partial r})]$$

$$- T_1 \frac{\partial}{\partial r}(\rho_0v_0\phi_{5n}) + (\gamma-1)p_1 \frac{\partial}{\partial r}(v_0\phi_{5n})\Big\} dr + \rho_0\phi_{1n}[R'u_1$$

$$+ \frac{\beta}{\rho_wc_w} p_1 (\sqrt{1+R'^2} - 1)]_{r=R} = 0 \tag{2.41}$$

Upon substitution of the assumed solution, Eqs. (2.18) and (2.19) into Eq. (2.41) one obtains the following N equations for the A's:

$$\sum_{n=1}^{N} f_{mn} \frac{dA_n}{dx} = \sum_{n=1}^{N} g_{mn}A_n \tag{2.42}$$

where m = 1,2,3,...,N and N designates the total number of modes considered so that the A_n's denote both left and right propagating modes. The coefficients, f_{mn} and g_{mn}, in these equations are evaluated from the following equations:

$$f_{mn} = [\int_0^R \{\phi_{1m}(\rho_0\psi_n^u + u_0\psi_n^\rho) + \phi_{2m}(\rho_0 u_0\psi_n^u + \psi_n^p) + \phi_{3m}\rho_0 u_0\psi_n^v$$

$$+ \phi_{4m}(\rho_0 u_0\psi_n^w) + \phi_{5m}(\rho_0 u_0\psi_n^T - (\gamma-1)u_0\psi_n^p)\}dr]e^{i\int k_n dx} \tag{2.43}$$

$$g_{mn} = -\Bigg[\int_0^R \Big\{\phi_{1m}[\frac{\partial}{\partial x}(\rho_0\psi_n^u + u_0\psi_n^\rho)] - rv_0\psi_n^\rho \frac{\partial}{\partial r}(\frac{\phi_{1m}}{r}) + \phi_{2m}[\rho_0 \frac{\partial}{\partial x}$$

$$(u_0\psi_n^u) + \psi_n^\rho(u_0 \frac{\partial u_0}{\partial x} + v_0 \frac{\partial u_0}{\partial r}) + \frac{\partial \psi_n^p}{\partial x}] - \psi_n^u \frac{\partial}{\partial r}(\rho_0 v_0\phi_{2m})$$

$$+ \phi_{3m}[\rho_0 u_0 \frac{\partial \psi_n^v}{\partial x} + \rho_0\psi_n^u \frac{\partial v_0}{\partial x} + \psi_n^\rho(v_0 \frac{\partial v_0}{\partial r} + u_0 \frac{\partial v_0}{\partial x})]$$

$$- v_0\psi_n^v \frac{\partial}{\partial r}(\rho_0\phi_{3m}) + \phi_{4m}[\frac{\rho_0 v_0\psi_n^w}{r} + \rho_0 u_0 \frac{\partial \psi_n^w}{\partial x}] - \psi_n^w \frac{\partial}{\partial r}(\rho_0 v_0\phi_{4m})$$

$$+ \phi_{5m}[\rho_0 u_0 \frac{\partial \psi_n^T}{\partial x} + \rho_0\psi_n^u \frac{\partial T_0}{\partial x} + \psi_n^\rho(v_0 \frac{\partial T_0}{\partial r} + u_0 \frac{\partial T_0}{\partial x}) - (\gamma-1) \times$$

$$(u_0 \frac{\partial \psi_n^p}{\partial x} + \psi_n^u \frac{\partial p_0}{\partial x} + \psi_n^v \frac{\partial p_0}{\partial r})] - \psi_n^T \frac{\partial}{\partial r}(\rho_0 v_0\phi_{5m}) + (\gamma-1)\psi_n^p \frac{\partial}{\partial r} \times$$

$$(v_0\phi_{5m}) + \phi_{1m} i(k_n - k_m)(\rho_0\psi_n^u + u_0\psi_n^\rho) + \phi_{2m} i(k_n - k_m)(\psi_n^p$$

$$+ \rho_0 u_0\psi_n^u) + \phi_{3m} i(k_n - k_m)\rho_0 u_0\psi_n^v + \phi_{4m} i(k_n - k_m)\rho_0 u_0\psi_n^w$$

$$+ \phi_{5m} i(k_n - k_m)u_0(\rho_0\psi_n^T - (\gamma-1)\psi_n^p)\Big\} dr + \rho_0\phi_{1m}[R'\psi_n^u$$

$$+ \frac{\beta}{\rho_w c_w}\psi_n^p(\sqrt{1+R'^2} - 1)]_{r=R}\Bigg] e^{i\int k_n dx} \tag{2.44}$$

Equation (2.42) can be written in matrix form as

$$F \frac{dA}{dx} = GA \tag{2.45}$$

where A is a column vector whose elements are the A_n, and both F and G are N×N matrices whose elements are the f_{mn} and g_{mn}, respectively. Under certain conditions there exists the possibility that two distinct quasiparallel wavenumbers, k_n, will approach each other as the numerical procedure progresses down the duct until they coincide at a particular axial location, and they will coincide only at this particular point. If this happens, the matrix F will be singular and the assumed solution, Eqs. (2.18) and (2.19), must be modified at this axial location. If $k_j = k_s$, the contributions by the j and s modes to Eq. (2.18) take the form[42]

$$[A_j(x) + xA_s(x)]\ \psi_j^p\ (r,x)\ \exp\ (i\int k_j dx)$$

with a similar expression for Eq. (2.19). Using this form in the solvability constraint Eq. (2.41) will change the row denoting the s mode in both the F and G matrices. These rows, for the case of a double root, become

$$f_{sn} = [\int_0^R \{\phi_{1s}(\rho_0\psi_n^u + u_0\psi_n^\rho) + \phi_{2s}(\rho_0 u_0\psi_n^u + \psi_n^p) + \phi_{3s}(\rho_0 u_0\psi_n^v) + \phi_{4s}(\rho_0 u_0\psi_n^w) + \phi_{5s}(\rho_0 u_0\psi_n^T - (\gamma-1)u_0\psi_n^p)\}dr]xe^{i\int k_n dx} \qquad (2.46)$$

$$g_{sn} = - \Bigg[\int_0^R \Big\{ \phi_{1s} [\frac{\partial}{\partial x} (x\rho_0\psi_n^u + xu_0\psi_n^\rho)] - xrv_0\psi_n^\rho \frac{\partial}{\partial r} (\frac{\phi_{1s}}{r}) + \phi_{2s} [\rho_0 \frac{\partial}{\partial x}$$

$$(xu_0\psi_n^u) + x\psi_n^\rho (u_0 \frac{\partial u_0}{\partial x} + v_0 \frac{\partial u_0}{\partial r}) + \frac{\partial (x\psi_n^p)}{\partial x}] - x\psi_n^u \frac{\partial}{\partial r} (\rho_0 v_0 \phi_{2s})$$

$$+ \phi_{3s} [\rho_0 u_0 \frac{\partial (x\psi_n^v)}{\partial x} + x\rho_0\psi_n^u \frac{\partial v_0}{\partial x} + x\psi_n^\rho (v_0 \frac{\partial v_0}{\partial r} + u_0 \frac{\partial v_0}{\partial x})]$$

$$- xv_0\psi_n^v \frac{\partial}{\partial r} (\rho_0\phi_{3s}) + \phi_{4s} [\frac{x\rho_0 v_0 \psi_n^w}{r} + \rho_0 u_0 \frac{\partial (x\psi_n^w)}{\partial x}] - x\psi_n^w \frac{\partial}{\partial r} (\rho_0 v_0 \phi_{4s})$$

$$+ \phi_{5s} [\rho_0 u_0 \frac{\partial (x\psi_n^T)}{\partial x} + x\rho_0\psi_n^u \frac{\partial T_0}{\partial x} + x\psi_n^\rho (v_0 \frac{\partial T_0}{\partial r} + u_0 \frac{\partial T_0}{\partial x}) - (\gamma-1) \times$$

$$(u_0 \frac{\partial (x\psi_n^p)}{\partial x} + x\psi_n^u \frac{\partial p_0}{\partial x} + x\psi_n^v \frac{\partial p_0}{\partial r})] - x\psi_n^T \frac{\partial}{\partial r} (\rho_0 v_0 \phi_{5s}) + (\gamma-1) x\psi_n^p \frac{\partial}{\partial r} \times$$

$$(v_0\phi_{5s}) + \phi_{1s} ix(k_n - k_s)(\rho_0\psi_n^u + u_0\psi_n^\rho) + \phi_{2s} ix(k_n - k_s)(\psi_n^p$$

$$+ \rho_0 u_0 \psi_n^u) + \phi_{3s} ix(k_n - k_s)\rho_0 u_0 \psi_n^v + \phi_{4s} ix(k_n - k_s)\rho_0 u_0 \psi_n^w$$

$$+ \phi_{5s} ix(k_n - k_s) u_0 (\rho_0 \psi_n^T - (\gamma-1)\psi_n^p) \Big\} dr + x\rho_0\phi_{1s} [R'\psi_n^u$$

$$+ \frac{\beta}{\rho_w c_w} \psi_n^p (\sqrt{1+R'^2} - 1)]_{r=R} \Bigg] e^{i\int k_n dx} \qquad (2.47)$$

2.2 Numerical Procedures

The coefficients f_{mn} and g_{mn} in Eq. (2.42) require the specification of all mean flow quantities, u_0, ρ_0, T_0, p_0, v_0, and their first partial derivatives with respect to both x and r. As can be seen g_{mn} also requires some second derivatives in its present form. In the computer routine integration by parts has been performed on the expressions which contain second derivatives so that only first derivatives of the mean flow are required for g_{mn}. Therefore the computer model must be supplied with the mean flow variables and their first derivatives and also the mean flow velocity profile has to satisfy the no-slip boundary condition at the wall.

Calculation of a steady, compressible mean flow requires a considerable computational effort; therefore one-dimensional gas dynamics theory is assumed to be sufficient to model the mean flow in the inviscid core in order that the calculation of the mean flow does not lead to an excessive amount of computer storage and time. This theory requires that u_0, ρ_0, T_0, and p_0 be constant across the duct section except in the region of the wall boundary layer. There are two options for the radial velocity v_o in the program. It can either be set equal to zero, which is consistent with the one-dimensional theory, or it can be calculated as a linear function of r, which is consistent with the mean-continuity equation and the flow-tangency condition at the wall. For the cases presented in this study a quadratic velocity profile in the boundary layer was used which has the following form:

$$\frac{u_o}{u_c} = \begin{cases} 1 - \left[1-\left(\frac{R-r}{\delta}\right)\right]^2 & \text{for } r \geq R-\delta \\ 1 & \text{for } r < R-\delta \end{cases} \tag{2.48}$$

The temperature profile is evaluated by[39]

$$\frac{T_o}{T_c} = 1 + r_1 \frac{\gamma-1}{2} M_c^2 \left[1 - \left(\frac{u_o}{u_c}\right)^2\right] + \frac{T_w - T_{ad}}{T_c} \left[1 - \frac{u_o}{u_c}\right] \tag{2.49}$$

$$\frac{T_{ad}}{T_c} = 1 + r_1 \frac{\gamma-1}{2} M_c^2 \tag{2.50}$$

where the subscript c denotes values in the inviscid core, T_w is the wall temperature, T_{ad} is the adiabatic wall temperature, δ is the boundary-layer thickness, r_1 is the recovery factor, and $\gamma = 1.4$ is the ratio of the gas specific heats. Equations (2.49) and (2.50) are regarded as rough approximations only for variable-area ducts. The computer model contains three input options in order to determine the wall temperature. A constant value can be input for the wall temperature, it can be set equal to the inviscid core temperature T_c, or it can be set equal to the adiabatic wall temperature T_{ad}. For the cases analyzed in this study, the boundary-layer displacement thickness δ^* is assumed to be a known function of the axial location. At $x = 0$, the mean flow Mach number is input which allows δ and M_c to be calculated at each axial station from the definition of displacement thickness and from mass flow considerations. The inviscid core variables T_c, ρ_c, u_c, etc. are evaluated from one-dimensional gas-dynamics theory and the boundary-layer profiles are computed from Eqs. (2.48), (2.49), and (2.50). Also, the sign convention used is that the mean Mach number is negative or positive if the flow is from right to left or left to right, respectively.

Two options are provided for the wall admittance of the duct liner. One choice is that the liner is point-reacting with constant properties whose specific admittance is described by

$$\beta = [R_e(1 - \frac{i\omega}{\omega_o}) + i \cot (\frac{\omega d}{\sqrt{T_w}})]^{-1} \tag{2.51}$$

where R_e is the resistance of the facing sheet, ω_0 is the characteristic frequency of the facing sheet, and d is the depth of the backing cavities in the liner. The other option is a continuously varying admittance given by

$$\beta = \beta_0 + (\beta_L - \beta_0)(3 - \frac{2x}{L})(\frac{x}{L})^2 \tag{2.52}$$

so that the admittance varies from a specified value β_0 at $x = 0$ to a specified value β_L at $x = L$.

In the inviscid core Eq. (2.28) reduces to Bessel's equation

$$\frac{\partial^2\psi^P}{\partial r^2} + \frac{1}{r}\frac{\partial\psi^P}{\partial r} + [\frac{\hat{\omega}^2}{T_0} - k^2 - \frac{m^2}{r^2}]\psi^P = 0 \tag{2.53}$$

so that ψ^P can be expressed as

$$\psi_n^P(r,x) = A_n(x)J_m(\kappa_{m,n}\, r) + B_n(x)Y_m(\kappa_{m,n}\, r) \tag{2.54}$$

at each axial station where J_m and Y_m are the Bessel functions of order m of the first and second kinds, respectively and $\kappa_{m,n}$ is the quasi-parallel eigenvalue and is related to the wavenumber by the following equation:

$$\kappa_{m,n}^2 = \frac{\hat{\omega}^2}{T_0} - k_{m,n}^2. \tag{2.55}$$

For ψ_n^P to be bounded at $r = 0$, $B(x)$ must be zero since $Y_m(0)$ is unbounded. Using the above facts, we implemented the following scheme to determine the quasiparallel wavenumbers and eigenfunctions. First an initial guess is made for the wavenumber so that in the inviscid core

$$\psi_n^P = J_m(\kappa_{m,n}\, r) \qquad 0 \le r < R - \delta \tag{2.56}$$

Now the values of ψ_n^P and $\frac{\partial\psi_n^P}{\partial r}$, evaluated at $r = R - \delta$, are used as initial conditions to integrate Eq. (2.28) to the duct wall. Once at

$r = R$ an iteration procedure is begun on Eq. (2.29) to determine the correct wavenumber.

The specific numerical methods used are a fourth-order Runge-Kutta integration routine and a modification of the Levenberg-Marquardt algorithm[43,44] (see Appendix A). The Levenberg-Marquardt algorithm minimizes the sum of the squares of M functions in N variables. With the initial wavenumber the integration is implemented on Eq. (2.28), which is

$$\frac{\partial^2 \psi_n^P}{\partial r} + [\frac{1}{r} + \frac{T_0'}{T_0} + \frac{2ku_0'}{\hat{\omega}}] \frac{\partial \psi_n^P}{\partial r} + [\frac{\hat{\omega}^2}{T_0} - k^2 - \frac{m^2}{r^2}]\psi_n^P = 0, \tag{2.28}$$

with the initial conditions

$$\psi_n^P = J_m(\kappa_{m,n}\, r), \quad r = R - \delta \tag{2.57}$$

$$\frac{\partial \psi_n^P}{\partial r} = \kappa_{m,n}\, J_m'(\kappa_{m,n}\, r), \quad r = R - \delta \tag{2.58}$$

where $\kappa_{m,n}$ is a function of the wavenumber $k_{m,n}$. Now at the duct wall the boundary condition is evaluated, and here the complex function $F(k_{m,n})$ is defined as

$$F(k_{m,n}) = \frac{\partial \psi_n^P}{\partial r} - i\, \frac{\omega \beta}{T_w^{\frac{1}{2}}}\, \psi_n^P \tag{2.59}$$

Since F and $k_{m,n}$ are complex, Eq. (2.59) can be separated into two real equations in two real unknowns. $|F(k_{m,n})|^2$ is minimized using the Levenberg-Marquardt algorithm. This procedure is done iteratively until $|F(k_{m,n})| \simeq 0$. A subroutine that is able to evaluate Bessel functions of a complex argument is supplied to the model. Therefore, the need to integrate Eq. (2.28) across the inviscid core is eliminated.

This method also provides consistent initial conditions, Eqs. (2.57) and (2.58), for the integration of Eq. (2.28). If $m = 0$ the flow is axisymmetric (no θ dependence) and if $m \neq 0$, then a particular spinning mode is analyzed. A note of caution is emphasized here concerning the wavenumbers. They should be examined throughout the duct to eliminate the possibility of any exponentially amplifying modes developing. This would violate the basic idea that the quasiparallel wavenumbers, $k_{m,n}$, are the wavenumbers that would exist in an infinite parallel duct, since they would become unbounded. If this does occur then that particular mode should be dropped in Eqs. (2.18), (2.19), etc.

Evaluation of the axial derivatives of the wavenumber k and the eigenfunctions ψ_n must be performed in order that the coefficients g_{mn} of Eq. (2.42) can be determined. These axial gradients are obtained by using a finite-difference quotient such as

$$\frac{dk}{dx} \approx \frac{k_{x+\Delta x} - k_{x-\Delta x}}{2\Delta x} \tag{2.60}$$

The adjoint functions are obtained from the quasiparallel flow variables ψ^p, $\frac{\partial\psi^p}{\partial x}$, and k by use of Eqs. (2.40) and (2.32)-(2.36). Equations (2.43) and (2.44) provide the coefficients f_{mn} and g_{mn} where the integrals across the duct in these relations are obtained from Simpson's rule. For the axial integrals $\int k_n dx$, the trapezoid rule is used.

Solving for $\frac{dA}{dx}$ in Eq. (2.45) results in

$$\frac{dA}{dx} = F^{-1}GA \tag{2.61}$$

and A is determined at each axial location by the integration of Eq. (2.61) using a fourth-order Runge-Kutta scheme. This problem is linear. Thus the solution for any problem subject to general boundary conditions at both ends of the duct can be obtained by a linear combination of N linear independent solutions. These linearly independent solutions are achieved by setting all mode amplitudes except one (which is set equal to unity) equal to zero at x = 0 and integrating Eq. (2.61) to x = L. Integrating each of the N modes in this fashion permits the introduction of the transfer matrices TR_1, TR_2, TR_3, TR_4 which satisfy (see Appendix B)

$$B^+(x) = TR_1(x)B^+(0) + TR_2(x)B^-(0) \tag{2.62}$$

$$B^-(x) = TR_3(x)B^+(0) + TR_4(x)B^-(0) \tag{2.63}$$

where $B^+(x)$ is a column vector whose elements are the values $A_n e^{i\int k_n dx}$ of the right-running modes and $B^-(x)$ is a column vector whose elements are the values $\tilde{A}_n e^{i\int \tilde{k}_n dx}$ of the left-running modes, let N_R denote the number of right-running modes and let N_L denote the number of left-running modes. The dimensions of the transfer matrices are: TR_1 - $N_R \times N_R$; TR_2 - $N_R \times N_L$; TR_3 - $N_L \times N_R$; and TR_4 - $N_L \times N_L$. From Eqs. (2.62) and (2.63) it is seen that the complex mode amplitudes at x = L can be determined from those at x = 0, that is,

$$B^+(L) = TR_1(L)B^+(0) + TR_2(L)B^-(0)$$

$$B^-(L) = TR_3(L)B^+(0) + TR_4(L)B^-(0).$$

Following reference 40, transmission and reflection coefficients are sought for the nonuniform ducts of this study. The transmission and reflection coefficients relate the complex magnitudes of the outgoing modes to those of the incoming modes, according to

$$B^+(L) = T^{L,0}B^+(0) + R^{L,L}B^-(L) \tag{2.64}$$

$$B^-(0) = T^{0,L}B^-(L) + R^{0,0}B^+(0) \tag{2.65}$$

which are evaluated from the transfer matrices by[45]

$$\begin{aligned} T^{0,L} &= TR_4^{-1} \\ R^{0,0} &= -TR_4^{-1}TR_3 \\ R^{L,L} &= TR_2TR_4^{-1} \\ T^{L,0} &= TR_1 + TR_2R^{0,0} \end{aligned} \tag{2.66}$$

where $T^{0,L}$, $R^{0,0}$, $R^{L,L}$, $T^{L,0}$ are $N_L \times N_L$, $N_L \times N_R$, $N_R \times N_L$, $N_R \times N_R$ matrices respectively. The (m,n) element of $T^{L,0}$ represents the transmission of the mth radial mode at x = L due to the nth radial mode being incident at x = 0, etc.

If the values of $B^+(0)$ and $B^-(L)$ are input, which are the amplitudes of the right-running modes that are incident on the duct section at x = 0 and the left-running modes that are incident on the duct section at x = L, respectively then acoustic pressure profiles are calculated. Equation (2.65) determines $B^-(0)$ and therefore the mode amplitudes can be calculated throughout the duct by using Eqs. (2.62) and (2.63). At each axial position acoustic pressure profiles can now be computed across the duct by using Eqs. (2.10) and (2.18) and the definition of B^+ and B^-:

$$p_1(r,x,\theta,t) = [\sum_{n=1}^{N_R} B_n^+(x)\psi_n^p(r,x) + \sum_{n=1}^{N_L} B_n^-(x)\tilde{\psi}_n^p(r,x)]e^{i(m\theta-\omega t)} \tag{2.67}$$

where the bracketed terms describe the spatial distribution of interest.

2.3 Initial Mode Identification

Equation (2.29) has an infinite number of roots and for the wave-envelope method to succeed the evaluation of the roots is quite critical. The approach adopted for the determination of the roots is to first determine a specified number of roots for the uniform duct section (which correspond to the left and right-running waves to be analyzed). These modes are the initial guess values at $x = 0$ for the computer model and Lagrangian interpolation is used for the initial guess of the wavenumbers, which are supplied to the Levenberg-Marquardt algorithm, as the solution scheme proceeds down the duct. It is apparent that achieving an accurate solution to the problem depends on the successful evaluation of the input modes at $x = 0$.

The determination of the input modes is accomplished by numerically integrating from the known hard-wall wavenumbers ($\beta = 0$) to the specified value of the liner admittance β. In the integration method, the initial conditions are the hard-wall wavenumbers and it is assumed that all soft-wall modes have a one-to-one correspondence with the hard-wall modes. The differential equations to be integrated are derived by considering a circular, parallel duct which is carrying an inviscid mean flow with uniform properties. For this situation the soft-wall boundary condition becomes

$$\kappa J_m'(\kappa) - i\beta\omega(1 - M\frac{k}{\omega})^2 J_m(\kappa) = 0 \tag{2.68}$$

where M is the mean flow Mach number. Also, the eigenvalue κ and the complex wavenumber k are related by

$$\kappa^2 = (Mk-\omega)^2 - k^2. \tag{2.69}$$

Differentiating Eqs. (2.68) and (2.69) with respect to β will yield

$$\frac{d\kappa^2}{d\beta} = \frac{-2i\hat{\omega}^2}{(1 - \frac{m^2}{\kappa^2})\omega + \frac{2i\hat{\omega}M\beta}{\hat{\omega}M+k} - \frac{\hat{\omega}^4}{\omega}\frac{\beta^2}{\kappa^2}} \tag{2.70}$$

$$\frac{dk}{d\beta} = \frac{-\frac{d\kappa^2}{d\beta}}{2(\hat{\omega}M + k)} \tag{2.71}$$

where $\hat{\omega} = \omega-kM$.

Integration of Eqs. (2.70) and (2.71) determines the soft-wall eigenvalues and wavenumbers. The initial conditions are

$$\kappa = \kappa_0 \text{ where } J_m'(\kappa_0) = 0 \text{ at } \beta = 0$$

and

$$k = \frac{-\omega M \pm \sqrt{\omega^2 - (1-M^2)\kappa_0^2}}{1 - M^2} \tag{2.72}$$

In Eq. (2.72) the sign on the radical determines which family of modes (right-running or left-running) is being considered. Equation (2.72) is used only to compute the initial value of k and the successive values of k are obtained from Eq. (2.71). For $d\kappa^2/d\beta$, the initial values at $\beta = 0$ are

$$\frac{d\kappa^2}{d\beta} = \frac{-2i\hat{\omega}^2}{(1 - \frac{m^2}{\kappa_0^2})\omega} \quad \text{if } \kappa_0^2 \neq 0 \tag{2.73}$$

and

$$\frac{d\kappa^2}{d\beta} = \frac{-2i\omega}{(1 \pm M)^2} \quad \text{if } \kappa_0 = 0 \tag{2.74}$$

The reason that Eq. (2.72) is used only for the initial value is that the complex quantity $\sqrt{\omega^2-(1-M^2)\kappa^2}$ can approach and cross a branch cut depending on the definition of the principal value in the computer routine. If this happens, the routine will then compute identical wavenumbers for both families of modes which is incorrect.

2.4 Results for a Converging Duct

All the results presented here are for the converging circular duct shown in Fig. 1. The duct radius is assumed to vary with axial distance according to

$$R = 1 + .15(-1 + \cos \frac{2\pi x}{L}) \tag{2.75}$$

where L/2 is the length of the duct. Thus, the radius of the duct decreases sinusoidally from 1 in the uniform section to 0.7 at the throat. The wall temperature is assumed to be equal to the adiabatic temperature so that Eq. (2.49) reduces to

$$\frac{T_o}{T_c} = 1 + \frac{1}{2} r_1(\gamma-1)M_c^2[1 - (\frac{u_o}{u_c})^2] \tag{2.76}$$

Also, the radial velocity v_o is calculated to be a linear function of r consistent with the mean-continuity equation and the flow tangency condition at the wall.

Figures 2 and 3 compare the acoustic pressure profiles for an axisymmetric mode and three spinning modes (m = 1, 2, 3) in a hard-wall duct. The input for these cases is the same except for the circumferential (spinning) mode number. The profiles for three axial stations are presented (x = 0, .5, 1). In all the results presented the throat of the converging duct is at $x = 1$. The throat mean Mach number is $-.883$, the inlet displacement thickness is .001, the frequency is 9 and four modes are considered. At $x = 0$ the lowest right-running mode is incident and it has the same value in all cases so that the acoustic signal propagates upstream. As is expected the maximum pressure amplitude in the axisymmetric case occurs at the centerline of the throat. With increasing spinning mode number one sees that the maximum amplitude decreases and shifts toward the duct wall at the throat. This indicates that whereas the refractive effect of the axial gradients is still present the focusing and intensification is weakened by the asymmetries.

Figures 4 and 5 depict the same cases except for the fact that the number of modes has been increased to seven. The decrease in amplitude and its shift toward the wall at the throat are still present. But there is a noticeable difference between the pressure profiles for the cases of $m = 0$ and $m = 1$ as compared to the cases using four modes. For $m = 2$ and $m = 3$ the profiles are little changed by considering seven modes. These differences can be explained by examining the quasi-parallel wavenumbers. The first four wavenumbers in each case are cut-on throughout the duct, but the next three can contain modes that are initially cut-off. In the axisymmetric case only one cut-off mode is added, for $m = 1$ two are added and for both $m = 2$ and $m = 3$ all three modes are cut-off. Also as the spinning mode number increases the attenuation factors increase. Therefore for the cases of $m = 2$ and $m = 3$ these modes are greatly attenuated as compared to $m = 0$ and m = 1. It can also be seen that for each case the inclusion of seven modes results in a greater peak pressure at the throat.

Figures 6 and 7 show the effect of the mean Mach number at the throat. The input parameters are the same as those used to construct the previous figures except for the Mach number variations. Figure 6 depicts the case for m = 2 and Fig. 7 for m = 3. Seven modes were included in each of these cases. They show the increase in the acoustic pressure amplitude as the throat Mach number increases toward unity. For partially-choked flows one should be aware of the limitations in using a linear model. As the mean Mach number increases the wavenumbers of the right-running (upstream) modes become very large. Consider the case for uniform flow where the wavenumber is given by

$$k = \frac{-\omega M_c \mp \sqrt{\omega^2 - (1 - M_c^2)\kappa^2}}{(1 - M_c^2)} \quad . \tag{2.77}$$

Here M_c is the Mach number and κ is the eigenvalue. As $M_c \to 1$, one of the values of k approaches infinity, whereas the other remains bounded. This unusual behavior of the solution is due to linearization of the acoustic equations, as demonstrated numerically by Eisenberg and Kao[13] and Hersh and Liu[32] and analytically by Myers and Callegari[33] for the one-dimensional case. Thus, the inclusion of the nonlinear terms becomes necessary at high Mach numbers.

The effect of the liner admittance, β, is demonstrated in Figs. 8 and 9 for m = 2 and m = 3. The acoustic pressure profiles at the throat are shown for four values of the admittance for each spinning mode. The throat Mach number is -.883, the inlet displacement thickness is .001, the frequency is 9 and seven modes are considered. The real part of the admittance is varied and the lowest right-running mode is input at x = 0 so that upstream propagation takes place. As is shown there is a significant reduction in the amplitude of the acoustic signal if the duct is lined, especially for m = 2. No definite trend in the amplitude reduction as a function of the real part of the liner admittance is apparent in contrast to the axisymmetric case[31].

The effect of transverse velocity (shear layers) and temperature gradients of the mean flow on the propagation and attenuation of sound waves in hard-walled as well as lined rectangular, circular, and annular ducts have been investigated in several studies[5]. In general, the shear layers refract the axisymmetric modes toward the wall for downstream propagation and away from the wall for upstream propagation. The degree of refraction tends to increase with increasing frequency and increasing boundary-layer thickness. Cooling the wall of a duct tends to refract the sound toward the wall for both upstream and downstream propagation, whereas heating the wall tends to refract the sound away from the wall.

Figure 10 shows the effect of boundary-layer thickness for m = 3 in a hard-wall duct. The acoustic pressure profiles presented were calculated at the throat and the relevant physical parameters are mean throat Mach number = -.883, frequency = 9, and four modes. The lowest right-running mode is incident at x = 0 so that the acoustic signal propagates upstream. As the inlet displacement thickness increases the peak acoustic pressure amplitude increases and the wall value decreases. Therefore it appears that the boundary-layer thickness has a strong refractive effect for spinning modes as well as axisymmetric modes. But as noted before the signal is not focused along the duct centerline.

The dependence on the frequency of the acoustic pressure is shown in Fig. 11. The input values for this case are the same as the previous case except that the inlet displacement thickness is set at .001 and the frequency is varied. Again the plots are constructed at the throat and four modes are included. The lowest right-running mode is incident at x = 0 which implies that upstream propagation takes place. Increasing the frequency results in an increase in the amplitude of the maximum acoustic pressure.

Figure 12 represents a case where the acoustic signal propagates downstream in a hard-wall duct. The lowest left-running mode is incident at x = 1 and seven modes are considered. The mean throat Mach number is -.883, m = 3, the frequency is 9 and the inlet displacement thickness is .001. Acoustic pressure profiles are shown at the three axial stations x = 0, .5 and 1. Notice that there is only a slight increase in the maximum acoustic pressure as the signal propagates downstream. It also appears that at x = 0 the signal has undergone significant refraction toward the wall where the maximum amplitude occurs in spite of the rather small bounday-layer thickness. Since there is no appreciable growth in the acoustic pressure here, resulting in the solution becoming unstable, one suspects that the linear theory is applicable to cases of waves propagating with the flow even if the mean Mach number is high.

2.5 Results for a Converging-Diverging Duct

Results for the converging-diverging duct depicted in Fig. 13 are presented in this section. The duct radius obeys Eq. (2.75) so that the converging portion of the duct is identical to the duct of the previous section and the diverging portion increases sinusoidally from 0.7 at the throat to 1 in the uniform section. For all cases presented the length of the duct is L = 2. The temperature profile is the same as in the previous section, i.e., Eq. (2.76) and the radial velocity v_o is a linear function of r.

Figure 14 shows the variation of the centerline acoustic pressure for the case of an axisymmetric acoustic wave in a hard-wall duct and the effect of the number of modes considered. The throat mean Mach number is -.883, the inlet displacement thickness is .02, the frequency is 9 and for the three cases presented the number of modes are 2, 4, and 6. At x = 0 the lowest right-running mode is incident and it has the same value in all cases. As can be seen the throat centerline pressure increases with an increase in the number of modes considered, which was also true in the analysis of the converging duct. At x = L the minimum centerline pressure is for the case of six modes but for four modes the pressure is greater than that produced by considering two modes. Figure 15 shows the acoustic pressure profiles across the duct radius at the three axial locations x = 0, L/2, L for the case of six modes. The peak acoustic pressure is greatly reduced at x = L as compared to the profile at the throat and this maximum value is shifted from the duct centerline. The continuous mode reflections that occur in the diverging section of the duct reduces the exit acoustic signal and refracts the sound to an annulus at about half the radius of the duct.

In Fig. 16 the effect of varying the mean flow Mach number on the centerline acoustic pressure is shown. The input data is the same as that used to produce the previous figures and six modes are considered. For a near sonic flow ($M_{th} = -.883$) the growth in the amplitude of the pressure at the throat contrasts sharply to those of the two lower speed flows. Also, at x = L the centerline pressure decreases with increasing Mach number. For $M_{th} = -.449$ and $-.65$ the maximum centerline pressure occurs upstream of the throat region.

Figure 17 is obtained by varying the liner admittance and the relevant physical parameters are the same as those in the previous cases. The centerline acoustic pressure for a hard-wall duct is compared to those for two soft-wall values. In the soft-wall cases the centerline acoustic pressure is significantly reduced but their values are greater at x = L than the hard-wall value. For $\beta = (1., .1)$ the peak centerline pressure occurs noticeably upstream of the throat. The radial pressure variations for these cases, at x = 0, L/2, L, are shown in Fig. 18. At the throat the presence of a liner does reduce the acoustic signal but at x = L the peak acoustic pressure is greater for $\beta = (1., .1)$ than that produced by the hard-wall duct. For parallel ducts carrying uniform mean flows where $|\beta| << 1$ the attenuation factor increases when the real part of the admittance increases. From Figs. 17 and 18 it appears that a lined duct does not necessarily reduce the maximum amplitude of the acoustic signal in a converging-diverging duct. The inclusion of more modes in the analysis will probably affect the hard-wall pressure profiles more than the soft-wall profiles. Generally the soft-wall wavenumbers have higher attenuation rates and more hard-wall wavenumbers are cut-on and therefore are attenuated less. Also an initially cut-off hard-wall mode is more likely to cut-on in the vicinity of the throat. Thus if all modes that are cut-on throughout the hard-wall duct are included the resulting acoustic signal at x = L might well be greater than that produced by a lined duct.

Figure 19 shows the effect of the boundary layer thickness on the centerline acoustic pressure for an axisymmetric flow case. For all cases shown in Fig. 19, the throat mean Mach number is -.883, the acoustic frequency is 9, the number of modes is 6 and the lowest right-running mode is incident at x = 0. It is seen that increasing the inlet displacement thickness does not necessarily increase the centerline pressure. Figures 20 and 21 show the development of the acoustic pressure profiles at x = 0, L/2, L for the cases depicted in Fig. 19. There is no apparent general trend in the acoustic pressure profiles as the inlet displacement thickness is increased. In fact the peak amplitude at the throat is obtained from $\delta_o^* = .01$ in contrast to the results achieved in the converging duct analysis of the previous section. At x = L the maximum acoustic pressure occurs for $\delta_o^* = .001$.

Figure 22 represents the variation of the acoustic pressure amplitude across the duct radius for a spinning mode case. The throat mean Mach number is -.883, $\delta_o^* = .02$, $\omega = 9$, $m = 2$, and 4 modes are considered. At $x = 0$ the lowest right-running mode is input so that upstream propagation takes place. For this particular case the acoustic signal is relatively undistorted at $x = L$ as compared to the profile at $x = 0$. As in the converging duct results the peak amplitude at the throat is not at the duct centerline.

Figures 23 and 24 represent a case when the lowest left-running mode is incident at $x = L$ and thus the acoustic disturbance propagates downstream. The physical parameters are the same as those that were used to obtain Fig. 14 for the case of six modes except that the signal is input at $x = L$. In Fig. 23 the axial variation of the centerline acoustic pressure amplitude is shown. There is no appreciable growth in the amplitude which is in marked contrast to Fig. 14 which depicts upstream propagation. Figure 24 shows the radial variation of the acoustic pressure amplitude. There is only a slight increase in the maximum pressure amplitude at the throat and the peak amplitude at $x = 0$ is greater than that at the throat.

CHAPTER THREE

Nonlinear Propagation in Near Sonic Flows

3.1 Problem Formulation and Method of Solution

The wave-envelope technique used in the previous chapter to study linear acoustic propagation, in which the linear acoustic disturbance is represented as a superposition of quasiparallel duct modes whose fast axial variation is explicitly given, will not be used in this chapter because of the singular behavior of the linear model in the region of interest. The singular behavior of the linear model as the Mach number approaches unity is illustrated in Fig. 25.

We consider a one-dimensional, inviscid, nonlinear flow in a hard-walled duct (Fig. 26). All flow quantities are expressed in non-dimensional form using the speed of sound c_a evaluated at some convenient point as a reference velocity, the radius R_o of the duct in the uniform region as the reference length, and R_o/c_a, $\rho_a c_a^2$, ρ_a, and T_a as the reference time, pressure, density, and temperature, respectively. The one-dimensional equations of motion are

Mass

$$A \frac{\partial \rho}{\partial t} + \frac{\partial}{\partial x} (\rho u A) = 0 \tag{3.1}$$

where A is the cross-sectional area of the duct.

Momentum

$$\rho[\frac{\partial u}{\partial t} + u \frac{\partial u}{\partial x}] + \frac{\partial p}{\partial x} = 0 \tag{3.2}$$

Energy

$$\rho[\frac{\partial T}{\partial t} + u \frac{\partial T}{\partial x}] - (\gamma - 1)(\frac{\partial p}{\partial t} + u \frac{\partial p}{\partial x}) = 0 \tag{3.3}$$

and, state

$$\gamma p = \rho T \tag{3.4}$$

where γ is the ratio of specific heats of the gas. The energy and state equations, (3.3) and (3.4), can be replaced with the isentropic state equation $p \propto \rho^{\gamma}$. However, the use of this apparently simpler equation would lead to difficulties in separating the effects of the several harmonics in the analysis which follows; therefore, the basic forms of the energy and state equations are used.

The flow variables are represented as the sum of a steady streaming term plus higher harmonics due to the acoustic disturbance[38]:

$$u(x,t) = u_{10}(x) + \sum_{n=1}^{N} (u_{1n}e^{-in\omega t} + \bar{u}_{1n}e^{in\omega t}) \tag{3.5}$$

$$\rho(x,t) = \rho_{10}(x) + \sum_{n=1}^{N} (\rho_{1n}e^{-in\omega t} + \bar{\rho}_{1n}e^{in\omega t}) \tag{3.6}$$

$$T(x,t) = T_{10}(x) + \sum_{n=1}^{N} (T_{1n}e^{-in\omega t} + \bar{T}_{1n}e^{in\omega t}) \tag{3.7}$$

with the pressure being eliminated with Eq. (3.4). The steady streaming terms are not solutions of the steady form of Eqs. (3.1)-(3.4). Reference conditions are chosen to be the mean-flow quantities in the straight duct section so that $T_{10}(0) = \rho_{10}(0) = 1$, $u_{10}(0) = M(0)$, and $p_{10}(0) = 1/\gamma$. The acoustic disturbance in Eqs. (3.5)-(3.7) is represented as a finite sum of harmonics, including steady-streaming terms u_{10} (which also include the effects of the mean flow), etc., and the complex conjugates must be explicitly stated since nonlinear interactions are considered. No assumptions about the relative sizes of the terms in Eqs. (3.5)-(3.7) are made, and no assumption about the axial variation of the acoustic quantities is made. Although the wavelengths of upstream propagating signals become small and thus a technique similar to the wave-envelope procedure would be very advantageous, no a priori assumption about that variation can be made.

Before proceeding with the nonlinear analysis let us consider the linear theory as it applies to a uniform duct. Linear theory will be used to relate the flow variables at the entrance of the nonuniform duct section in order to insure consistent impedance conditions for the nonlinear problem. Assume that the mean flow in the straight duct is uniform, that is u_o, T_o, ρ_o and p_o are constant. The flow variables are assumed to consist of a constant part due to the mean flow and a perturbed part due to the acoustic disturbance, that is,

$$\begin{aligned} \rho &= \rho_o + \rho_1(x,t) \\ u &= u_o + u_1(x,t) \\ T &= T_o + T_1(x,t) \end{aligned} \tag{3.8}$$

Substituting Eq. (3.8) into Eqs. (3.1)-(3.3) and ignoring nonlinear terms results in the following equations:

$$\frac{\partial \rho_1}{\partial t} + u_o \frac{\partial \rho_1}{\partial x} + \rho_o \frac{\partial u_1}{\partial x} = 0 \tag{3.9}$$

$$\rho_o \frac{\partial u_1}{\partial t} + \rho_o u_o \frac{\partial u_1}{\partial x} + \frac{\partial p_1}{\partial x} = 0 \tag{3.10}$$

$$\rho_o\left(\frac{\partial T_1}{\partial t} + u_o \frac{\partial T_1}{\partial x}\right) = (\gamma-1)\left(\frac{\partial p_1}{\partial t} + u_o \frac{\partial p_1}{\partial x}\right) \tag{3.11}$$

The pressure is eliminated from these equations by using the isentropic state equation

$$p = A\rho^{\gamma} \tag{3.12}$$

This can be rewritten as,

$$p_o + p_1 = A(\rho_o + \rho_1)^\gamma = A\rho_o^{\ \gamma} \left(1 + \frac{\rho_1}{\rho_o}\right)^\gamma \tag{3.13}$$

where $\left|\frac{\rho_1}{\rho_o}\right| << 1$.

Expanding Eq. (3.13) and retaining terms through first-order yields

$$p_o + p_1 = A\rho_o^{\ \gamma} + A\rho_o^{\ \gamma} \frac{\rho_1}{\rho_o} \gamma \tag{3.14}$$

but,

$$p_o = A\rho_o^{\ \gamma} \tag{3.15}$$

so that

$$p_1 = \frac{p_o \rho_1 \gamma}{\rho_o} = c_o^{\ 2} \rho_1 \tag{3.16}$$

where $c_o = \sqrt{\gamma p_o/\rho_o} = \sqrt{T_o}$.

Using Eq. (3.16) one can write the governing Eqs., (3.9)-(3.11) as

$$\frac{\partial \rho_1}{\partial t} + u_o \frac{\partial \rho_1}{\partial x} + \rho_o \frac{\partial u_1}{\partial x} = 0 \tag{3.17}$$

$$\rho_o \frac{\partial u_1}{\partial t} + \rho_o u_o \frac{\partial u_1}{\partial x} + c_o^2 \frac{\partial \rho_1}{\partial x} = 0 \tag{3.18}$$

$$\rho_o\left(\frac{\partial T_1}{\partial t} + u_o \frac{\partial T_1}{\partial x}\right) = (\gamma - 1)T_o\left(\frac{\partial \rho_1}{\partial t} + u_o \frac{\partial \rho_1}{\partial x}\right) \tag{3.19}$$

Assuming harmonic traveling waves for the uniform duct and letting $q_1(x,t)$ represent any of the flow variables of the acoustic disturbance allows the following form for the disturbance:

$$q_1(x,t) = \sum_{n=1}^{N} [q_{nR} e^{in(k_R x - \omega t)} + q_{nL} e^{in(k_L x - \omega t)} + \text{complex conjugate}] \tag{3.20}$$

In this expression the complex quantities q_{nR} and q_{nL} represent the amplitude and phase of the nth right and left-running waves, respectively, and are constants. Here, nk_R and nk_L are the wavenumbers for the right- and left-running waves, respectively, and they are also constant. Since the above discussion deals with linear theory we can superpose solutions and therefore analyze only one component of Eq. (3.20) which will be expressed as

$$q_1(x,t) = q_n e^{i(k_n x - \omega_n t)} \tag{3.21}$$

where

$$k_n = nk \tag{3.22}$$

$$\omega_n = n\omega \tag{3.23}$$

The phase speed of the waves will be determined by substituting

$$\rho_1(x,t) = \rho_n e^{i(k_n x - \omega_n t)} \tag{3.24}$$

$$u_1(x,t) = u_n e^{i(k_n x - \omega_n t)} \tag{3.25}$$

into Eqs. (3.17) and (3.18). This results in the following system of equations:

$$\begin{bmatrix} (-\omega + u_o k) & \rho_o k \\ c_o^2\, k & (-\rho_o \omega + \rho_o u_o k) \end{bmatrix} \begin{bmatrix} \rho_n \\ u_n \end{bmatrix} = 0 \tag{3.26}$$

The determinant of the matrix must be zero for non-trivial solutions to exist. This implies that

$$(-\omega + u_o k)^2 = c^2_o k^2 \tag{3.27}$$

or

$$-\omega + u_o k = \pm c_o k \tag{3.28}$$

Choosing the positive sign will give

$$\frac{\omega_n}{k_n} = \frac{\omega}{k_L} = u_o - c_o \tag{3.29}$$

which corresponds to the left-running waves. Choosing the negative sign will give

$$\frac{\omega_n}{k_n} = \frac{\omega}{k_R} = u_o + c_o \tag{3.30}$$

which corresponds to the right-running waves. Looking at the first equation (the mass equation) in Eq. (3.26) results in

$$(-\omega + u_o k)\rho_n + \rho_o k u_n = 0 \tag{3.31}$$

so that,

$$u_n = (\frac{\omega}{k} - u_o)\frac{\rho_n}{\rho_o} \tag{3.32}$$

Now Eqs. (3.20) and (3.30) are substituted into Eq. (3.32) so that we arrive at

$$u_{nR} = \frac{c_o}{\rho_o}\rho_{nR} \tag{3.33}$$

$$u_{nL} = -\frac{c_o}{\rho_o}\rho_{nL} \tag{3.34}$$

Replacing the acoustic temperature and density by their respective harmonic wave representations in the energy equation, Eq. (3.19), relates the temperature coefficients to the density coefficients according to

$$T_{nR} = (\gamma-1)\frac{T_o}{\rho_o}\rho_{nR} \tag{3.35}$$

$$T_{nL} = (\gamma-1)\frac{T_o}{\rho_o}\rho_{nL} \tag{3.36}$$

With these relations from the linear theory for a uniform duct the impedance conditions at the duct entrance can be formulated. The assumption here is that the linear theory is valid at the duct entrance so that it should approach the nonlinear expressions at x = 0.

Therefore Eqs. (3.8) are equated to Eqs. (3.5)-(3.7) respectively at x = 0, with the use of Eq. (3.20) also. For the density, this becomes

$$\rho_o + \sum_{n=1}^{N} [\rho_{nR}e^{-in\omega t} + \rho_{nL}e^{-in\omega t} + \bar{\rho}_{nR}e^{in\omega t} + \bar{\rho}_{nL}e^{in\omega t}] =$$

$$\rho_{10}(0) + \sum_{n=1}^{N} [\rho_{1n}(0)e^{-in\omega t} + \bar{\rho}_{1n}(0)e^{in\omega t}] \tag{3.37}$$

Equating coefficients of equal powers of exp ($\pm$ $in\omega t$) results in the following equations

$$\rho_{10}(0) = \rho_o \tag{3.38}$$

$$\rho_{1n}(0) = \rho_{nR} + \rho_{nL} \tag{3.39}$$

$$\bar{\rho}_{1n}(0) = \bar{\rho}_{nR} + \bar{\rho}_{nL} \tag{3.40}$$

By matching the velocity one obtains the following expressions:

$$u_{10}(0) = u_o \tag{3.41}$$

$$u_{1n}(0) = u_{nR} + u_{nL} \tag{3.42}$$

$$\bar{u}_{1n}(0) = \bar{u}_{nR} + \bar{u}_{nL} \tag{3.43}$$

Using Eqs. (3.33) and (3.34) in Eq. (3.42) relates the velocity to the density according to

$$u_{1n}(0) = \frac{c_o}{\rho_o}(\rho_{nR} - \rho_{nL}) \tag{3.44}$$

Finally, matching the temperature results in

$$T_{10}(0) = T_o \tag{3.45}$$

$$T_{1n}(0) = T_{nR} + T_{nL} \tag{3.46}$$

$$\overline{T}_{1n}(0) = \overline{T}_{nR} + \overline{T}_{nL} \tag{3.47}$$

and using Eqs. (3.35) and (3.36) in Eq. (3.46) implies that

$$T_{1n}(0) = (\gamma-1)\frac{T_o}{\rho_o}(\rho_{nR} + \rho_{nL}) \tag{3.48}$$

Equations (3.39), (3.44) and (3.48) establish the impedance conditions for the velocity and temperature in terms of the density at x = 0 for the nonlinear problem. The next step now is to establish the impedance condition for the nonlinear problem at the duct exit (x = L). This is accomplished by again matching the nonlinear problem to the linear problem at x = L. For x > L it is assumed that the duct has an infinite uniform termination. This is equivalent to having only right-running waves in the uniform section of the duct for x > L. Since the linear theory holds for x > L the following relations can be written

$$u(x,t) = u_o + \sum_{n=1}^{N} [u_{nR}e^{in(k_R x-\omega t)} + \overline{u}_{nR}e^{-in(k_R x-\omega t)}] \tag{3.49}$$

$$\rho(x,t) = \rho_o + \sum_{n=1}^{N} [\rho_{nR}e^{in(k_R x-\omega t)} + \overline{\rho}_{nR}e^{-in(k_R x-\omega t)}] \tag{3.50}$$

$$T(x,t) = T_o + \sum_{n=1}^{N} [T_{nR}e^{in(k_R x-\omega t)} + \overline{T}_{nR}e^{-in(k_R x-\omega t)}] \tag{3.51}$$

Equating Eq. (3.6) to Eq. (3.50) at x = L implies that

$$\rho_o = \rho_{10}(L) \tag{3.52}$$

$$\rho_{1n}(L) = \rho_{nR} e^{ink_R L} \tag{3.53}$$

Similar relations are obtained by equating Eq. (3.5) to Eq. (3.49), that is,

$$u_o = u_{10}(L) \tag{3.54}$$

$$u_{1n}(L) = u_{nR} e^{ink_R L} \tag{3.55}$$

Recalling the linear relation, Eq. (3.33), one can write Eq. (3.55) as

$$u_{1n}(L) = \frac{c_o}{\rho_o} \rho_{nR} e^{ink_R L} = \frac{c_o}{\rho_o} \rho_{1n}(L) \tag{3.56}$$

but,

$$c_o = \sqrt{T_{10}(L)} \tag{3.57}$$

$$\rho_o = \rho_{10}(L) \tag{3.58}$$

so that

$$u_{1n}(L) = \frac{\sqrt{T_{10}(L)}}{\rho_{10}(L)} \rho_{1n}(L) \tag{3.59}$$

Equation (3.59) is the impedance condition at x = L for an infinite duct. With the impedance conditions established let us now derive the differential equations for the nonlinear region ($0 < x < L$).

Substituting the expansion of the flow variables, Eqs. (3.5)-(3.7), into the governing Eqs. (3.1)-(3.4), and equating coefficients of equal powers of $\exp(in\omega t)$ for n = 0,1,2,... to zero, one obtains a set of coupled, nonlinear ordinary-differential equations of the form

$$A(x,y) \frac{dy}{dx} = B(x,y) \tag{3.60}$$

where y is a column vector of the unknowns. The coefficient matrix A(x,y) and the inhomogeneous vector B(x,y) are given in Appendix C.

We choose to solve Eq. (3.60) in real form. To accomplish this we rewrite Eq. (3.60) as

$$(A_r + iA_i)\left(\frac{dy_r}{dx} + i\,\frac{dy_i}{dx}\right) = (B_r + iB_i) \tag{3.61}$$

Separation of the real and imaginary parts leads to

$$A_r\,\frac{dy_r}{dx} - A_i\,\frac{dy_i}{dx} = B_r \tag{3.62}$$

$$A_i\,\frac{dy_r}{dx} + A_r\,\frac{dy_i}{dx} = B_i \tag{3.63}$$

Since the steady streaming is always real, its imaginary part in Eqs. (3.62) and (3.63) is discarded. This manipulation reduces Eqs. (3.60) to

$$A^*(x,y^*)\,\frac{dy^*}{dx} = B^*(x,y^*) \tag{3.64}$$

where A^* is a $3(2N + 1) \times 3(2N + 1)$ real matrix and y^* and B^* are real $3(2N + 1)$ column vectors with

$$
y^* = \begin{bmatrix} u_{10} \\ Re(u_{11}) \\ Im(u_{11}) \\ R_e(u_{12}) \\ Im(u_{12}) \\ \vdots \\ Im(u_{1n}) \\ \rho_{10} \\ Re(\rho_{11}) \\ Im(\rho_{11}) \\ \vdots \\ Im(\rho_{1n}) \\ T_{10} \\ Re(T_{11}) \\ Im(T_{11}) \\ \vdots \\ Im(T_{1n}) \end{bmatrix}
$$

With the appropriate impedance boundary conditions specified at both ends of the duct, Eqs. (3.39), (3.44), (3.48) and (3.59), Eqs. (3.64) can be numerically solved.

The numerical results that will be presented are for the case of a fundamental wave entering a duct at its left end when its right end is infinite in length.

The initial conditions at the duct entrance are specified in terms of reflection coefficients. Conditions in the straight duct section are assumed to be such that linear theory is adequate. Thus the acoustic signal at the duct entrance is resolved into left-and-right running waves. The magnitude of the input signal, of the density disturbance, for the fundamental frequency and a reflection coefficient for each harmonic are specified as input at x = 0. By matching the linear and nonlinear expressions at x = 0, the initial conditions for the nonlinear problem are determined in terms of the right-running and left-running waves at x = 0.

The density disturbance specified represents the right-running wave of the fundamental frequency and a reflection coefficient, which is input, determines the left-running wave. For the higher modes, it was assumed that only left-running waves would exist and these were assumed to be a product of the right-running fundamental wave. Therefore the acoustic disturbance will be specified by the right-running complex coefficient of the fundamental mode (n = 1), so that if ρ_I represents the acoustic signal then

$$\rho_{1R} = \rho_I \tag{3.65}$$

and ρ_{1L} is determined from the reflection coefficient c_{r1} by

$$\rho_{1L} = c_{r1}\rho_I \tag{3.66}$$

Substituting Eqs. (3.65) and (3.66) into Eq. (3.39) implies that

$$\rho_{11}(o) = (1 + c_{r1})\rho_I \tag{3.67}$$

Making use of Eq. (3.44) implies that

$$u_{11}(0) = \frac{c_o}{\rho_o}(1 - c_{r1})\rho_I = (1 - c_{r1})\rho_I \tag{3.68}$$

since $c_o = \rho_o = 1$. The temperature is determined from Eq. (3.48) to be

$$T_{11}(0) = (\gamma-1)\frac{T_o}{\rho_o}(1+c_{r1})\rho_I = (\gamma-1)(1+c_{r1})\rho_I \tag{3.69}$$

For $n \geq 2$

$$\rho_{1n}(0) = c_{rn}\rho_I \tag{3.70}$$

$$u_{1n}(0) = -c_{rn}\rho_I \tag{3.71}$$

$$T_{1n}(0) = (\gamma-1)c_{rn}\rho_I \tag{3.72}$$

and Eqs. (3.70)-(3.72) are a statement of the fact that the incident acoustic disturbance at $x = 0$ is the fundamental wave and therefore for $n \geq 2$ only left-running waves are present for $x < 0$.

Here, u_{10}, ρ_{10}, and T_{10} are determined from the mean-flow values. With these conditions set, the program then integrates through the duct to determine the corresponding conditions at $x = L$. Determination of the transmission and reflection characteristics of the duct section then would require an iteration on the assumed values of the reflection coefficients until the desired impedance conditions at $x = L$ are achieved. In the results presented here, we consider the case in which the duct has an infinite uniform termination. This is equivalent to having only right-running waves in the uniform section of the duct for $x > L$.

Mathematically Eq. (3.59) must be satisfied at $x = L$ to guarantee this situation and a complex vector $F(c_{rn})$ is defined as

$$F(c_{rn}) \equiv u_{1n}(L) - \frac{\sqrt{T_{1\theta}(L)}}{\rho_{10}(L)}\,\rho_{1n}(L) \tag{3.73}$$

Separating the real and imaginary parts of Eq. (3.73) results in 2N equations to be solved. The scheme followed then is to initially assume values for the reflection coefficients (there will be 2N of these since they are complex) and iterate on these assumed values by integrating to $x = L$. An optimization routine is used to determine updated values of the reflection coefficients until $F(c_{rn}) \simeq 0$.

In a previous analysis[38] the system represented by Eq. (3.64) was solved by using matrix inversion and a fourth-order Runge-Kutta integration routine. It was determined that if the strength of the input signal and/or the throat Mach number was increased, the numerical procedure produces either a strong oscillation or abrupt jumps in the acoustic signal. These irregular results are not a consequence of the physical occurrence of a shock. Refinement of the numerical step size produces no qualitative change. Except for these isolated jumps, the results appear entirely plausible. Examination of a large number of cases indicates that the difficulty results from a combination of the basic properties of the coefficient matrix and numerical error. Since the linear problem is singular as $|M| \to 1$, the determinant of matrix A^* is non-zero only as a result of the nonlinear terms, which are small. Since the matrix A^* becomes nearly singular, it is very ill-conditioned with a very small determinant; the addition of more harmonics makes the situation more critical and under certain conditions the numerical round-off errors eliminate the possibility of proper resolution of the terms of the equations. In fact, cases are calculated in which a doubling of the number of harmonics causes a discontinuity to develop. Previously the size of the determinant was used to monitor the singularity of A*. This is not done in the present analysis because a well conditioned matrix A* may still have a very small determinant.

The integration routine that will be employed is an Adams-PECE (Predictor Evaluate Corrector Evaluate) variable step-variable order method[46]. To avoid the problems associated with matrix inversion, the singular value decomposition (SVD)[47] of A* is performed at each axial step. The numerical problems encountered in the original analysis are due to the fact that the Runge-Kutta, because of its fixed step size, cannot detect when a singularity is occurring in the system represented by Eq. (3.64). The reflection coefficients determine the initial conditions and it is found that there is only a certain range of values for the reflection coefficients that will produce a non-singular system. Since the Runge-Kutta routine cannot recognize the presence of a singularity, it will integrate across a singular component as if it were continuous. The result of this is rapid fluctuations in the amplitudes of the harmonics and in some cases this is accompanied by unstable growth in one or more of the harmonics, which will result in the termination of the program.

To summarize, in the region of the duct throat for near sonic flows two extremely critical numerical problems are occurring in the solution of the system of equations represented by Eq. (3.64). In order to integrate this system $\frac{dy^*}{dx}$ must be solved for explicitly and supplied to the integration routine. This normally is done by inverting A*, but in this case A* is nearly singular and hence numerically inverting it is quite unstable. By using the SVD routine this particular problem is eliminated and an explicit expression for $\frac{dy^*}{dx}$ can be obtained. Now after computing $\frac{dy^*}{dx}$ care must be taken in the choice of the integration scheme. If a fixed step method (such as Runge-Kutta) is used it is more than likely that it will not recognize the presence of a singularity. For the Runge-Kutta methods highly accurate local discretization error estimates are somewhat difficult to obtain which would help to determine the step size. Also, in the Runge-Kutta methods the solution at y^*_{n+1} depends only on the solution y^*_n at the previous point x_n and the step size h_n. Multistep methods (such as the Adams methods) are based on the idea that more accuracy might be obtained by using information at previous points, such as y^*_{n-1}, y^*_{n-2}, . . . and $\frac{dy^*_{n-1}}{dx}$, $\frac{dy^*_{n-2}}{dx}$, . . . The multistep methods usually are more efficient than one-step methods and an estimate of the local discretization error is, in general, readily obtained. The order of a numerical integration scheme is the power of the step size that appears in the local error estimate, ε_n, which can be written as

$$\varepsilon_n = O(h_n^{p+1}) \tag{3.74}$$

where the integer p is then said to be the order of the method.

From this expression it can be seen that the discretization error estimate can be decreased by either increasing the order (if $h_n < 1$) or decreasing the step size. Therefore by monitoring the local discretization error estimate, multistep methods provide the capability of automatically changing the order or step size to insure the accuracy of the solution. An example of a multistep scheme is the fourth-order Adams predictor-corrector method[48]:

$$\text{predictor:}\quad y^*_{n+1} = y^*_n + \frac{h}{24}\left(55\,\frac{dy^*_n}{dx} - 59\,\frac{dy^*_{n-1}}{dx} + 37\,\frac{dy^*_{n-2}}{dx} - 9\,\frac{dy^*_{n-3}}{dx}\right)$$

$$\text{corrector:}\quad y^*_{n+1} = y^*_n + \frac{h}{24}\left(9\,\frac{dy^*_{n+1}}{dx} + 19\,\frac{dy^*_n}{dx} - 5\,\frac{dy^*_{n-1}}{dx} + \frac{dy^*_{n-2}}{dx}\right)$$

These are fourth order formulas, but the order can be increased by including more terms in these relations corresponding to $\frac{dy^*_{n-4}}{dx}$, $\frac{dy^*_{n-5}}{dx}$, etc. The Adams-PECE routine for calculating y^*_{n+1} is as follows:

1. Use the predictor to calculate $y^{*(0)}_{n+1}$, an initial approximation to y^*_{n+1}.

2. Evaluate the derivative function and set $\frac{dy^{*(0)}_{n+1}}{dx} = \frac{dy^*}{dx}(y^{*(0)}_{n+1}, x_{n+1})$

3. Calculate a more accurate approximation $y^{*(1)}_{n+1}$ using the corrector formula with $\frac{dy^*_{n+1}}{dx} = \frac{dy^{*(0)}_{n+1}}{dx}$.

4. Evaluate the derivative function using $y^{*(1)}_{n+1}$ obtained in step 3 (from the corrector formula) for the next integration step.

If a singularity exists in the solution to Eq. (3.64), the Adams-PECE scheme is much more likely to discover this fact than a Runge-Kutta method.

The SVD procedure decomposes the matrix A* into the following form:

$$A^* = USV^T \tag{3.75}$$

where U and V^T are orthogonal matrices and S is a diagonal matrix that shows if A* is singular (see Appendix D). If one or more of the diagonal elements of S is zero then A* is singular. Also the number of non-zero diagonal elements of S is the rank of A*. The SVD of A* is accomplished by first using Householder transformations to reduce A* to bidiagonal form and then the singular values of the bidiagonal matrix are determined by using a variant of the QR algorithm. This decomposition explicitly shows if A* is singular and monitoring S will show if a singularity is encountered. The fact that the SVD is based on orthogonal matrices makes it numerically stable, which is essential in a neighborhood of a numerical singularity.

Substituting this decomposition for A* produces a very simple method for determining when a component of $\frac{dy^*}{dx}$ is unbounded. This procedure is shown by expressing Eq. (3.64) as

$$USV^T \frac{dy^*}{dx} = B^* \tag{3.76}$$

which implies that

$$SV^T \frac{dy^*}{dx} = U^T B^* = G \tag{3.77}$$

Now since S is a diagonal matrix, then

$$V^T \frac{dy^*}{dx} = \begin{bmatrix} \frac{G_1}{\sigma_1} \\ \frac{G_2}{\sigma_2} \\ \cdot \\ \cdot \\ \cdot \\ \frac{G_n}{\sigma_n} \end{bmatrix} = H$$

where the σ_i are the diagonal elements of S. The vector H determines if any of the derivatives is unbounded. There is no need to solve explicitly for $\frac{dy^*}{dx}$ to realize that the system is singular because V is orthogonal. Pre-multiplying H by V might shift the singularity to another component but it will not eliminate the singularity from Eq. (3.64). By examining a number of cases it was found that a tolerance could be set on the components of H when the system is singular. The singularity always occurs at the throat and when the Adams-PECE routine encounters this singular behavior it will not be able to integrate further. But it is quite inefficient to discover the singularity in this manner, since the integration routine will keep trying to integrate across the singularity until it runs out of time. Therefore, if $|G_i/\sigma_i| \geq 100$ the program stops since this indicates that $\frac{dy^*}{dx}$ is becoming too large for the integration routine to handle. If this is the case then incorrect reflection coefficients have been chosen.

Now, with a systematic procedure for integrating to x = L, the iteration on Eq. (3.73) can be implemented. For a particular case, the only variables in Eq. (3.73) are the reflection coefficients. The reflection coefficients that satisfy Eq. (3.73) are determined by iteration. This is accomplished by using a subroutine that tries to minimize the sum of the squares of 2N nonlinear functions in 2N variables by a modification of the Levenberg-Marquardt algorithm[43,44] (see Appendix A). The algorithm calculates corrected reflection coefficients which are then passed to the integration routine. This is done successively until $F(c_{rn}) \approx 0$ is satisfied to within a certain tolerance.

3.2 Numerical Results

The numerical procedure has been applied to examine acoustic propagation through a simple converging-diverging duct section. The radius of the duct wall in the variable-area section is given by

$$R = 1 - \frac{1}{10} \left(1 - \cos \frac{2\pi x}{L}\right)$$

and the duct connects to straight sections at $x = 0$ and $x = L$, see Fig. 26.

In order to implement the iteration procedure, reflection coefficients that will permit Eq. (3.64) to be integrated to the right-end of the duct without encountering a singularity are first determined. To begin with, we consider only one reflection coefficient c_{r1} and assume the other coefficients to be zero. This is equivalent to setting the boundary conditions at $x = 0$ for the higher harmonics to be zero. By varying c_{r1}, we obtain the plot in Fig. 27 showing the region of admissible reflection coefficients c_{r1}. The region is determined using two harmonics. Cases using four and ten harmonics indicate that the region does not shrink appreciably. Using these values for c_{r1} and the other $c_{ri} = 0$ as initial values, we start the iteration to determine all the coefficients c_{ri}.

Equation (3.5) can be written in real form as

$$u(x,t) = u_{10}(x) + \sum_{n=1}^{N} D_n(x) \cos [n\omega t - \phi_n(x)] \tag{3.78}$$

where the amplitude functions $D_n(x)$ are related to the complex coefficients by

$$D_n(x) = 2 \sqrt{[\mathrm{Re}(u_{1n})]^2 + [\mathrm{Im}(u_{1n})]^2} = 2 \; |u_{1n}(x)| \tag{3.79}$$

and the phase angle $\phi_n(x)$ can be determined from

$$\phi_n(x) = \tan^{-1} \frac{\mathrm{Im}(u_{1n})}{\mathrm{Re}(u_{1n})} \tag{3.80}$$

In the following figures $|u_{1n}(x)|/|u_{11}(0)|$ represents the development of the amplitude of the nth harmonic as compared to the fundamental wave at the duct entrance.

In Figures 28, 29, and 30 the original Runge-Kutta version of the program is compared with the version using the Adams-PECE and SVD routines. The figures represent plots of the velocity amplitudes versus the axial distance through the duct. They are determined using the above mentioned procedure (i.e., $c_{ri} = 0$ for $n \geq 2$). Figure 28 demonstrates the weakness of the original numerical procedure. In the case depicted in Fig. 28, $c_{r1} = 0$. But from Fig. 27 it is seen that this value for c_{r1} is not in the region of admissible c_{r1}. Therefore the Runge-Kutta scheme, as shown in Fig. 28, has integrated to $x = L$

without realizing that the solution is singular near the throat. In Fig. 29 the same case is shown except here four harmonics are used. The unstable growth of the amplitudes near the throat, which resulted in the termination of the program, indicates that the results in Fig. 28 are incorrect. Using the Adams-PECE and SVD methods shows that $c_{r_1} = 0$ is incorrect for the case of two harmonics. The program will terminate at the throat and not integrate to x = L as the Runge-Kutta does. Figure 30 is obtained from the Adams-PECE and SVD schemes. There are no unstable growth patterns or large jumps in the amplitudes near the throat both of which develop in the Runge-Kutta method.

The successful integration to the right end of the duct allows the iteration to begin on the impedance conditions at x = L. Figures 31-34 depict the variation of the velocity amplitude of each harmonic through the duct for a case where the impedance conditions at x = L are satisfied by the iteration. Several cases were calculated using different reflection coefficients to initiate the iteration. In each case the iteration converged to the same solution. Also, the flow in the vicinity of the throat is in the near sonic region. The parameters for each case are identical except for the number of harmonics. These figures illustrate the dominance of the fundamental signal. The fundamental signal in Fig. 34 computed using four harmonics is not appreciably different from that in Fig. 31 using one harmonic. Also shown is the rapid increase in the intensity of the disturbance near the throat region. The higher harmonics do not become significant until the throat is approached. For the fundamental signal there is a reduction of its amplitude at the exit. Including higher harmonics reduces the amplitude of the fundamental signal to a still lower value at the exit, thus the increased intensity near the throat appears to transfer energy from the fundamental to the higher harmonics. The results of the case using four harmonics were used as input for a case using ten harmonics. No iteration was performed on this case due to the large computation time that would have been required for ten harmonics. Integration to the exit would be performed to determine if a singularity would appear that was undetected by using four harmonics. Also the impedance conditions at $x = L$ were evaluated to determine if they were still satisfied. This example confirms the results of Fig. 34. For the first two harmonics the results are essentially the same as that obtained by using four harmonics in the computation of the solution. The only significant result of this case not shown in Fig. 34 is the reduction of the third and fourth harmonics at the exit due to their interaction with the higher harmonics. Since this case has a high maximum Mach number (-.983 for $N = 4$) at the throat (which implies significant nonlinear effects), it should serve as a limiting case to guarantee a subsonic flow eliminating the possibility of shocks being formed. Therefore in less severe flows (i.e., lower Mach numbers), the use of four harmonics is probably sufficient to analyze the problem.

Figures 35 and 36 illustrate the growth in the intensity of the fundamental signal at the throat that develops by increasing the density disturbance ρ_I and the mean flow Mach number M_0, respectively. Each case is computed using three harmonics and the last point plotted approximately locates where the problem becomes singular.

Figures 37 and 38 are similar to the two previous figures, but here the reduction in the intensity of the fundamental signal at the duct exit by increasing ρ_I and M_0, respectively, is shown. Input values for these figures are identical to those used to compute the cases in Figs. 35 and 36.

Investigating a number of cases where the derivatives become unbounded indicates that the singularity is due to shock formation. That is, if the input parameters which determine the flow produce a singularity, then these parameters are not consistent for an isentropic solution to the governing equations. In each singular case analyzed (also, these cases will not converge in the iteration scheme) the Mach number exceeds unity at certain values of time. In all of the singular cases, the singularity is encountered downstream of the throat. A particular case is taken for three harmonics and what occurs for a singular case by varying ρ_I is shown in Fig. 39. The density disturbance ρ_I is varied between $.0049 \leq \rho_I \leq .008$ while the mean flow Mach number is held constant, $M_0 = -.4$. For these particular values the problem is singular. Figure 39 shows that as the density disturbance is increased, the singularity occurs farther downstream of the throat. A similar result would be expected by varying the mean flow Mach number. Therefore it appears that ρ_I and M_0 affect the location of the shock and that the shock approaches the duct entrance if either value is increased or both are increased.

In Fig. 40, the Mach number variation with time is plotted for two cases. These curves are periodic in time with period 2π. Each curve is determined using three harmonics and the same mean flow Mach number. For the case $\rho_I = .0049$, a singularity is produced just downstream of the throat and this is where the Mach number is computed ($x = .98851$). As is seen, this Mach number curve exceeds unity in its time variation which is a necessary condition for a shock to appear. In the case where $\rho_I = .0045$ no singularity is encountered and the iteration scheme converges. The Mach number plot for this value is computed at the throat ($x = 1$). Throughout its time variation it is subsonic.

CHAPTER FOUR

Conclusions

Acoustic propagation in nonuniform circular ducts carrying partially choked mean flows is studied using two models. The wave-envelope technique is employed to analyze axisymmetric and spinning mode linear propagation. In the second model a one-dimensional nonlinear analysis is developed since for near sonic flows it is known that nonlinear effects become important. Linearization was performed in the first problem because the number of physical parameters included in the analysis would lead to extreme mathematical and computational complexity if the nonlinear terms were retained.

Computer codes were developed for both theories and results were obtained. The linear analysis investigates the effects of such physical variables as the liner admittance, boundary-layer thickness, acoustic frequency, spinning mode number, and mean Mach number.

Two duct geometries were investigated in the linear analysis: a converging duct and a converging-diverging duct. The numerical results indicate that the diverging portion of the duct can have a strong reflective effect for near sonic flows. For a converging duct it appears that with increasing inlet boundary layer displacement thickness the maximum pressure amplitude increased while the refractive effect of the axial gradients is strongest for axisymmetric disturbances. Also, the largest peak pressure occurrs for axisymmetric disturbances. The presence of a liner reduces the acoustic signal for a converging duct.

In the converging-diverging duct study no general trend was found in the acoustic pressure profiles by varying the boundary-layer thickness or liner admittance for axisymmetric disturbances. The wave-envelope technique is probably more accurate for lined ducts and spinning mode propagation, since in these cases the modes are more cut-off initially and therefore are less likely to cut-on. Hence, they are greatly attenuated in the duct.

A numerical procedure for analysis of nonlinear acoustic propagation through nearly sonic mean flows, which is stable for cases of strong interaction, has been developed. This procedure is a combination of the Adams-PECE integration scheme and the SVD scheme. It does not develop the numerical instability associated with the Runge-Kutta and matrix inversion methods for nearly sonic duct flows. The numerical results show that an impedance condition can be satisfied at the duct exit and a corresponding solution can be obtained. The numerical results confirm that the nonlinearity intensifies the acoustic disturbance in the throat region, reduces the intensity of the fundamental frequency at the duct exit, and increases the reflections. This implies that the mode conversion properties of variable area ducts can refract and focus the acoustic signal to the vicinity of the throat in high subsonic flows. Also the numerical results indicate that a shock develops if certain limits on the input parameters are exceeded.

REFERENCES

1. Greatrex, F. B., "By-Pass Engine Noise," Trans. SAE, Vol. 69, pp. 312-324, 1961.
2. Sobel, J. A. and Welliver, A. D., "Sonic Block Silencing for Axial and Screw-Type Compressors," Noise Control, Vol. 7, No. 5, pp. 9-11, Sept/Oct. 1961.
3. Nayfeh, A. H., Kaiser, J. E. and Shaker, B. S., "A Wave-Envelope Analysis of Sound Propagation in Nonuniform Circular Ducts with Compressible Mean Flows," NASA Contractor Report 3109, 1979.
4. Nayfeh, A. H., Shaker, B. S. and Kaiser, J. E., "Transmission of Sound Through Nonuniform Circular Ducts with Compressible Mean Flows," AIAA Paper 79-0622; AIAA Journal, Vol. 18, No. 5, pp. 515-525, May 1980.
5. Nayfeh, A. H., Kaiser, J. E., and Telionis, D. P., "Acoustics of Aircraft Engine-Duct Systems," AIAA Journal, Vol. 13, pp. 130-153, 1975.
6. Nayfeh, A. H., "Sound Propagation Through Nonuniform Ducts," NASA CP-2001 3, 821-833, November 1-3, 1976.
7. Vaidya, P. G. and Dean, P. D., "State of the Art of Duct Acoustics," AIAA Paper 77-1279, 1977.
8. Baumeister, K. J., "Numerical Techniques in Linear Duct Acoustics--A Status Report," NASA Technical Memorandum 81553, 1980.
9. Powell, A., "Theory of Sound Propagation through Ducts Carrying High-Speed Flows," Journal of the Acoustical Society of America, Vol. 32, pp. 1640-1946, 1960.

10. Davis, S. S. and Johnson, M. L., "Propagation of Plane Waves in a Variable Area Duct Carrying a Compressible Subsonic Flow," presented at the 87th Meeting of the Acoustical Society of America, New York, 1974.

11. Huerre, P. and Karamcheti, K., "Propagation of Sound through a Fluid Moving in a Duct of Varying Area," in Interagency Symposium of University Research in Transportation Noise, Stanford, Vol. II, pp. 397-413, 1973.

12. King, L. S. and Karamcheti, L., "Propagation of Plane Waves in the Flow Through a Variable Area Duct," AIAA Paper 73-1009, 1973.

13. Eisenberg, N. A. and Kao, T. W., "Propagation of Sound Through a Variable-Area Duct with a Steady Compressible Flow," J. Acous. Soc. Am., Vol. 49, pp. 169-175, 1971.

14. Nayfeh, A. H., Telionis, D. P., and Lekoudis, S. G., "Acoustic Propagation in Ducts with Varying Cross Sections and Sheared Mean Flow," AIAA Paper No. 73-1008, 1973.

15. Nayfeh, A. H., Kaiser, J. E., and Telionis, D. P., "Transmission of Sound Through Annular Ducts of Varying Cross Sections," AIAA Journal, Vol. 13, No. 1, pp. 60-65, 1975.

16. Nayfeh, A. H., Kaiser, J. E., "Effect of Compressible Sheared Mean Flow on Sound Transmission Through Variable-Area Plane Ducts," AIAA Paper 75-128, 1975.

17. Nayfeh, A. H., "Acoustic Waves in Ducts with Sinusoidally Perturbed Walls and Mean Flow," Journal of the Acoustical Society of America, Vol. 57, pp. 1036-1039, 1975.

18. Quinn, D. W., "A Finite Difference Method for Computing Sound Propagation in Nonuniform Ducts," AIAA Paper No. 75-130, 1975.

19. Baumeister, K. J. and Rice, E. J., "A Difference Theory for Noise Propagation in an Acoustically Lined Duct with Mean Flow," AIAA Paper 73-1007, 1973.

20. Baumeister, K. H., "Wave Envelope Analysis of Sound Propagation in Ducts with Variable Axial Impedance," Progress in Astronautics and Aeronautics: Aeroacoustics, Vol. 44, edited by I. R. Schwarz, AIAA, New York, pp. 451-474, 1976.

21. Eversman, W., "A Multimodal Solution for the Transmission of Sound in Nonuniform Hard Wall Ducts with High Subsonic Flow," AIAA Paper No. 76-497, 1976.

22. Sigman, R. K., Majjigi, R. K., and Zinn, B. T., "Determination of Turbofan Inlet Acoustics Using Finite Elements," AIAA J., Vol. 16, No. 11, pp. 1139-1145, 1978.

23. Majjigi, R. K., Sigman, R. K., and Zinn, B. T., "Wave Propagation in Ducts Using the Finite Element Method," AIAA Paper No. 79-0659, March 1979.

24. Tag, I. and Lumsdaine, E., "An Efficient Finite Element Technique for Sound Propagation in Axisymmetric Hard Wall Ducts Carrying High Subsonic Mach Number Flows," AIAA Paper, No. 78-1154, July 1978.

25. Quinn, D. W., "A Finite Element Method for Computing Sound Propagation in Ducts Containing Flow," AIAA Paper No. 79-0661, March 1979.

26. Abrahamson, A. L., "A Finite Element Model of Sound Propagation in a Non-uniform Circular Duct Containing Compressible Flow," AIAA Paper 77-1301, 1977.

27. Abrahamson, A. L., "Acoustic Duct Liner Optimization Using Finite Elements," AIAA Paper No. 79-0662, March 1979.

28. Eversman, W., Astley, R. J., and Thanh, V. P., "Transmission in Nonuniform Ducts--A Comparative Evaluation of Finite Element and Weighted Residuals Computational Schemes," AIAA Paper 77-1299, 1977.

29. Astley, R. J., and Eversman, W., "The Application of Finite Element Techniques to Acoustic Transmission in Lined Ducts with Flow," AIAA Paper No. 79-0660, March 1979.

30. Astley, R. J., Walkington, N. J., and Eversman, W., "Transmission in Flow Ducts with Peripherally Varying Linings," AIAA Paper No. 80-1015, June 1980.

31. Nayfeh, A. H., "Intensification and Refraction of Acoustic Signals in Partially-Choked Converging Ducts," Journal of Sound and Vibration, Vol. 73, No. 3, December 1980.

32. Hersh, A. S. and Liu, C. Y., "Sound Propagation in Choked Ducts," NASA CR-135123, 1976.

33. Myers, M. K. and Callegari, A. J., "On the Singular Behavior of Linear Acoustic Theory in Near-Sonic Duct Flows," J. Sound Vib., Vol. 51, No. 4, pp. 517-531, 1977.

34. Callegari, A. J. and Myers, M. K., "Nonlinear Effects on Sound in Nearly Sonic Duct Flows," AIAA Paper 77-1296, 1977.

35. Myers, M. K. and Callegari, A. J., "Transmission of Sound Through High-Subsonic Flows in Non-Uniform Ducts," AIAA Paper 78-1155, 1978.

36. Callegari, A. J. and Myers, M. K., "Sound Transmission in Ducts Containing Nearly Choked Flows," AIAA Paper 79-0623, 1979.

37. Myers, M. K. and Callegari, A. J., "Acoustic Shocks in Nearly Choked Duct Flows," AIAA Paper 80-1019, 1980.

38. Nayfeh, A. H., Shaker, B. S., and Kaiser, J. E., "Computation of Nonlinear One-Dimensional Waves in Near-Sonic Flows," AIAA J., Vol. 16, pp. 1154-1159, 1978.

39. Schlicting, H., Boundary Layer Theory, 6th Ed., McGraw-Hill, New York, pp. 61-254, 1968.

40. Zorumski, W. E., "Acoustic Theory of Axisymmetric Multisectioned Ducts", NASA TR R-419, May 1974.

41. Nayfeh, A. H., Introduction to Perturbation Techniques, Wiley-Interscience, Chap. 15, 1981.

42. Zorumski, W. E., and Mason, J. P., "Multiple Eigenvalues of Sound Absorbing Circular and Annular Ducts," J. Acoust. Soc. Am., Vol. 55, No. 6, pp. 1158-1165, 1974.

43. Brown, K. M., and Dennis, J. E., "Derivative Free Analogues of the Levenberg-Marquardt and Gauss Algorithms for Nonlinear Least Squares Approximations," Numer. Math, Vol. 18, pp. 289-297, 1972.

44. Garbow, B. S., Hillstrom, K. E., and More, J. J., MINPACK Documentation, Argonne National Lab, Argonne, IL, 1979.

45. Kaiser, J. and Nayfeh, A. H., "A Wave-Envelope Technique for Wave Propagation in Nonuniform Ducts," AIAA Journal, Vol. 15, No. 4, pp. 533-537, April 1977.

46. Shampine, L. F. and Gordon, M. K., Computer Solution of Ordinary Differential Equations: The Initial Value Problem, Freeman, San Francisco, 1975.

47. Wilkinson, J. H. and Reinsch, C., Handbook for Automatic Computation, Vol. II, Springer-Verlag, Berlin, 1971.

48. Forsythe, G. E., Malcolm, M. A., and Moler, C. B., Computer Methods for Mathematical Computations, Prentice-Hall, Englewood Cliffs, N.J., 1977.

49. Fulks, W., Advanced Calculus, Wiley, New York, 1961.

50. Gill, P. E., and Murray, W., "Algorithms for the Solution of the Nonlinear Least-Squares Problem," SIAM Numer. Anal., Vol. 15, No. 5, pp. 977-992, October 1978.

51. Bard, Y., "Comparison of Gradient Methods for the Solution of Nonlinear Parameter Estimation Problems," SIAM J. Numer. Anal., Vol. 7, No. 1, pp. 157-186, March 1970.

52. Noble, B. and Daniel, J. W., Applied Linear Algebra, Prentice-Hall, Englewood Cliffs, N. J., 1977.

53. Meirovitch, L., Computational Methods in Structural Dynamics, Sijthoff & Noordhoff, Alphen aan den Rijn, The Netherlands, Chapter 5, 1980.

54. Wilkinson, J., "Global Convergence of Tridiagonal QR Algorithm with Origin Shifts," Lin. Alg. and its Appl. 1, pp. 409-420, 1968.

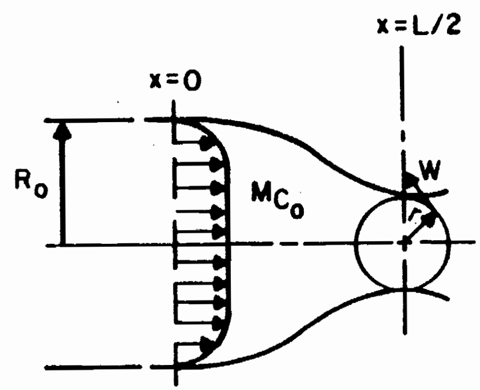

Figure 1 Flow configuration for the converging duct.

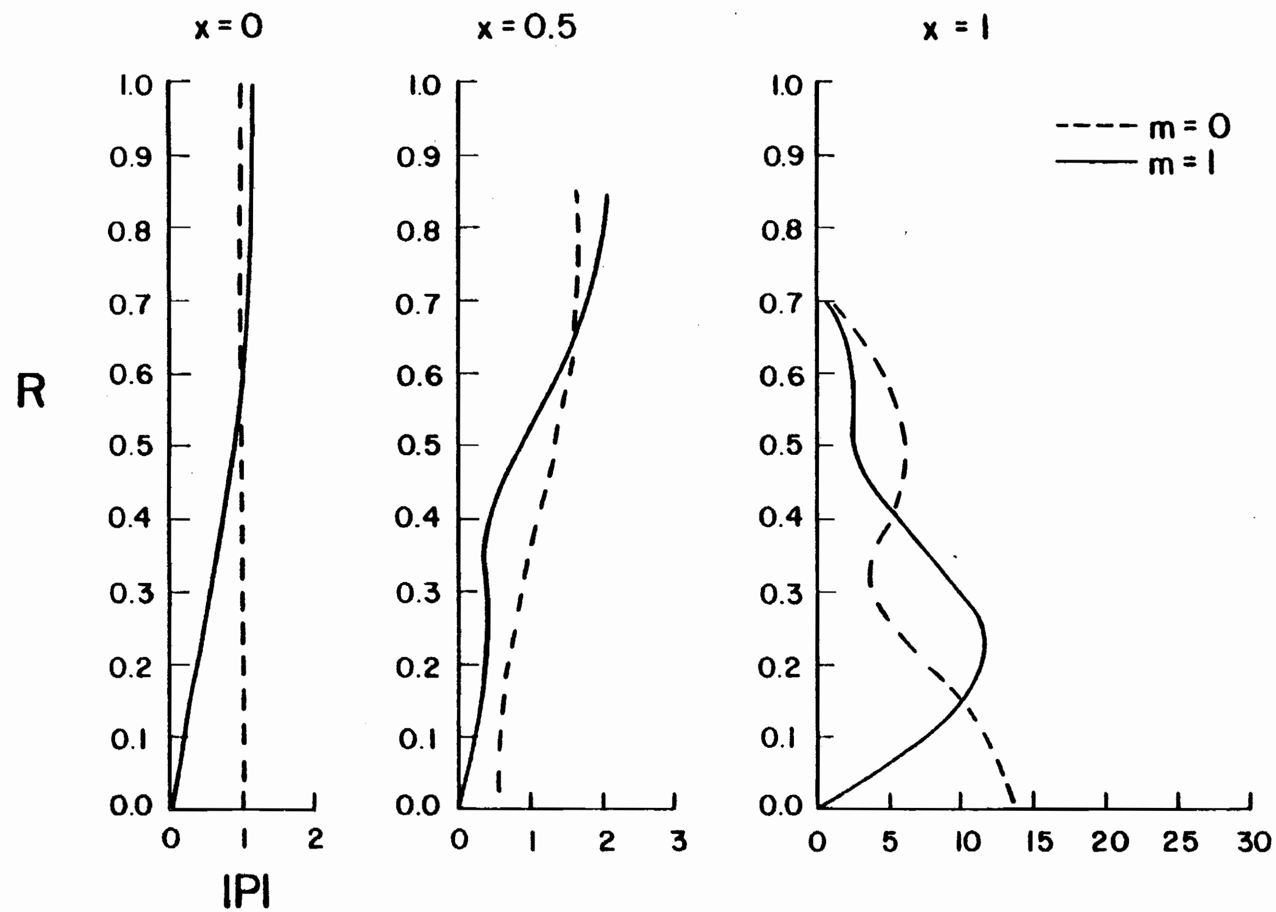

Figure 2 Comparison of the acoustic pressure profiles for m = 0 and 1 when the first upstream mode is incident at $\underset{\cdot}{x} = 0$, $\beta = 0$, $\omega = 9$, $M_t = -.883$, $\delta_0^* = .001$ and $N = 4$.

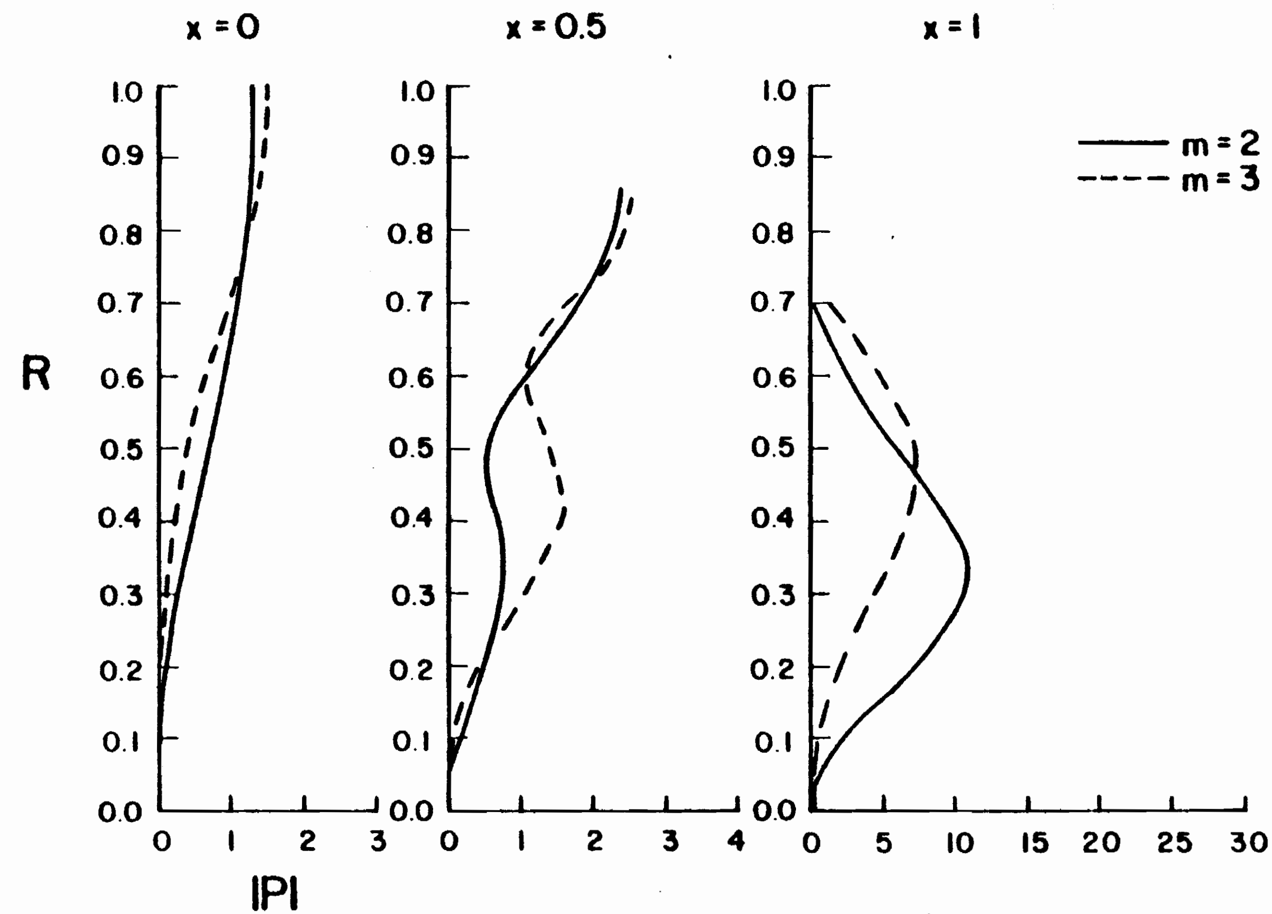

Figure 3 Comparison of the acoustic pressure profiles for m = 2 and 3 where the first upstream mode is incident at x = 0, $\beta = 0$, $\omega = 9$, $M_t = -.883$, $\delta_0^* = .001$ and N = 4.

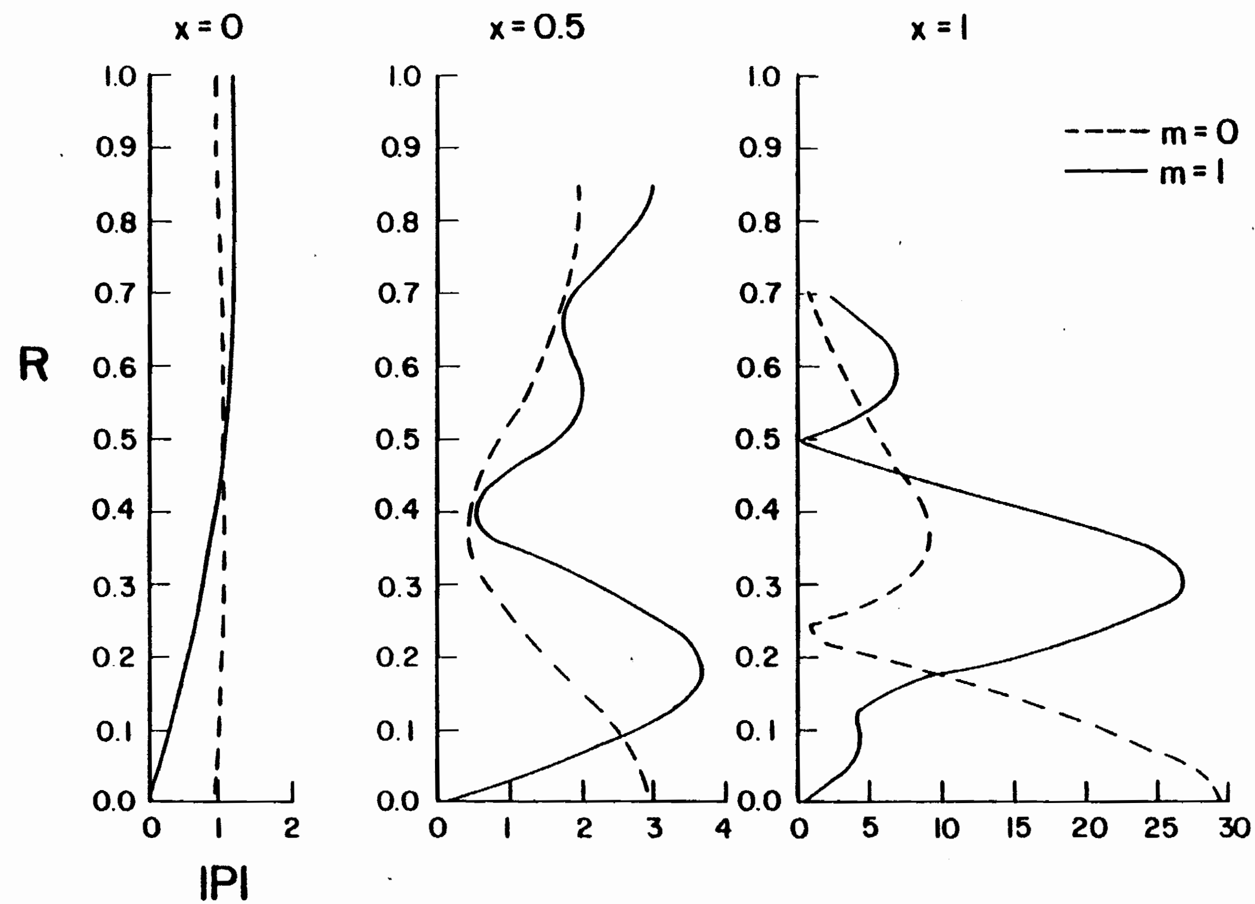

Figure 4 Comparison of the acoustic pressure profiles for m = 0 and 1 where the first upstream mode is incident at $x = 0$, $\beta = 0$, $\omega = 9$, $M_t = -.883$, $\delta_0^* = .001$ and $N = 7$.

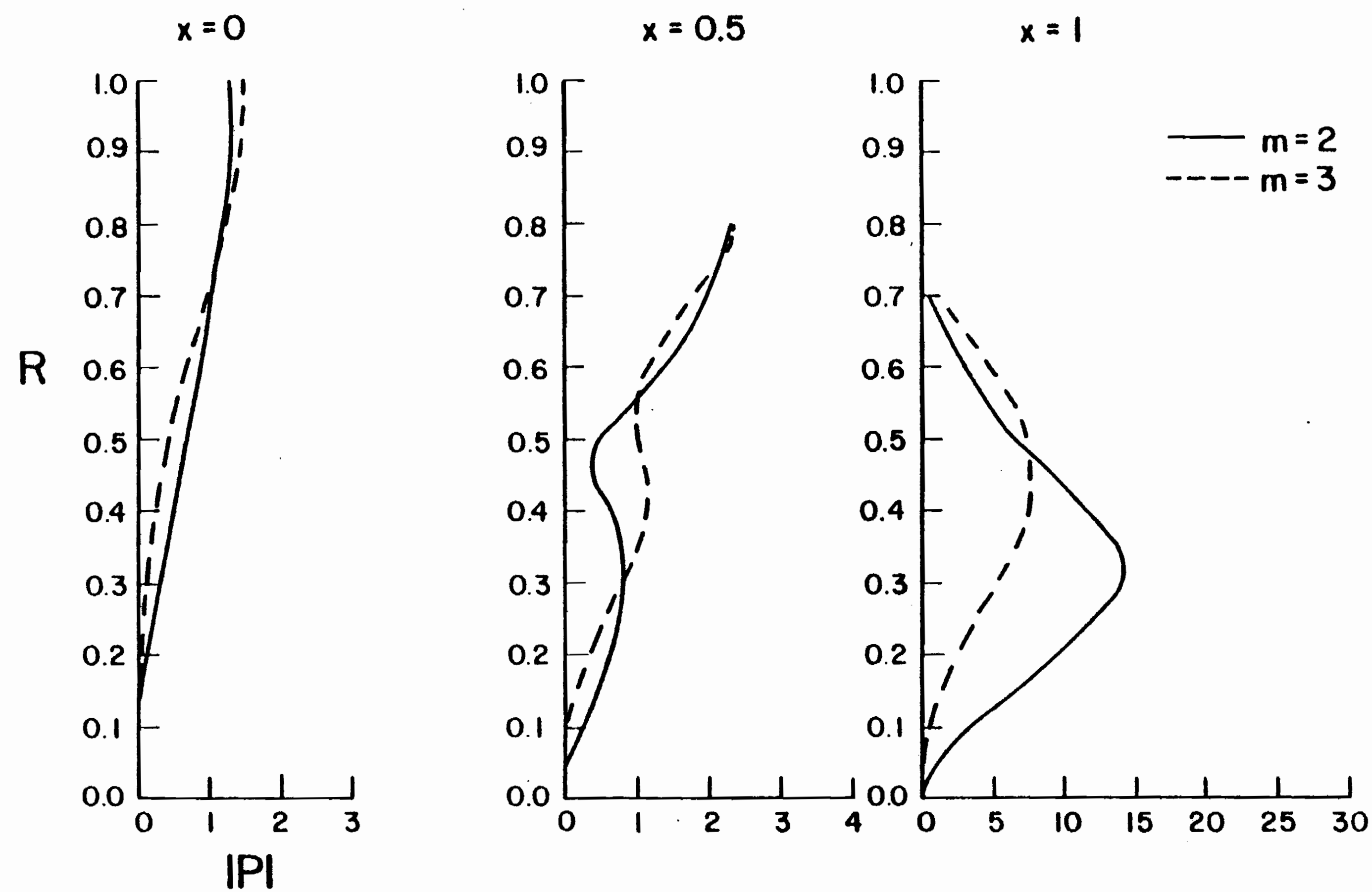

Figure 5 Comparison of the acoustic pressure profiles for m = 2 and 3 when the first upstream mode is incident at x = 0, $\beta = 0$, $\omega = 9$, $M_t = -.883$, $\delta_0^* = .001$ and N = 7.

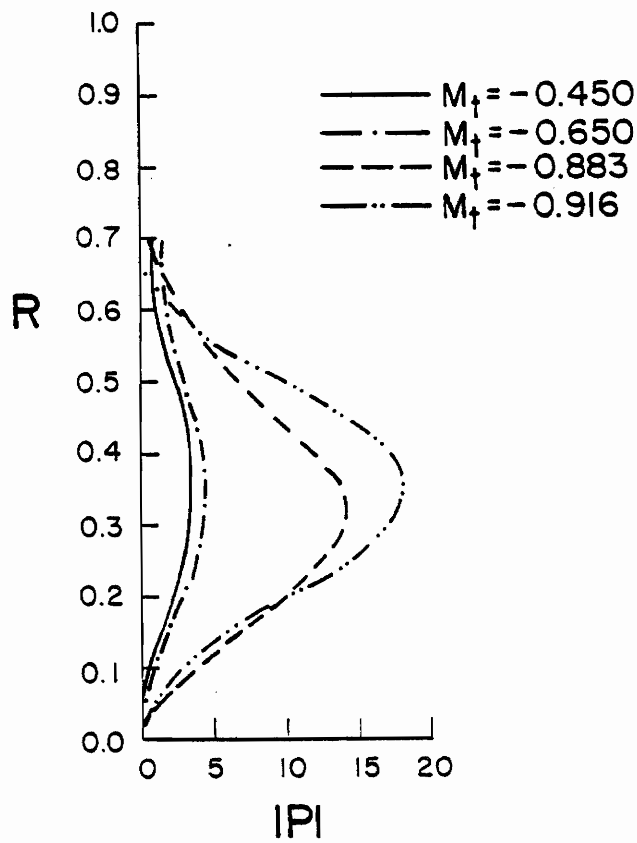

Figure 6 Effect of mean Mach number on the acoustic pressure profile at the throat for m = 2 when the first upstream mode is incident at x = 0, β = 0, ω = 9, δ_0^* = .001 and N = 7.

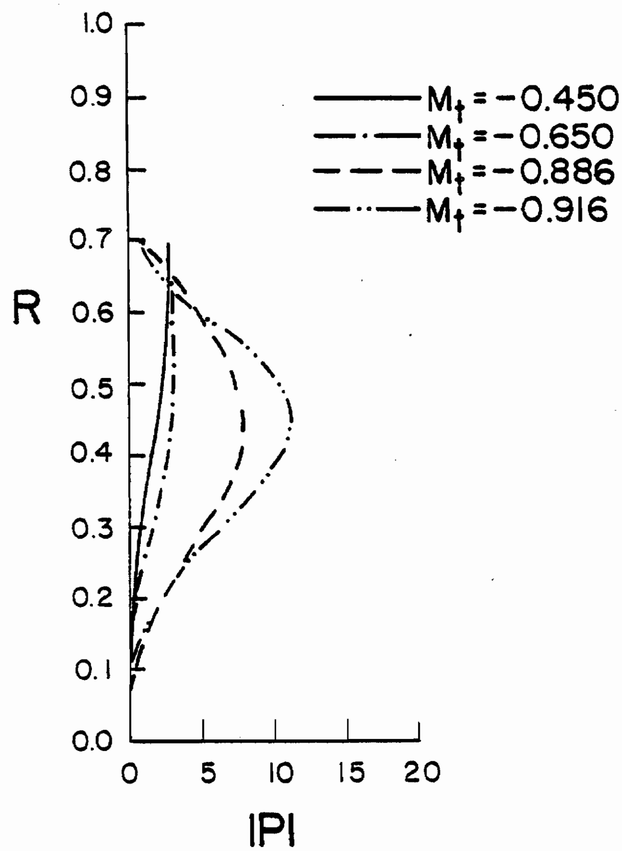

Figure 7 Effect of mean Mach number on the acoustic pressure profile at the throat for m = 3 when the first upstream mode is incident at x = 0, $\beta = 0$, $\omega = 9$, $\delta_0^* = .001$ and N = 7.

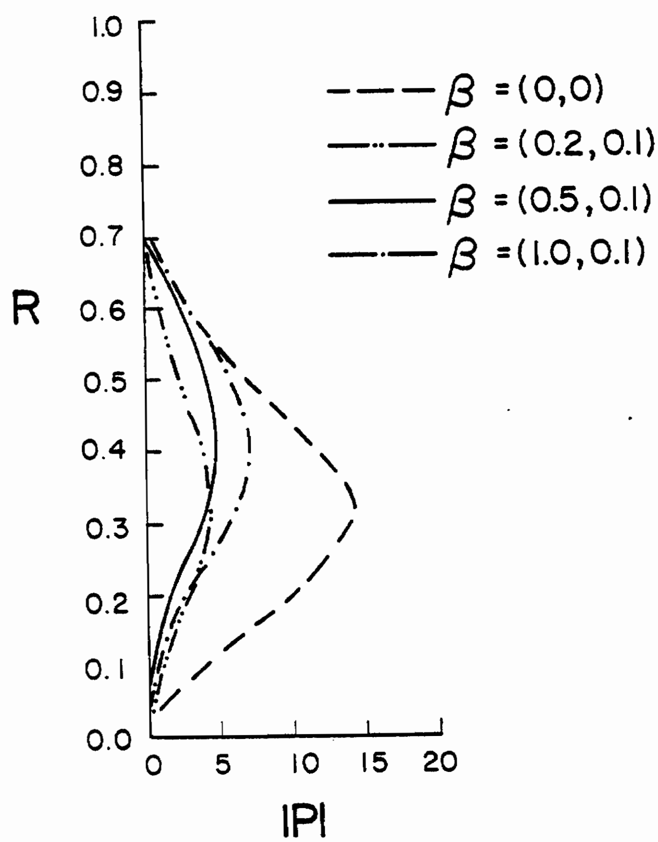

Figure 8 Effect of admittance on the acoustic pressure profile at the throat of a lined duct for m = 2 when the first upstream mode is incident at x = 0, M_t = −.883, ω = 9, δ_0^* = .001 and N = 7.

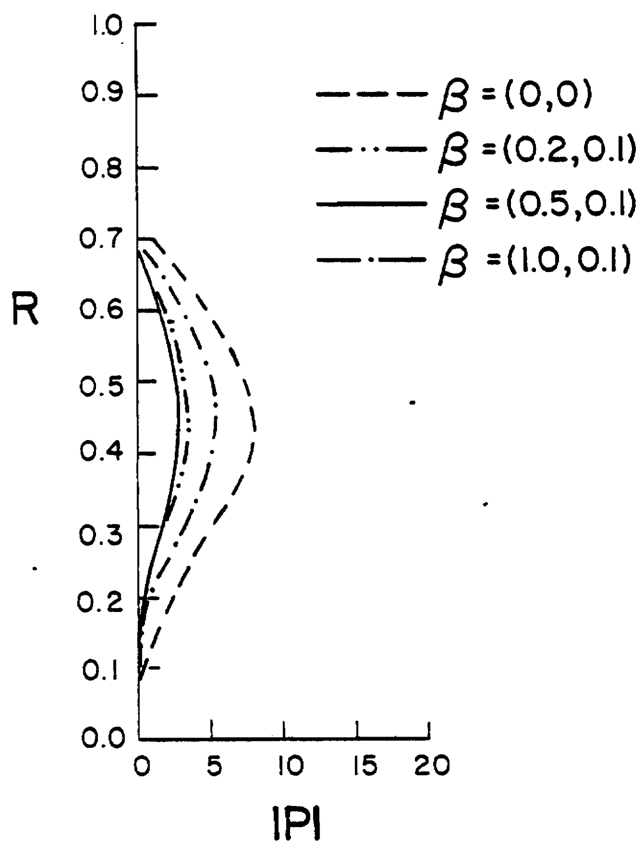

Figure 9 Effect of admittance on the acoustic pressure profile at the throat of a lined duct for m = 3 where the first upstream mode is incident at x = 0, M_t = −.883, ω = 9, δ_0^* = .001 and N = 7.

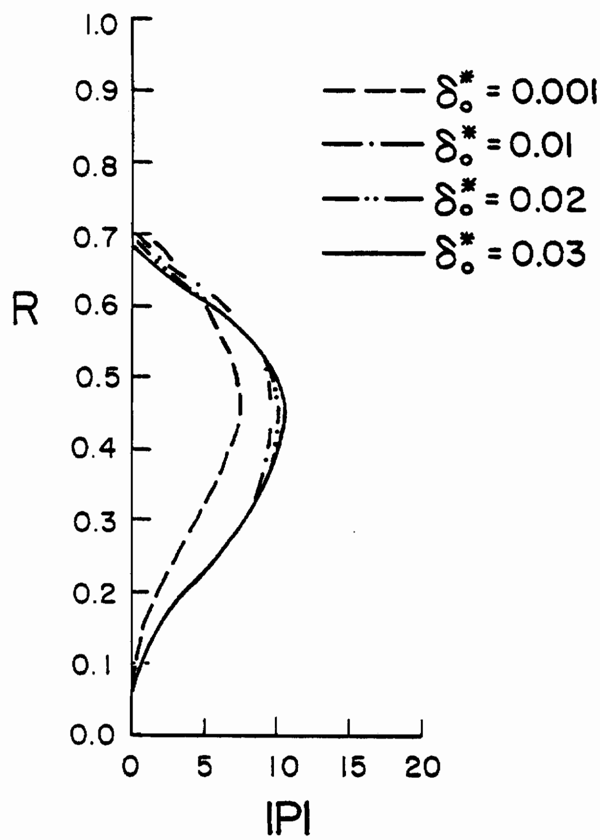

Figure 10 Effect of boundary-layer thickness on the acoustic pressure profile at the throat for m = 3 where the first upstream mode is incident at x = 0, $\beta = 0$, $M_t = -.883$, $\omega = 9$ and N = 4.

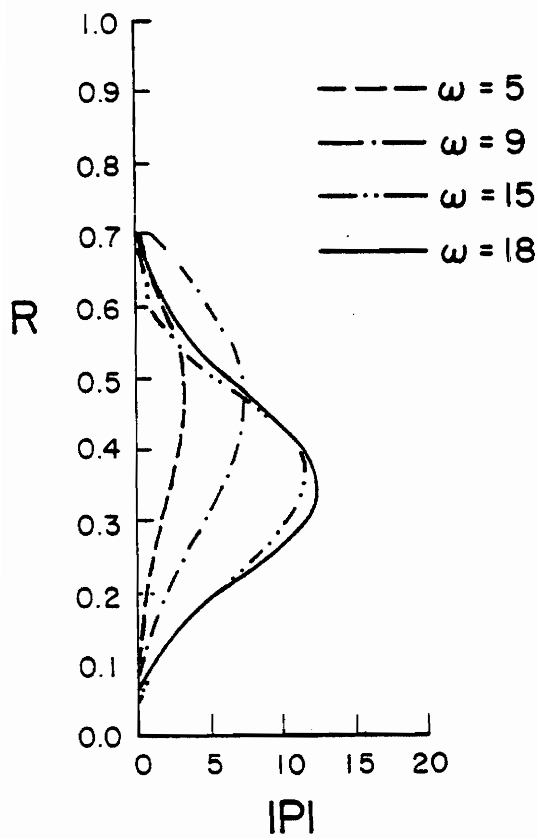

Figure 11 Effect of the acoustic frequency on the acoustic pressure profile at the throat for m = 3 where the first upstream mode is incident at $x = 0$, $\beta = 0$, $M_t = -.883$, $\delta_0^* = .001$ and $N = 4$.

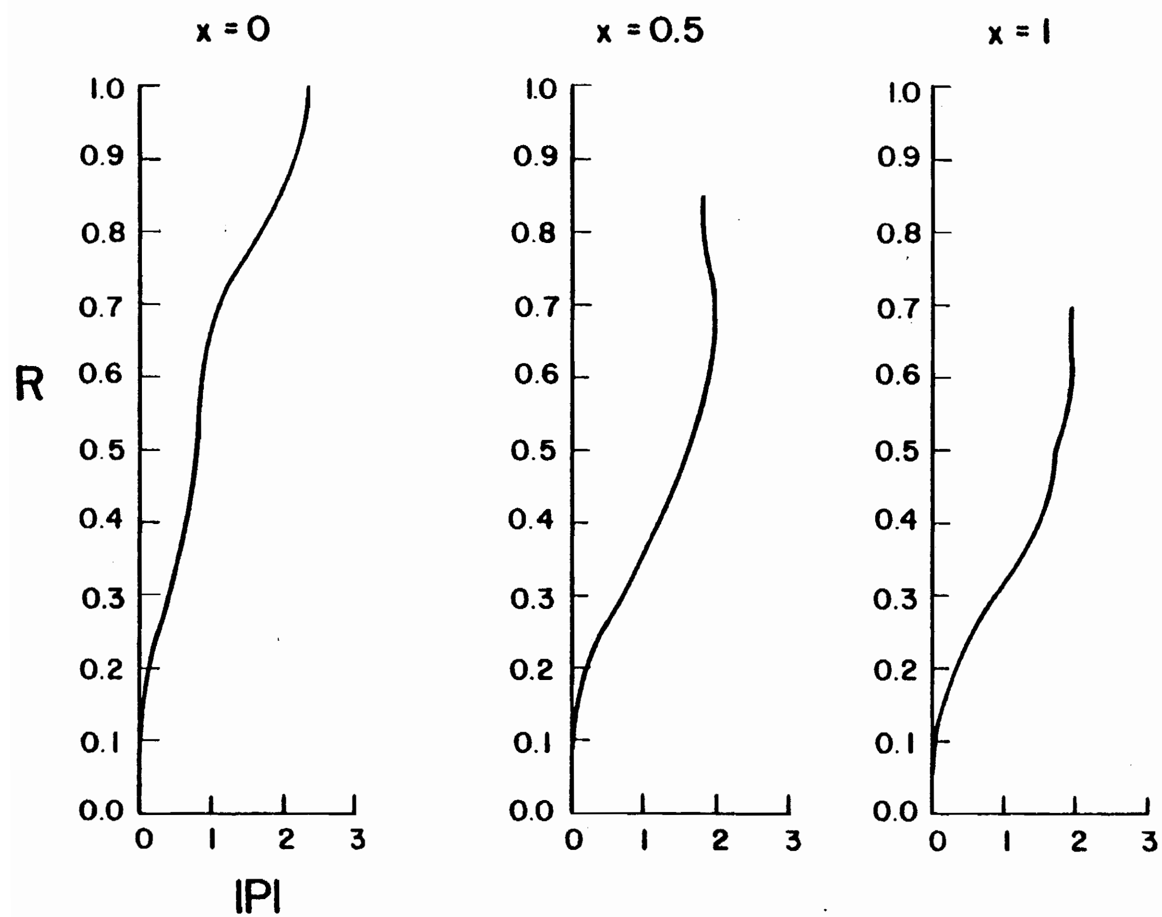

Figure 12 Acoustic pressure profiles for m = 3 when the first downstream mode is incident at x = 1, $\beta = 0$, $M_t = -.883$, $\delta_0^* = .001$ and N = 7.

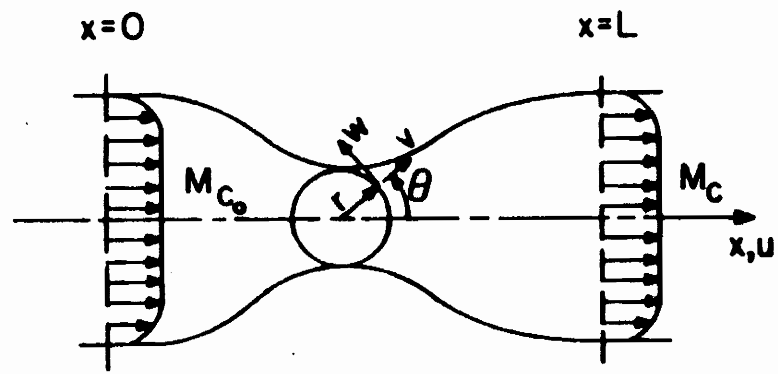

Figure 13 Flow configuration for the converging-diverging duct.

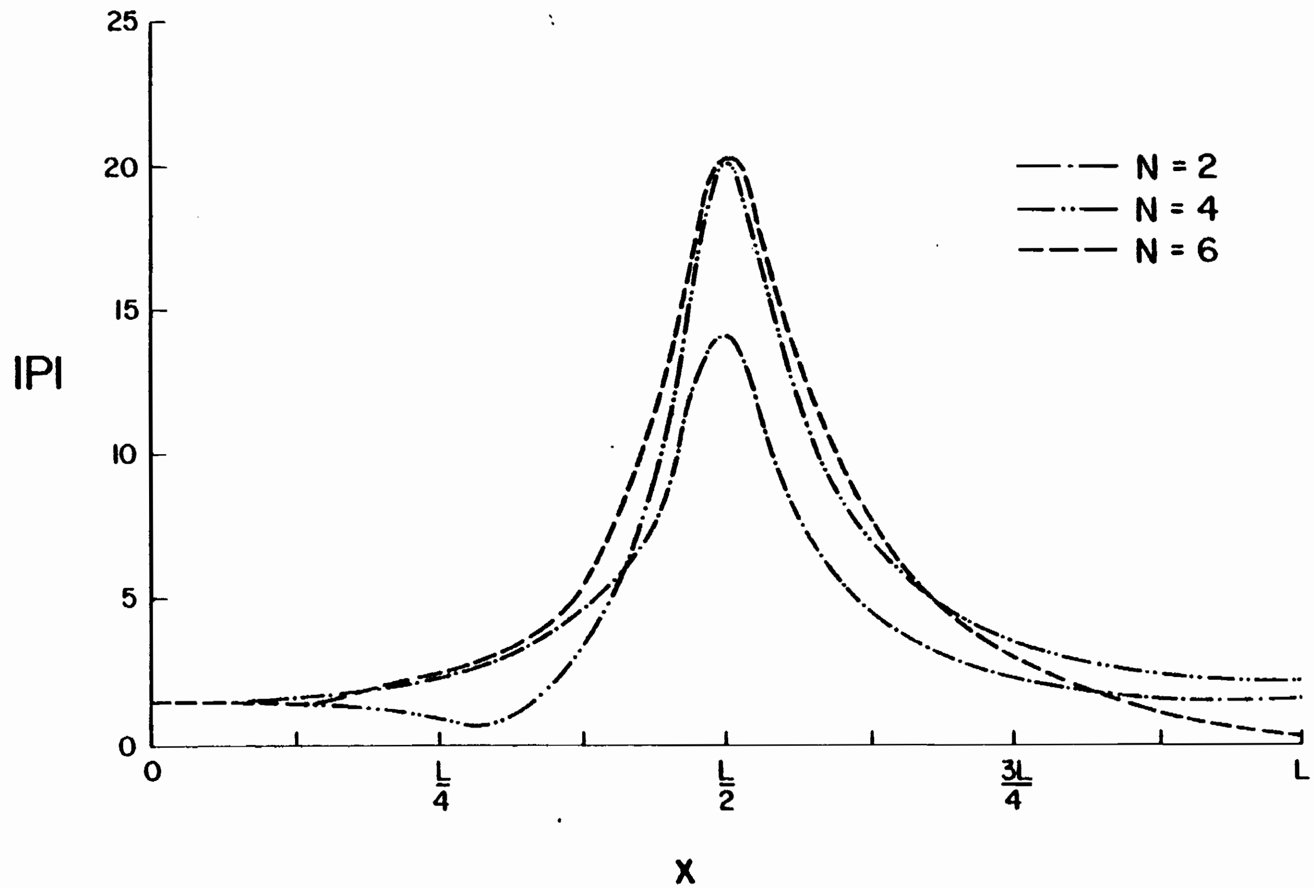

Figure 14 Axial variation of the centerline acoustic pressure for $N = 2$, 4, and 6, $m = 0$, $\beta = 0$, $\omega = 9$, $M_t = -.883$, $\delta_0^* = .02$.

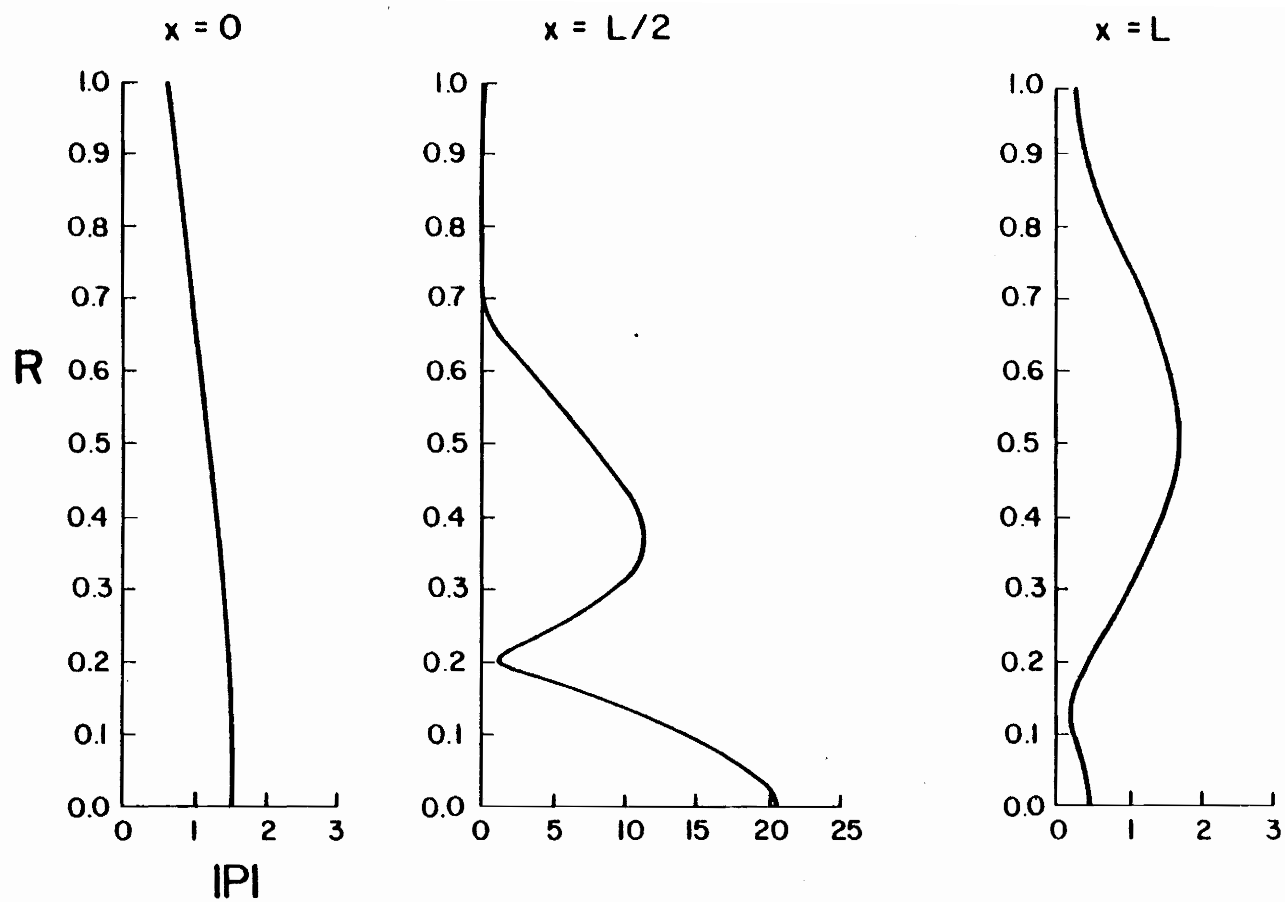

Figure 15 Radial variation of the acoustic pressure for N = 6, m = 0, $\beta = 0$, $\omega = 9$, $M_t = -.883$, $\delta_0^* = .02$.

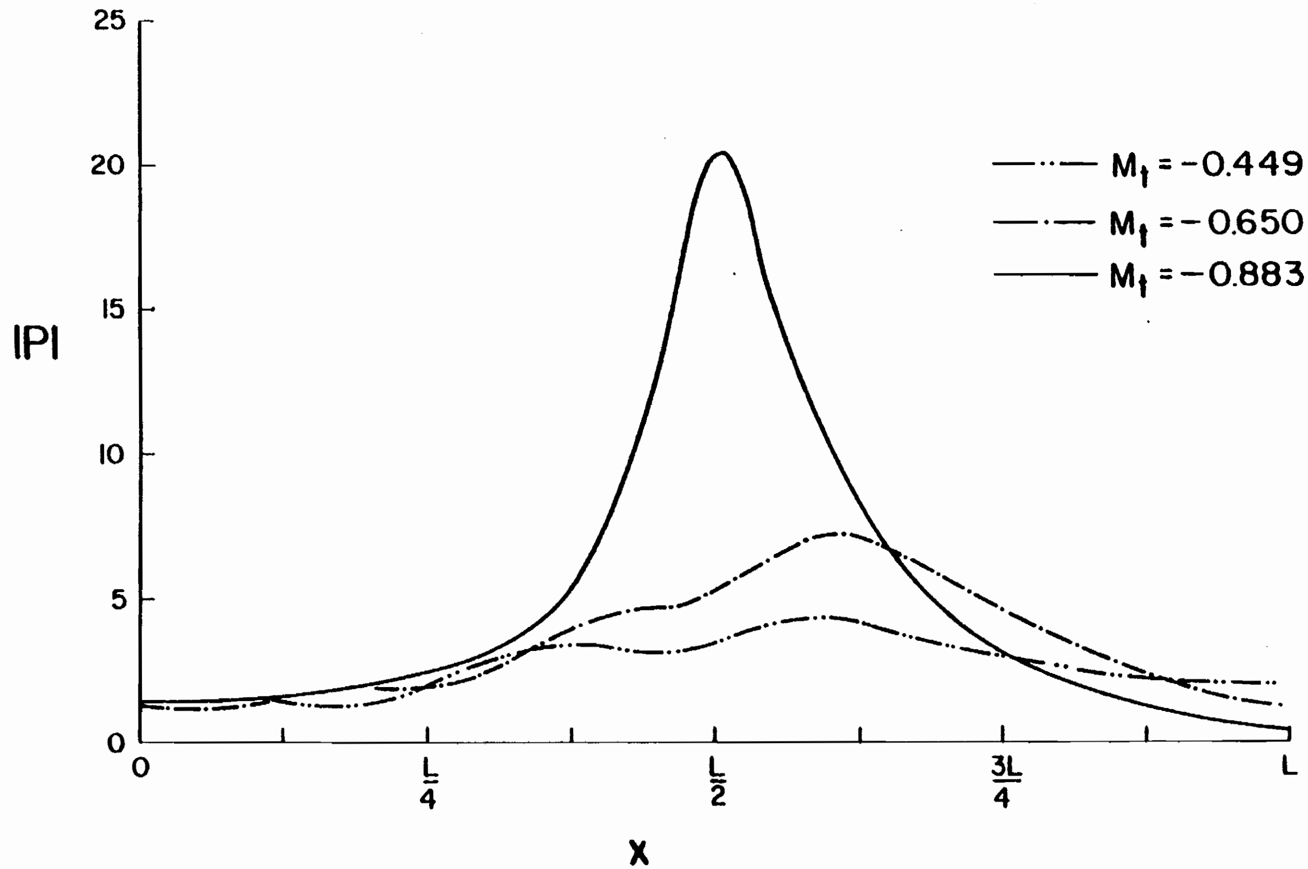

Figure 16 Effect of Mach number on the centerline acoustic pressure, m = 0,

$\beta = 0$, $N = 6$, $\omega = 9$, $\delta_0^* = .02$

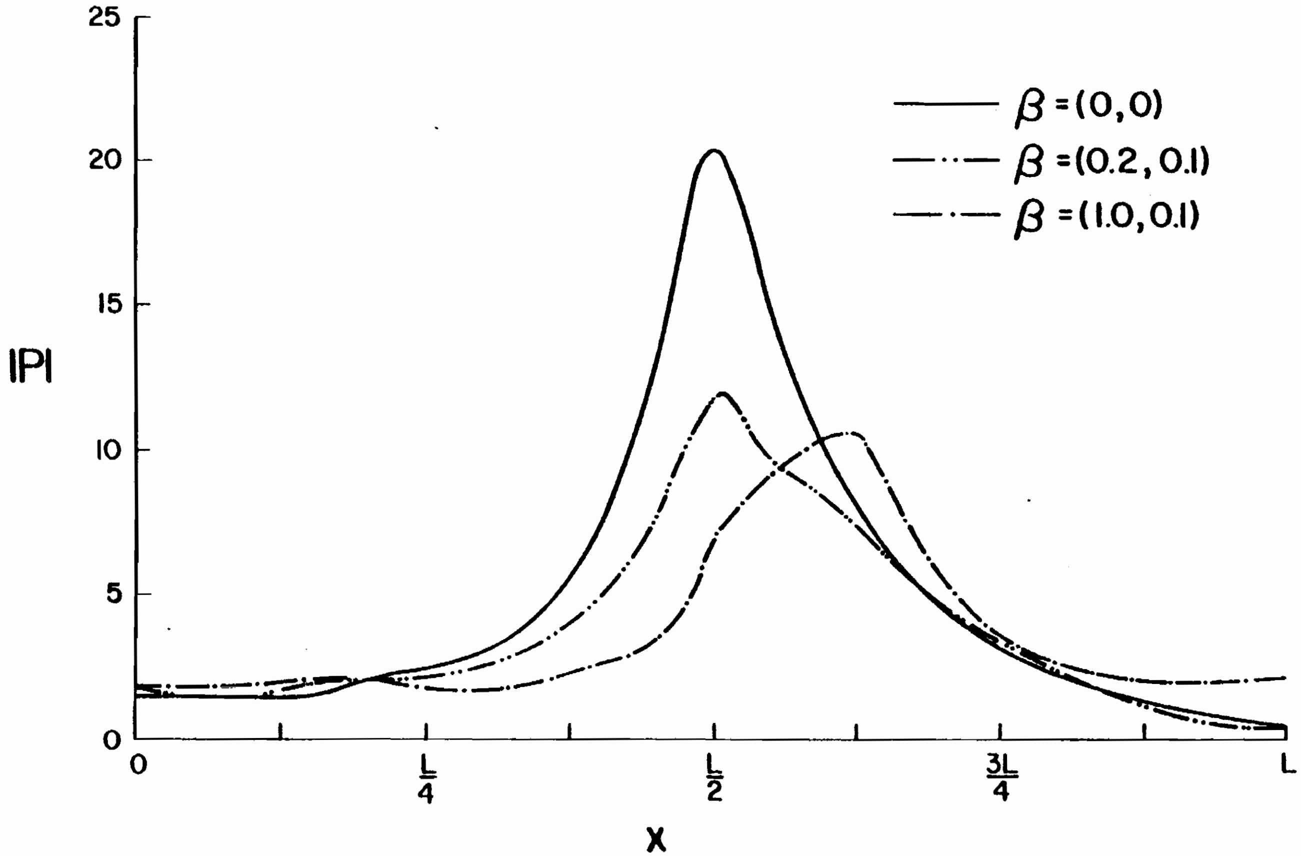

Figure 17 Effect of admittance on the centerline acoustic pressure, m = 0, N = 6, $\omega = 9$, $\delta_0^* = .02$, $M_t = -.883$.

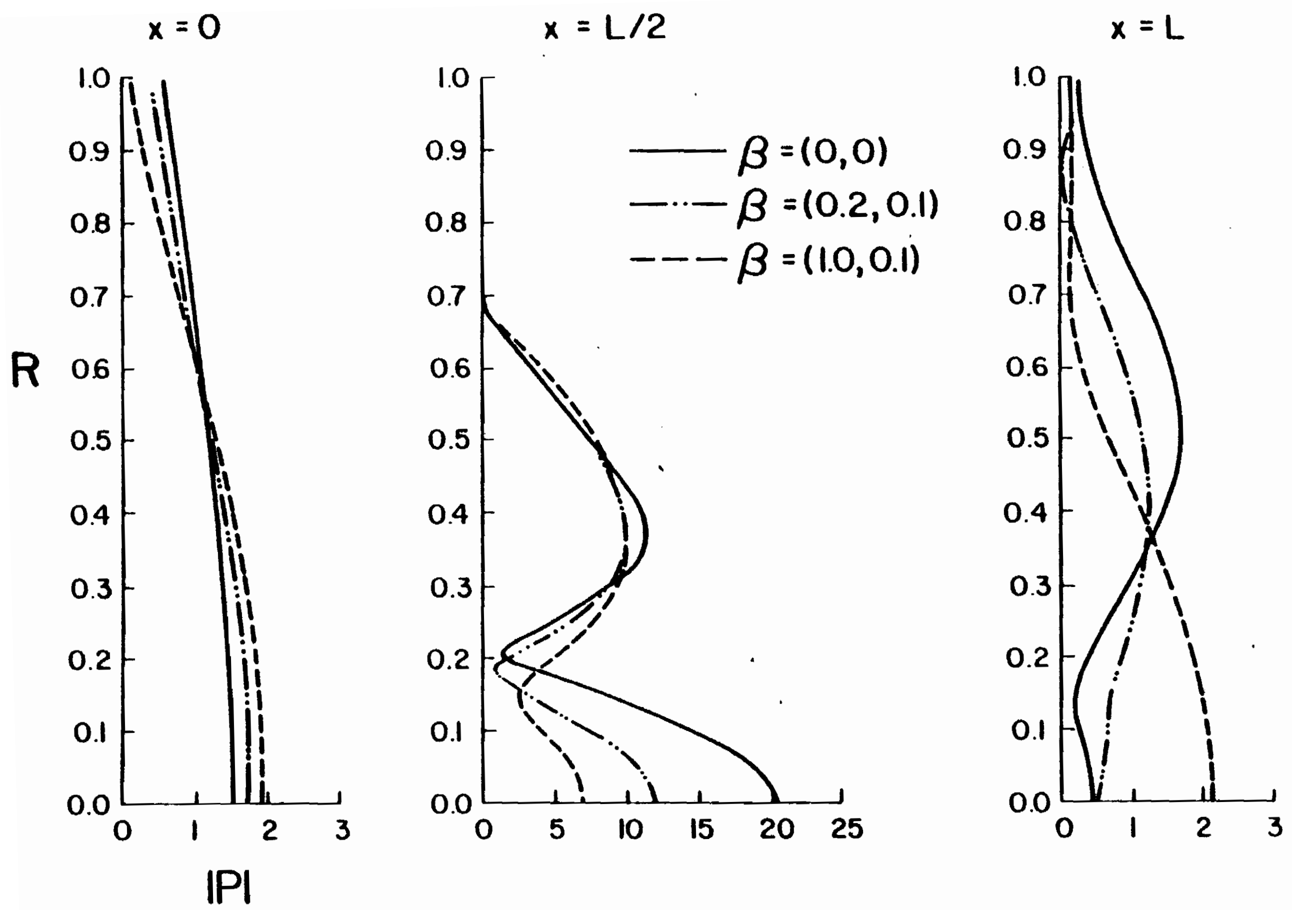

Figure 18 Effect of admittance on the radial acoustic pressure, $m = 0$, $N = 6$, $\omega = 9$, $\delta_0^* = .02$, $M_t = -.883$.

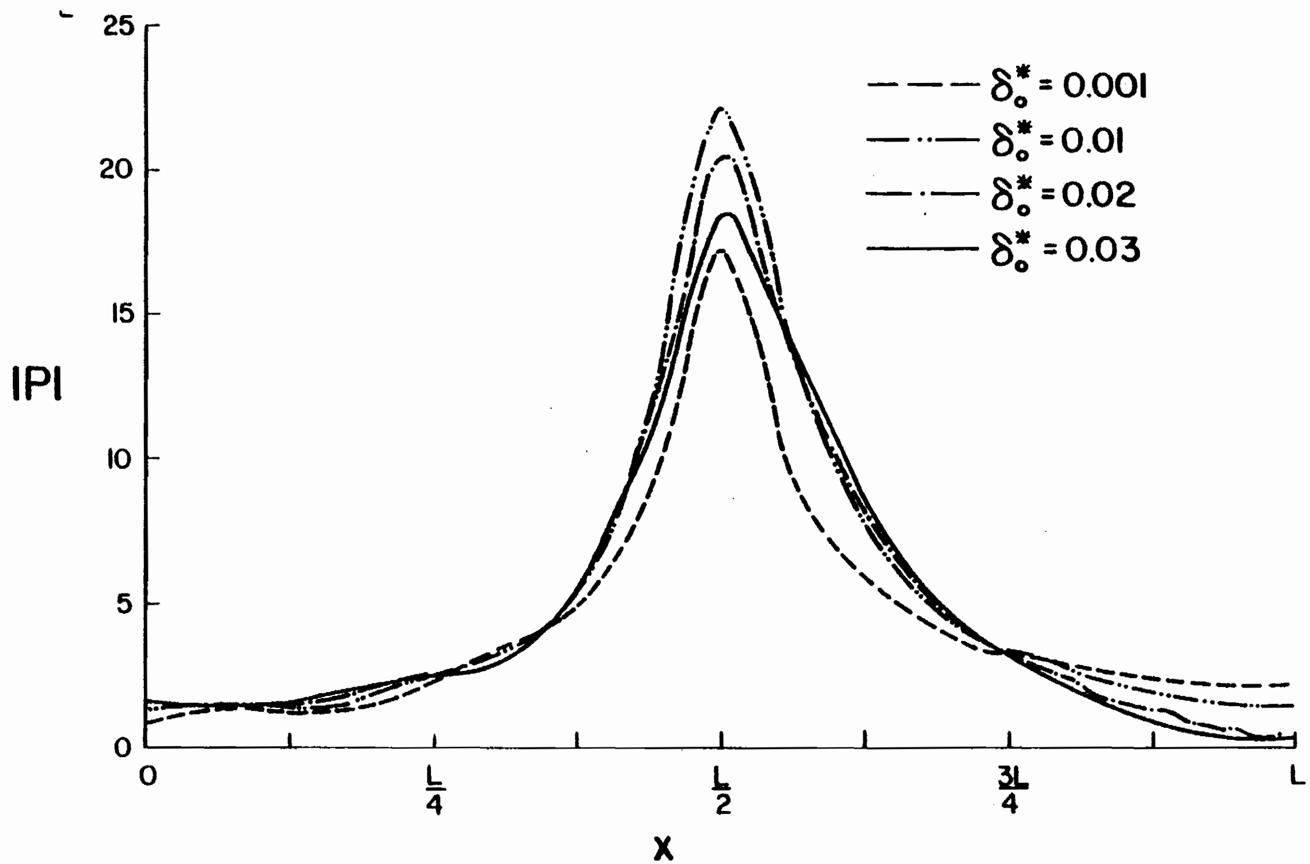

Figure 19 Effect of boundary-layer thickness on centerline acoustic pressure, $m = 0$, $\beta = 0$, $\omega = 9$, $N = 6$, $M_t = -.883$.

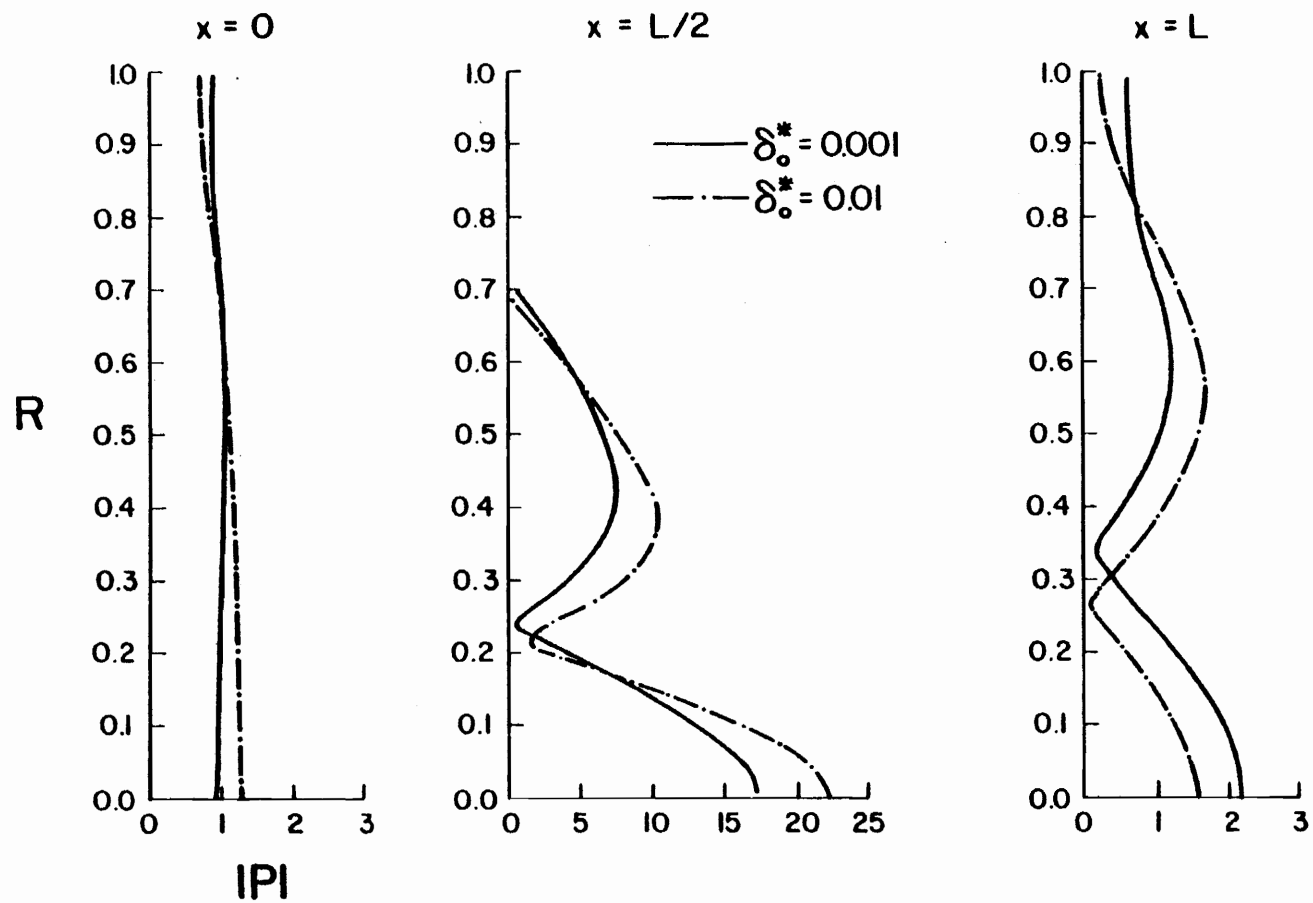

Figure 20 Effect of boundary-layer thickness on radial acoustic pressure, $\delta_0^* = .001, .01$.

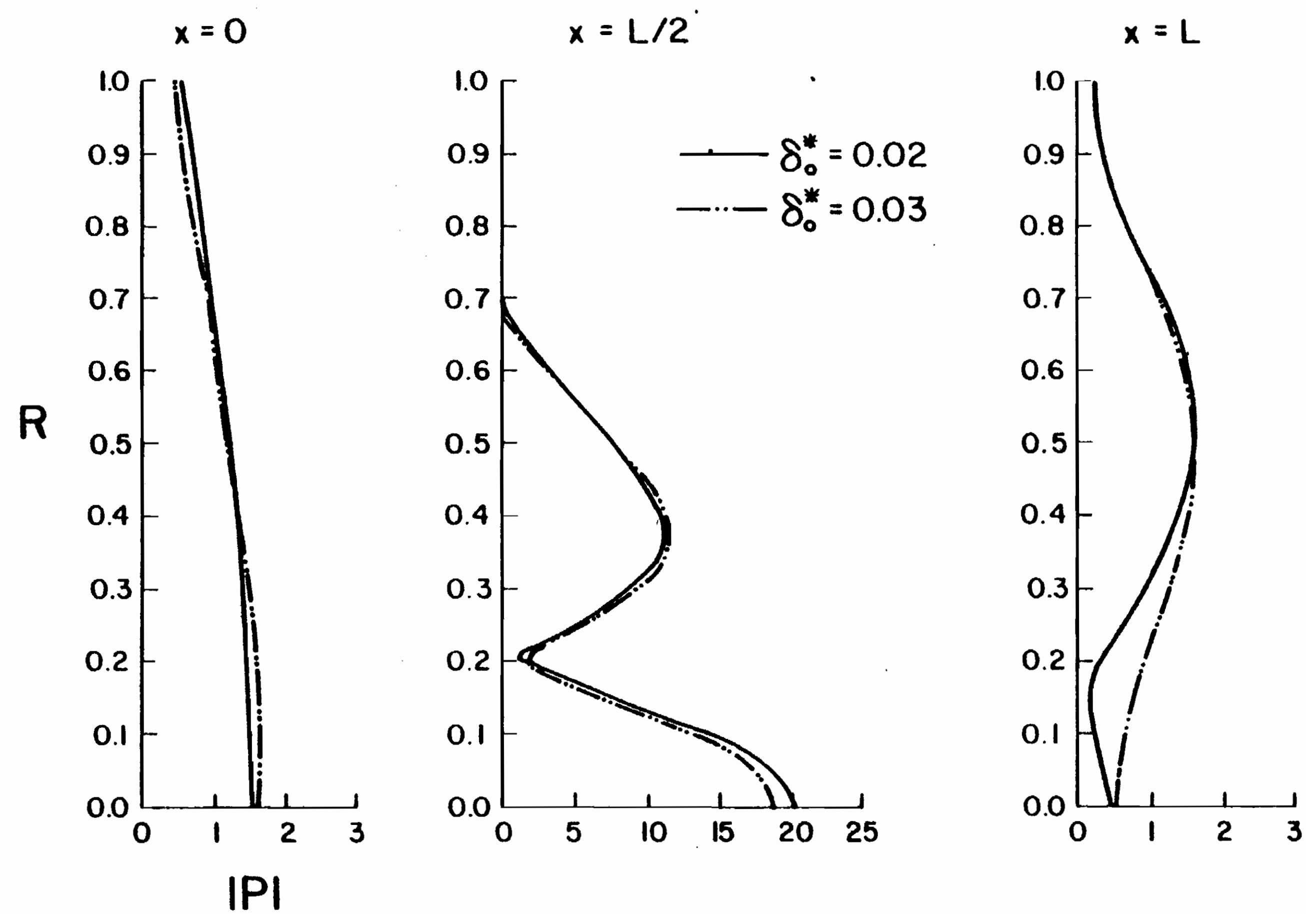

Figure 21 Effect of boundary-layer thickness on radial acoustic pressure, $\delta_0^* = .02, .03$.

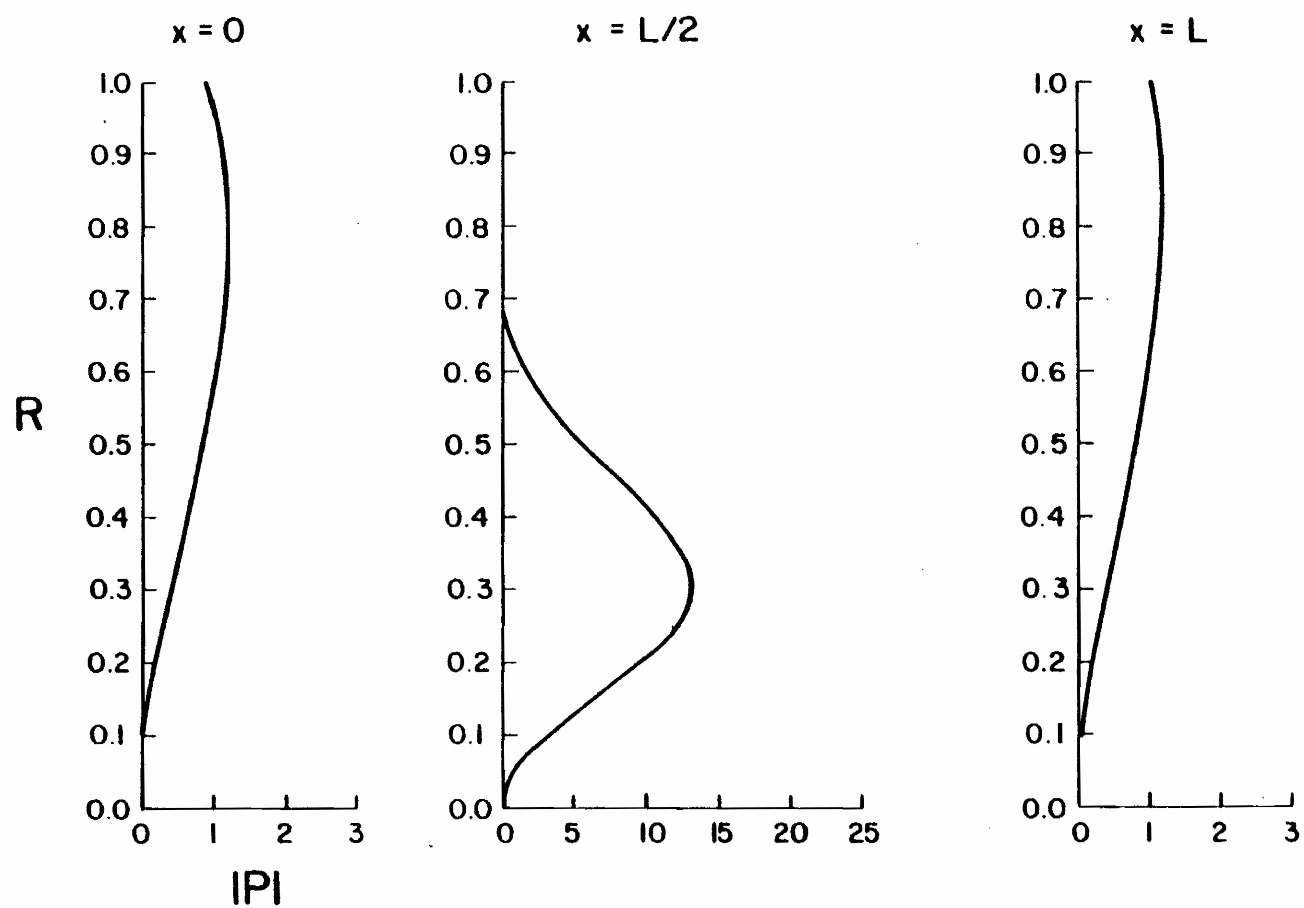

Figure 22 Radial variation of the acoustic pressure, $m = 2$, $\beta = 0$, $M_t = -.883$, $\delta_0^* = .02$, $\omega = 9$, $N = 4$.

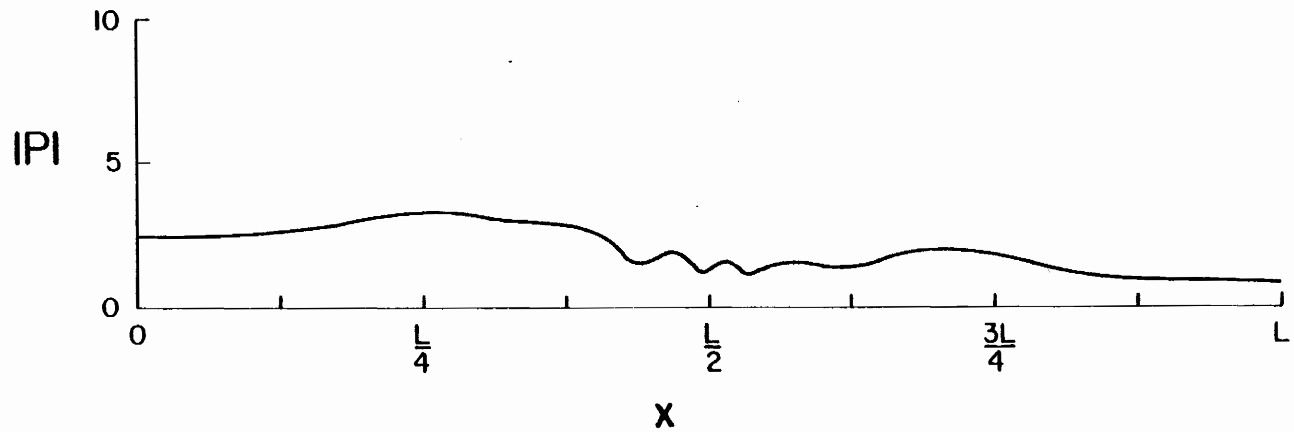

Figure 23 Axial variation of the acoustic pressure for downstream propagation, m = 0, $\beta = 0$, $\omega = 9$, $M_t = -.883$, $\delta_0^* = .02$, N = 6.

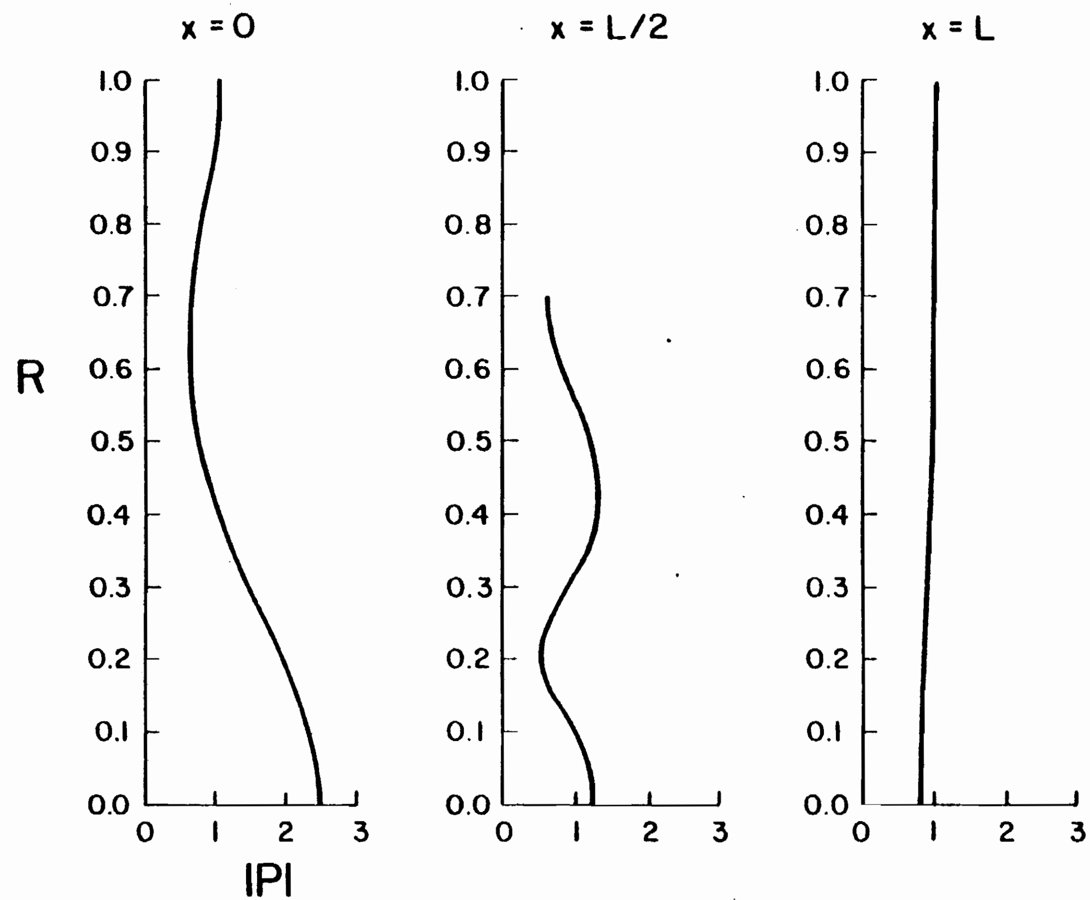

Figure 24 Radial variation of the acoustic pressure for downstream propagation, $m = 0$ $\beta = 0$, $\omega = 9$, $M_t = -.883$, $\delta_0^* = .02$, $N = 6$.

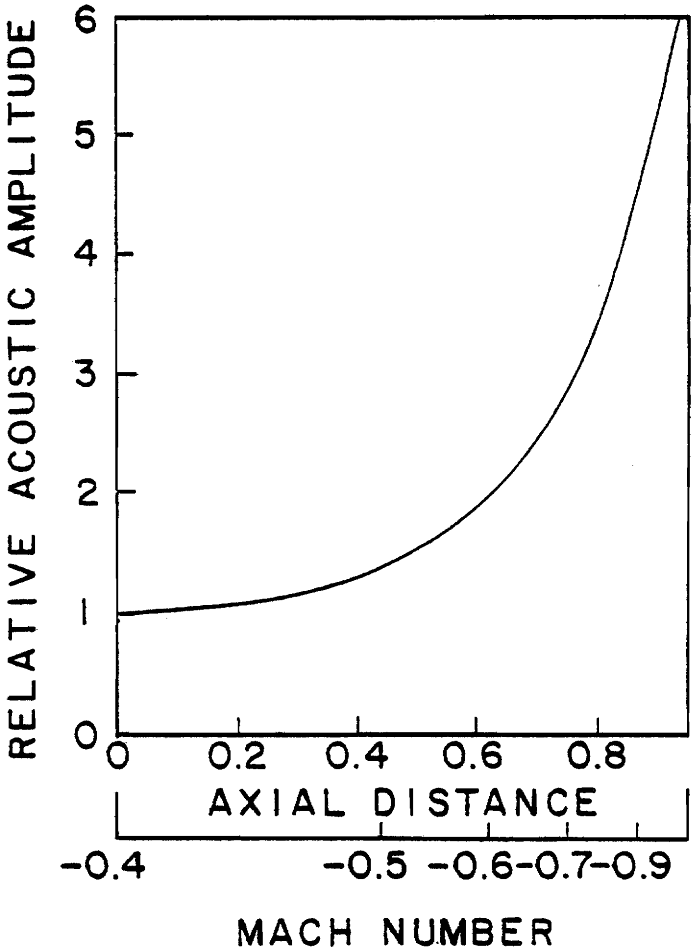

Figure 25 Increase of linear acoustic amplitude with mean-flow Mach number, $\omega = 1$.

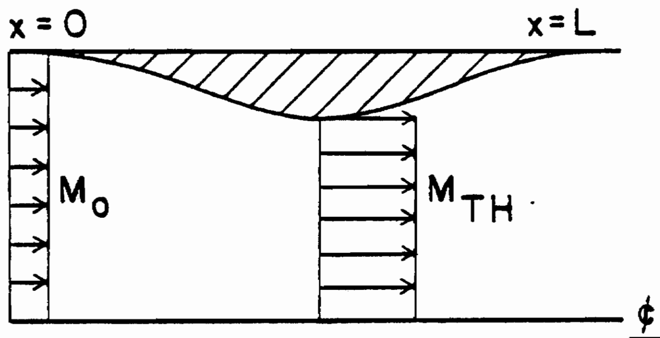

Figure 26 Duct geometry.

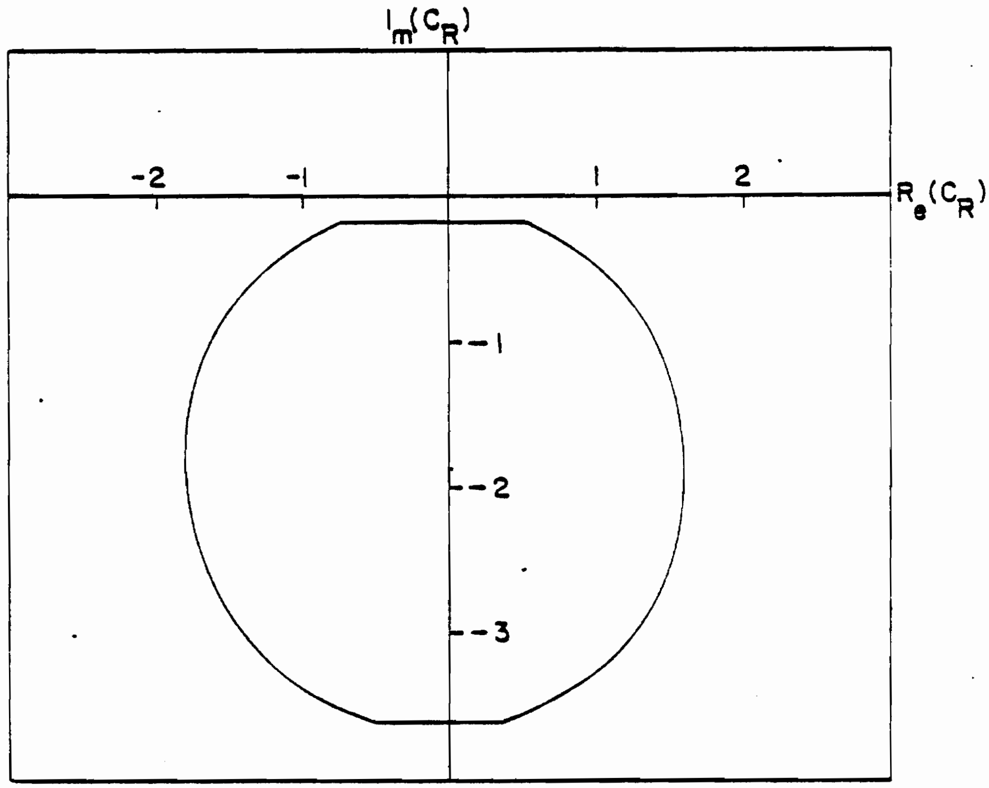

Figure 27 Region of admissible reflection coefficients using two harmonics and one reflection coefficient, $\omega = 1$, $\rho_I = .005$, $M_0 = -.4$.

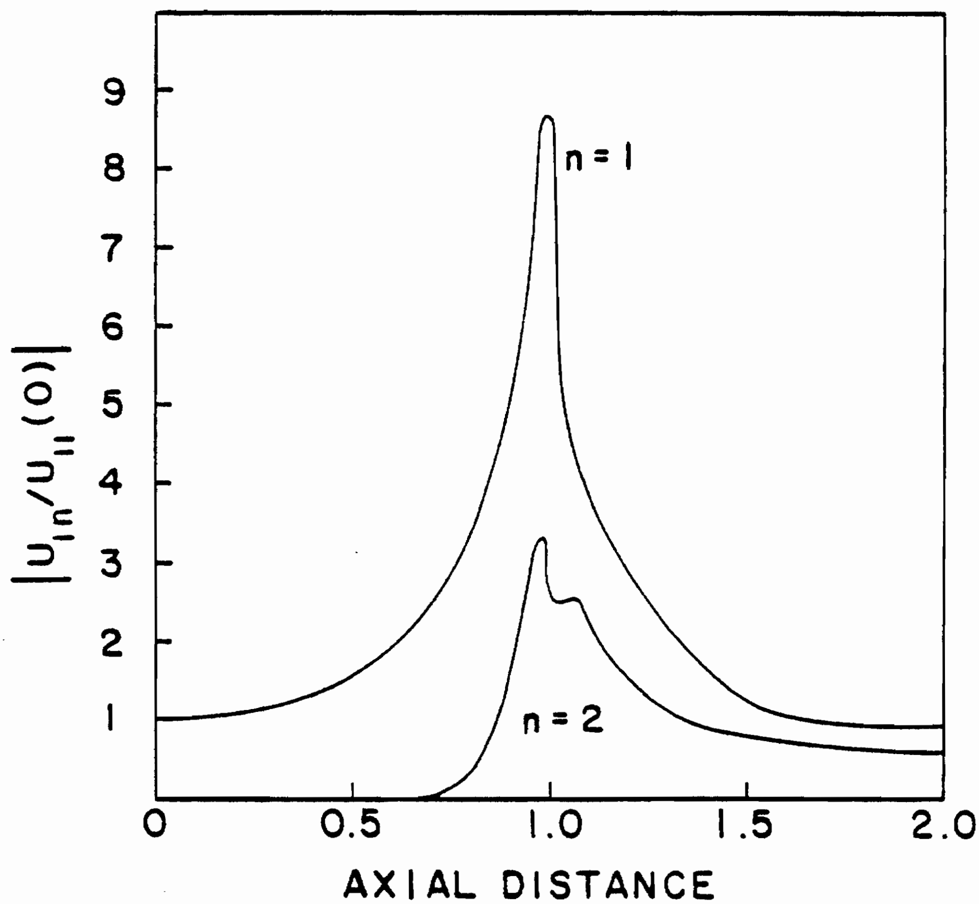

Figure 28 Development of harmonic amplitudes (Runge-Kutta method), ω = 1, M_0 = -.4, ρ_I = .005, N = 2, C_R = 0.

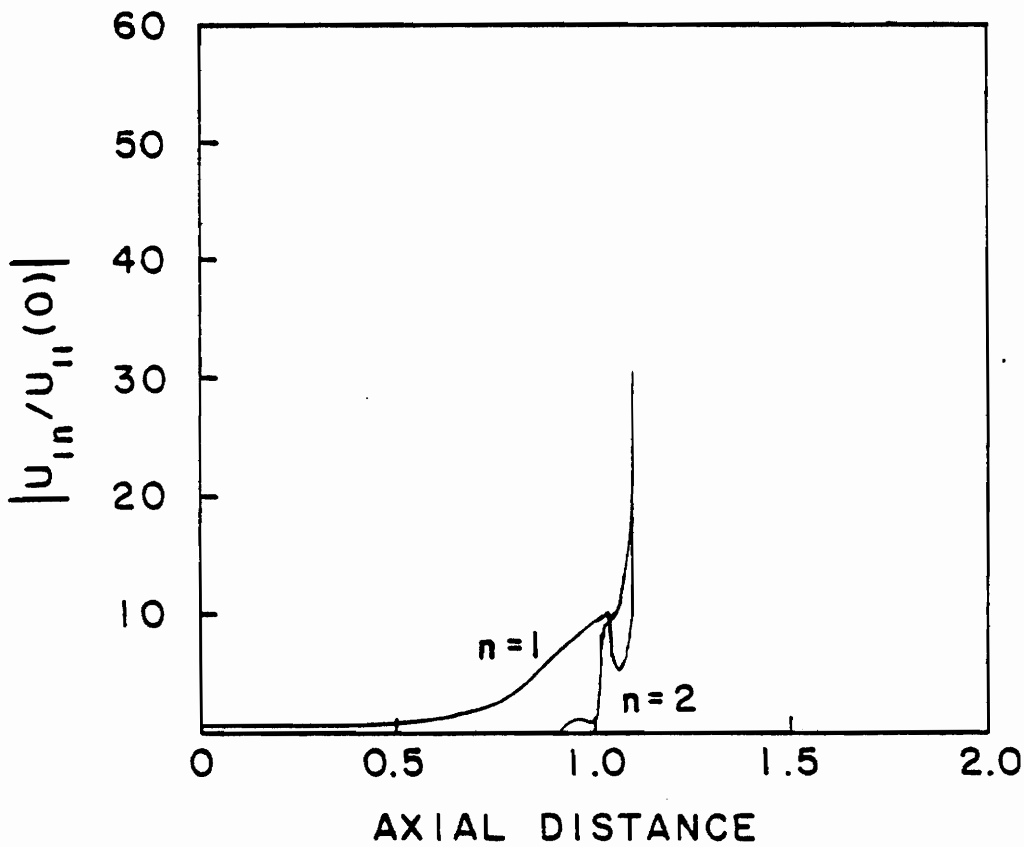

Figure 29 Development of harmonic amplitudes (Runge-Kutta method), $\omega = 1$, $M_0 = -.4$, $\rho_I = .005$, $N = 4$, $C_R = 0$.

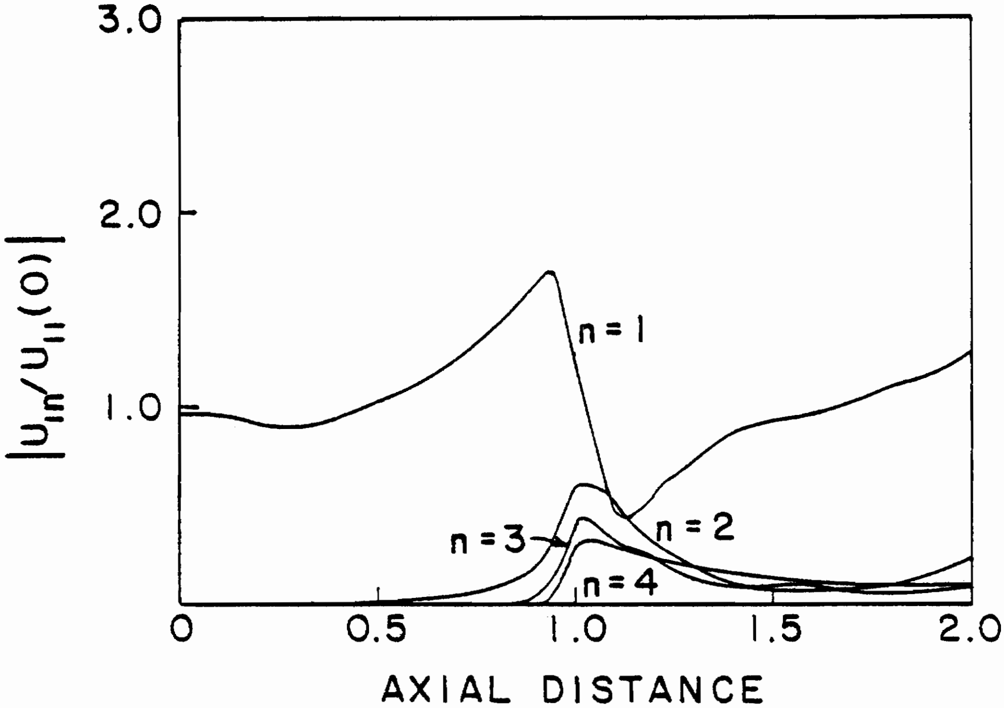

Figure 30 Development of harmonic amplitudes (Adams-PECE and SVD methods), $\omega = 1$, $M_0 = -.4$, $\rho_I = .005$, $N = 4$, $C_r = -.5 - 3.3i$.

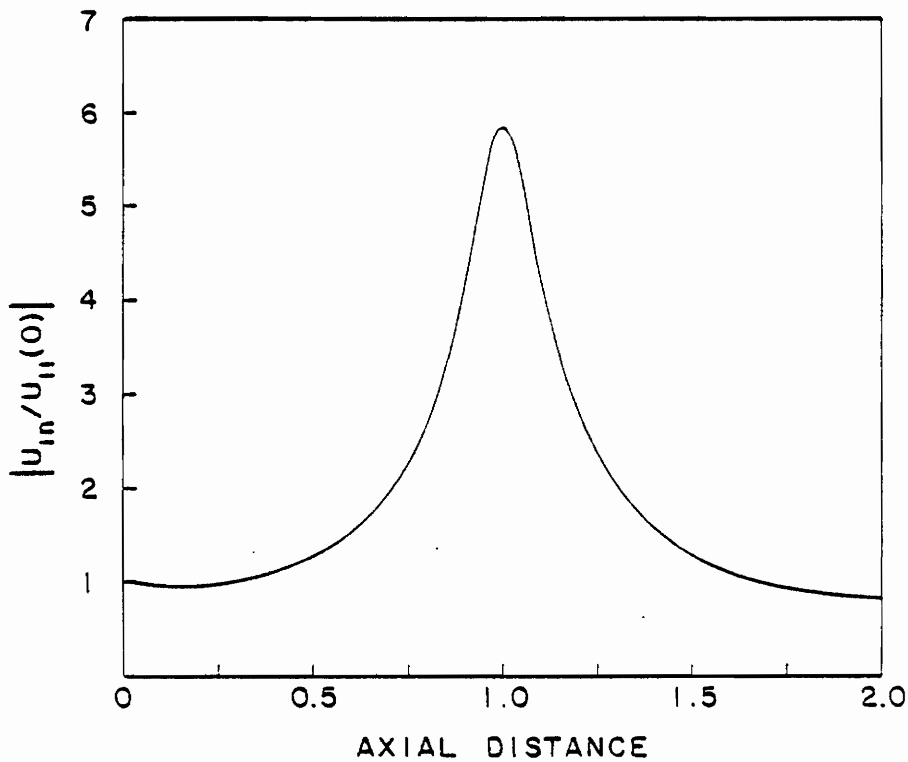

Figure 31 Development of harmonic amplitudes,

$\omega = 1$, $M_0 = -.4$, $\rho_I = .0045$, $N = 1$.

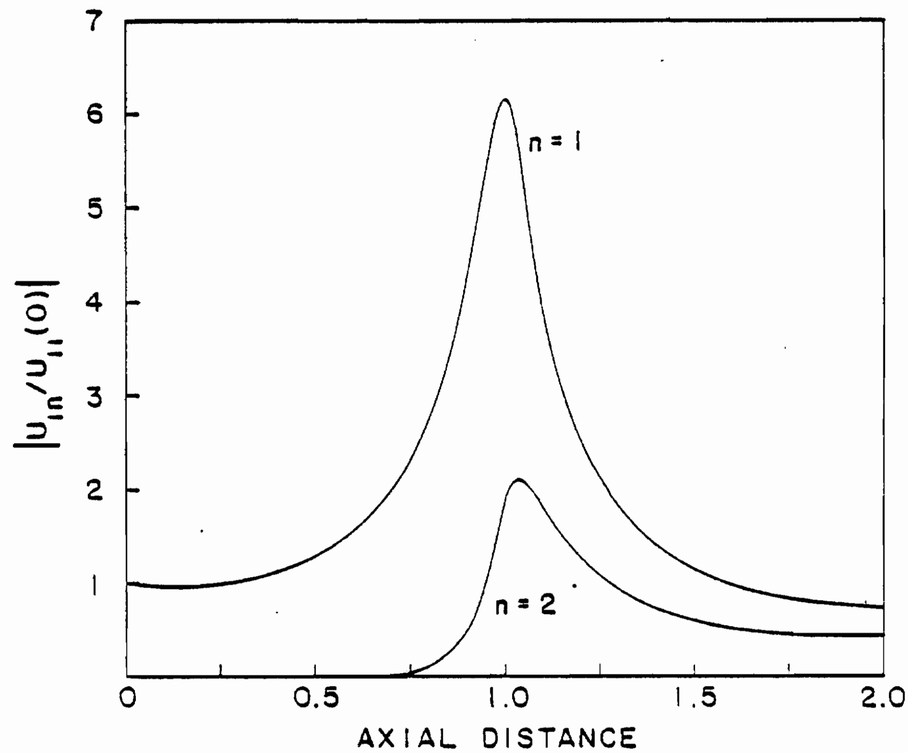

Figure 32 Development of harmonic amplitudes,

$\omega = 1$, $M_0 = -.4$, $\rho_I = .0045$, $N = 2$.

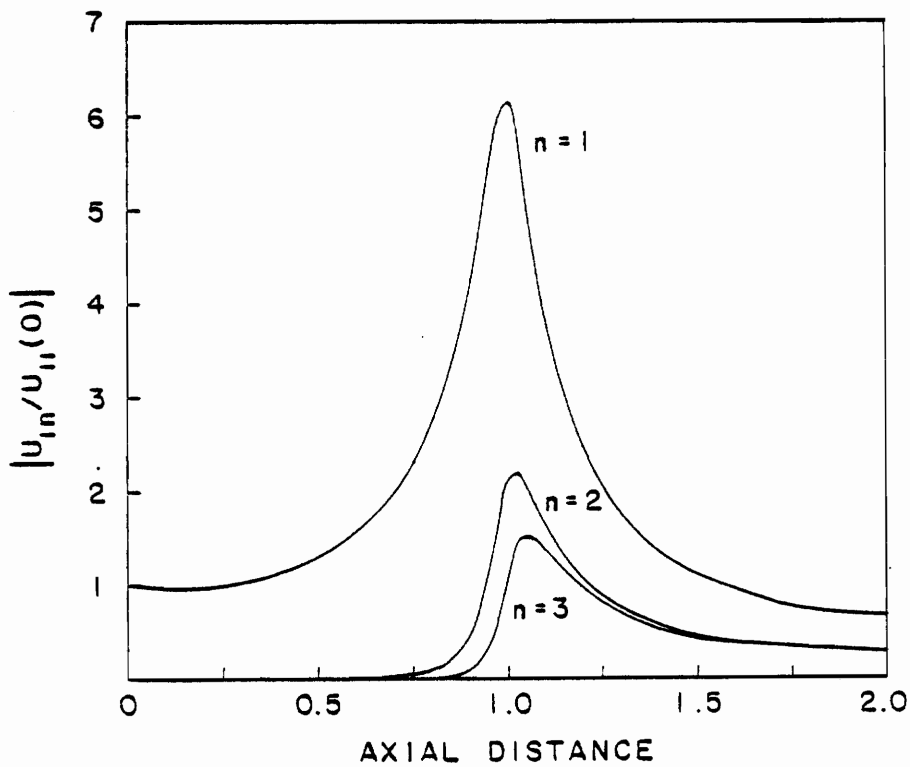

Figure 33 Development of harmonic amplitudes,

$\omega = 1$, $M_0 = -.4$, $\rho_I = .0045$, $N = 3$.

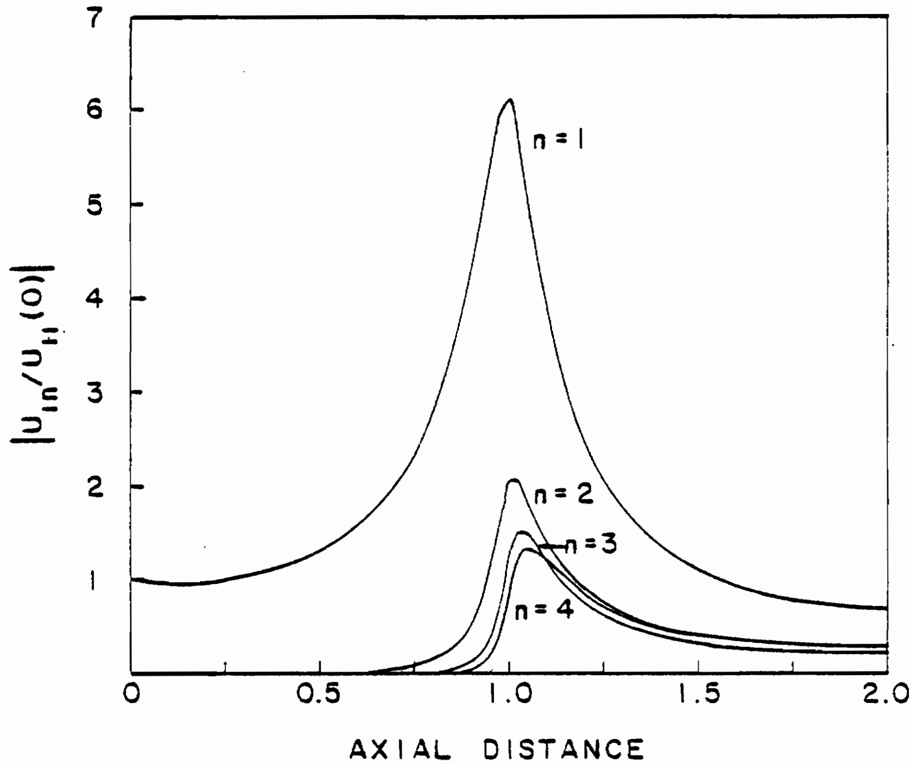

Figure 34 Development of harmonic amplitudes,

$\omega = 1$, $M_0 = -.4$, $\rho_I = .0045$, $N = 4$.

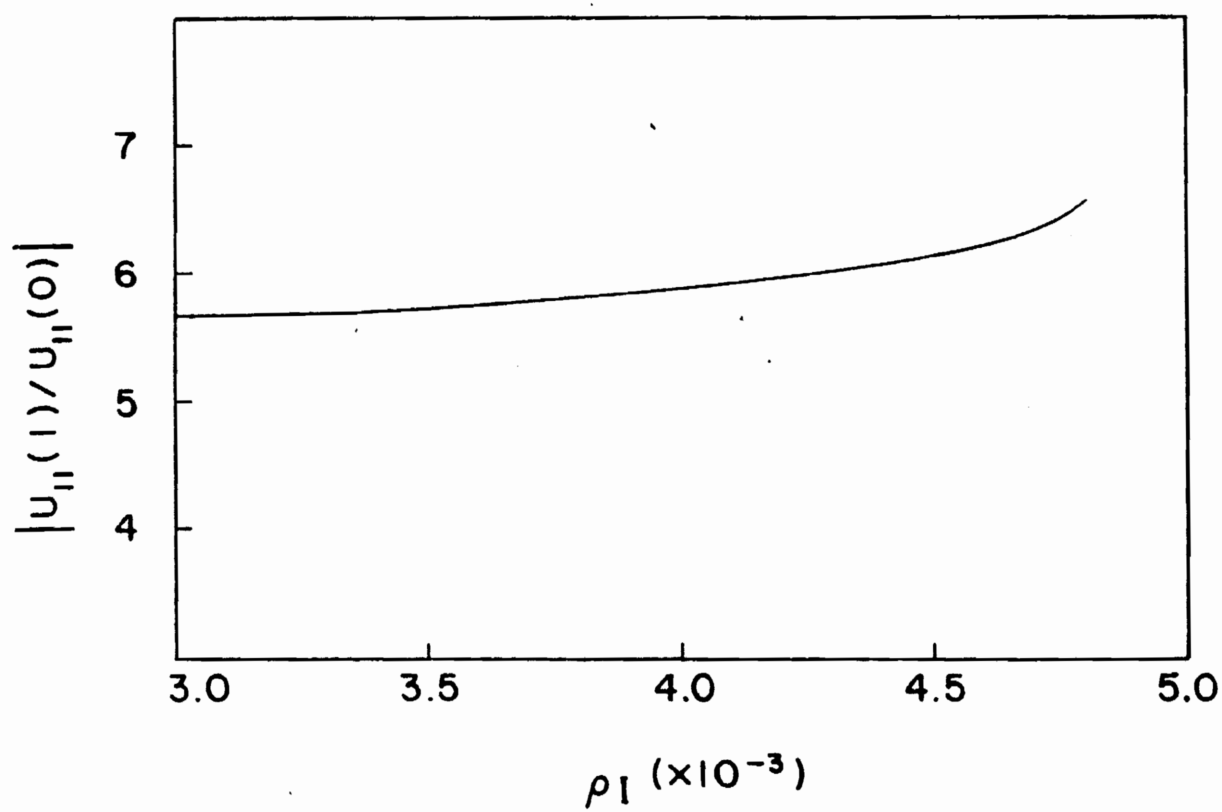

Figure 35 Growth of the fundamental harmonic at the throat as the density disturbance increases, $\omega = 1$, $M_0 = -.4$, $N = 3$.

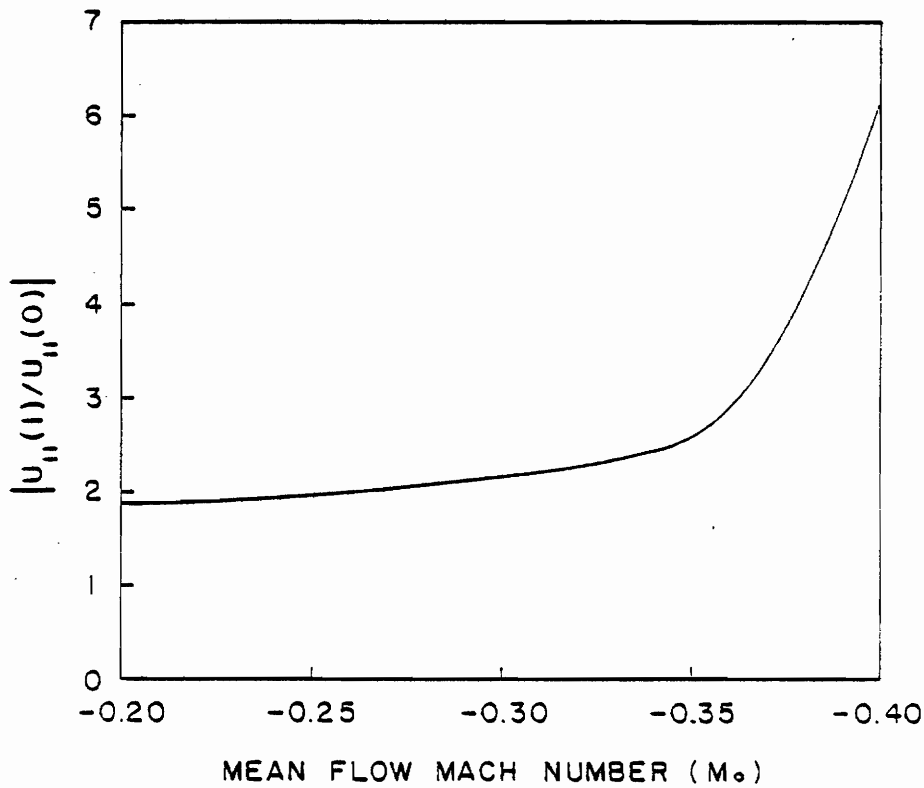

Figure 36 Growth of the fundamental harmonic at the throat as the mean flow Mach number increases, ω = 1, N = 3, ρ_I = .0045.

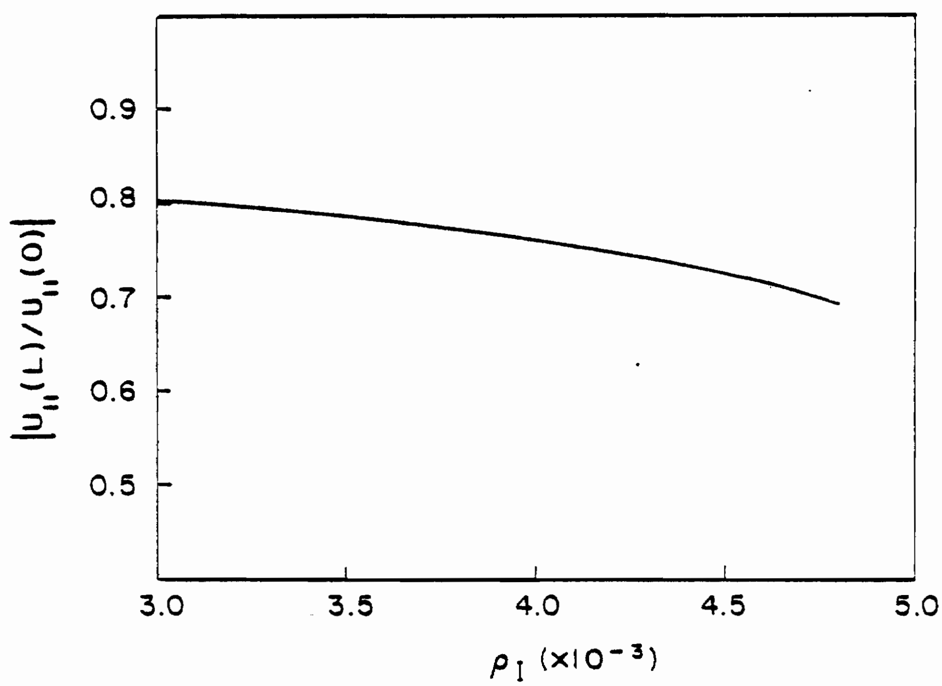

Figure 37 Reduction of the fundamental harmonic at the exit as the density disturbance increases, $\omega = 1$, $N = 3$, $M_0 = -.4$.

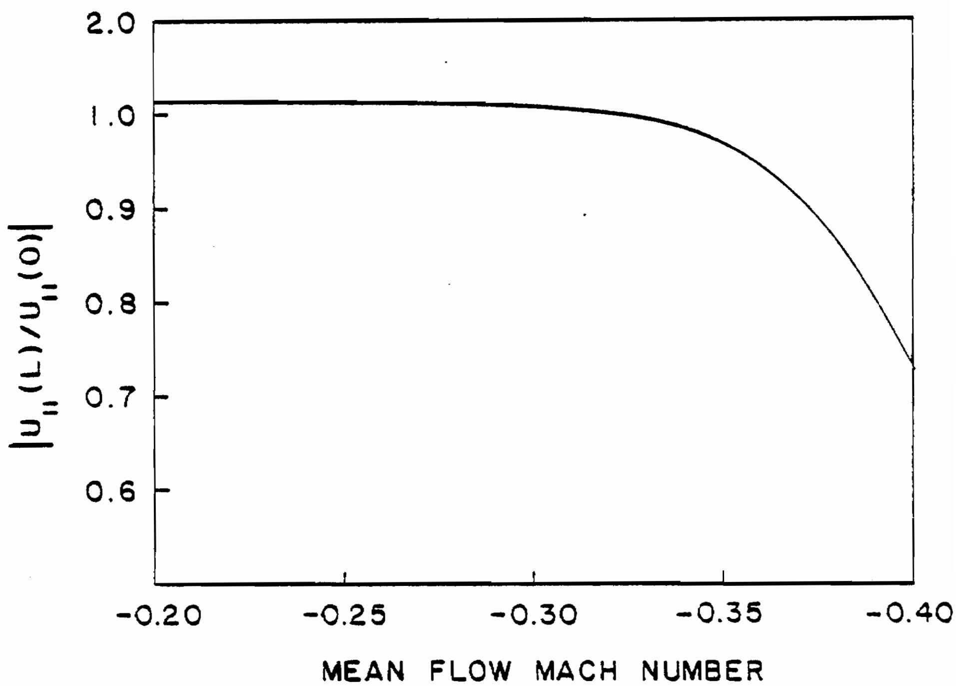

Figure 38 Reduction of the fundamental harmonic at the exit as the mean flow Mach number increases, $\omega = 1$, $\rho_I = .0045$, $N = 3$.

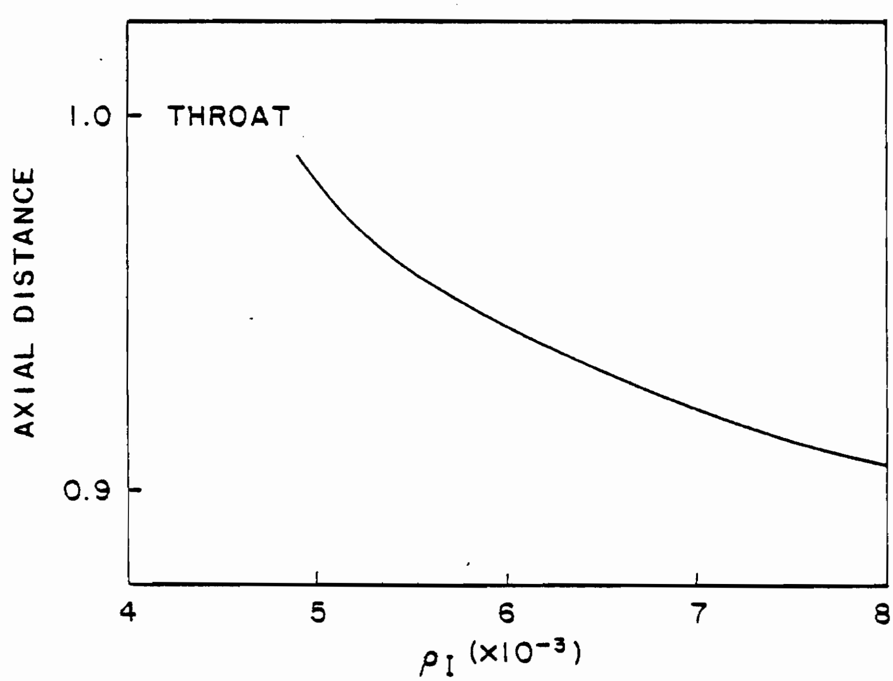

Figure 39 The movement downstream of the singularity as the density disturbance increases, $\omega = 1$, $N = 3$, $M_0 = -.4$.

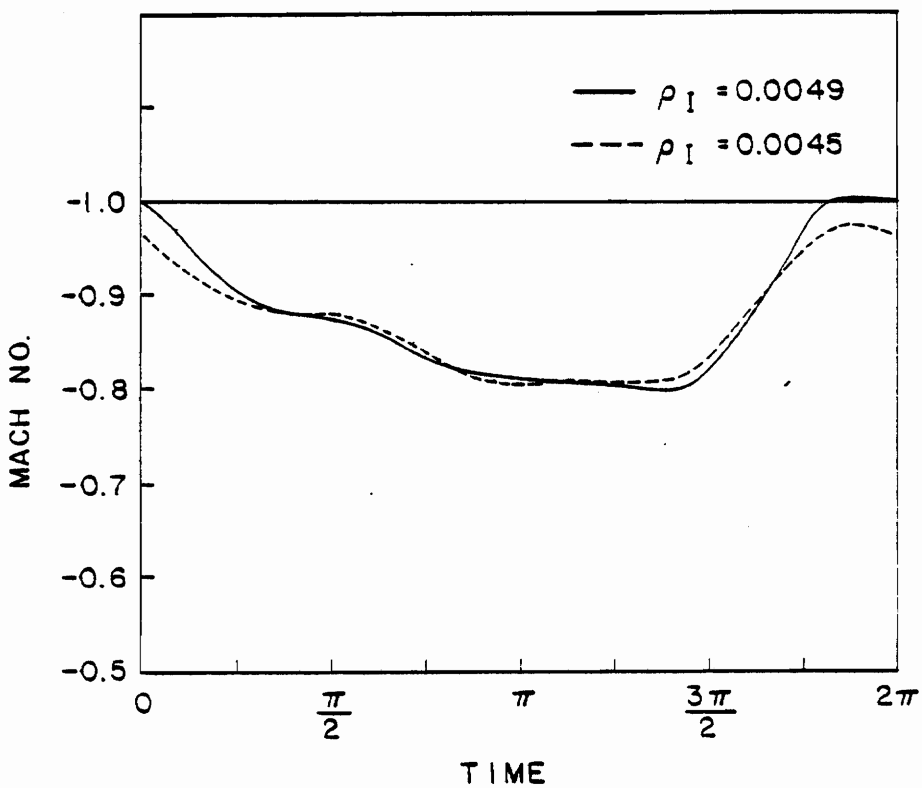

Figure 40 Comparison of Mach number variation between a singular case and a nonsingular case, $\omega = 1$, $N = 3$, $M_0 = -.4$.

Appendix A

Nonlinear Least-Squares Optimization

A scalar function $\phi(\underline{x})$ in n variables where

$$\underline{x} = \begin{bmatrix} x_1 \\ x_2 \\ \cdot \\ \cdot \\ \cdot \\ x_n \end{bmatrix}$$

can be expanded about an arbitrary point, $\underline{a}$, by Taylor's theorem according to

$$\phi(\underline{x}) = \phi(\underline{a}) + (\underline{x}-\underline{a})^T\underline{g}(\underline{a}) + \frac{1}{2}(\underline{x}-\underline{a})^T B(\underline{a})(\underline{x}-\underline{a}) + \ldots \tag{A1}$$

In this formula $\underline{g}$ is the gradient of ϕ and B is the Hessian matrix of ϕ where $\underline{g}$ and B are

$$g_i = \frac{\partial\phi}{\partial x_i} \tag{A2}$$

$$b_{ij} = \frac{\partial^2\phi}{\partial x_i x_j} \tag{A3}$$

Suppose the local minimum of ϕ is desired and this minimum occurs at $\underline{a}$. Then $\underline{g}(\underline{a}) = \underline{0}$ and the Hessian matrix, B(a), must be positive definite[49]. For quadratic ϕ Eq. (A1) becomes

$$\phi(\underline{x}) = \phi(\underline{a}) + \frac{1}{2}(\underline{x}-\underline{a})^T B(\underline{x}-\underline{a}) \tag{A4}$$

Therefore the gradient $\underline{g}$ at $\underline{x}$ is given by

$$\underline{g}(\underline{x}) = B(\underline{x}-\underline{a}) \tag{A5}$$

so that for an arbitrary point $\underline{x}$, the value of $\underline{a}$ can be evaluated from

$$\underline{a} = \underline{x} - B^{-1}\underline{g}(\underline{x}) \tag{A6}$$

From this it is apparent that the minimum of a quadratic ϕ can be obtained by knowing the gradient direction $\underline{g}$ at $\underline{x}$ and B^{-1}. Define the matrix H as

$$H = B^{-1} \tag{A7}$$

One can now view the matrix H as an operator which turns the local direction of steepest descent $-\underline{g}$ at $\underline{x}$ into the true direction from $\underline{x}$ to the minimum point of ϕ. Replacing B^{-1} by H in Eq. (A6) results in

$$\underline{a} = \underline{x} - H\underline{g}(\underline{x}) \tag{A8}$$

Equation (A8) can be considered as the Newton method for solving the system of equations $\underline{g}(\underline{x}) = 0$. Using the form of Eq. (A8) an iteration procedure can be formulated to find the minimum of any function ϕ[48]. The iteration equation is of the following form

$$\underline{x}_{k+1} = \underline{x}_k - \alpha_k H_k \underline{g}_k \tag{A9}$$

in which

$$\underline{g}_k = \underline{g}(\underline{x}_k) \tag{A10}$$

and H_k is a kth approximation to the inverse H of the Hessian matrix B of the function ϕ at $\underline{a}$, the minimum. Also α_k is a positive scalar which is determined at each step of the iteration in order that a local minimum of ϕ is achieved along the direction $-H_k\underline{g}_k$ from $\underline{x}_k$. This iteration scheme attempts to achieve the minimum point $\underline{a}$ and the inverse Hessian matrix H simultaneously.

Let us now consider the case where ϕ is the sum of squares of m nonlinear functions in n variables that is,

$$\phi(\underline{x}) = \underline{f}^T\underline{f} = \sum_{i=1}^{m} [f_i(\underline{x})]^2 \tag{A11}$$

where

$$\underline{x} = (x_1, x_2, \ldots, .x_n)^T \tag{A12}$$

$$\underline{f} = (f_1, f_2, \ldots, f_m)^T \tag{A13}$$

and assume for convenience that $m \geq n$. For our purposes the column vector $\underline{f}$ represents the residuals of the boundary conditions so that minimizing ϕ will minimize the residuals in a least-squares sense. The gradient and Hessian matrix of ϕ will now be determined by expressing ϕ in index notation

$$\phi = f_k f_k \tag{A14}$$

which implies that

$$\underline{g}(\underline{x}) = \phi_{,i} = (f_k f_k)_{,i} = f_{k,i} f_k + f_k f_{k,i} \tag{A15}$$

so that

$$\underline{g}(\underline{x}) = 2J^T \underline{f} \tag{A16}$$

In Eq. (A16) J is the $m \times n$ Jacobian matrix of $\underline{f}$ which has the form

$$J = j_{pq} = \frac{\partial f_p}{\partial x_q} \tag{A17}$$

The Hessian matrix B is given by

$$\begin{aligned} b_{pq} &= \phi_{,pq} \\ &= (f_k f_k)_{,pq} = (2f_{k,p} f_k)_{,q} \\ &= 2(f_{k,pq} f_k + f_{k,p} f_{k,q}) \quad \text{or} \end{aligned}$$

$$B = 2(C + J^T J) \tag{A18}$$

where

$$c_{pq} = f_{k,pq} f_k \ , \tag{A19}$$

a n × n matrix.

If the Hessian matrix of second derivatives, B, can be calculated then Newton's method, Eq. (A9), can be used. This scheme[50] constructs a sequence of vectors $\{\underline{x}_k\}$ such that

$$\underline{x}_{k+1} = \underline{x}_k + \alpha_k \underline{p}_k \tag{A20}$$

Comparing Eq. (A20) with Eq. (A9) shows that $\underline{p}_k$, the direction of search, satisfies

$$B(\underline{x}_k)\underline{p}_k = -\underline{g}(\underline{x}_k) \tag{A21}$$

where the Hessian matrix is approximated by evaluating it at $\underline{x}_k$. If ϕ is a sum of squares of nonlinear functions then the special form of the Hessian matrix and gradient vector, Eqs. (A18) and (A16) respectively, can be substituted into Eq. (A21) so that,

$$[C(\underline{x}_k) + J^T(\underline{x}_k)J(\underline{x}_k)]\underline{p}_k = -J^T(\underline{x}_k)\underline{f}(\underline{x}_k) \tag{A22}$$

Neglecting the second-derivative matrix $C(\underline{x}_k)$ in Eq. (A22) results in

$$J^T(\underline{x}_k)J(\underline{x}_k)\underline{p}_k = -J^T(\underline{x}_k)\underline{f}(\underline{x}_k) \tag{A23}$$

This is known as the Gauss-Newton method and is intended for problems where $||C(\underline{x})||$ is small compared to $||J^T(\underline{x})J(\underline{x})||$.

The Levenberg-Marquardt iteration[43] generates a sequence of approximations to the minimum point by

$$\underline{x}_{k+1} = \underline{x}_k - \alpha_k[\mu_k I + J^T(\underline{x}_k)J(\underline{x}_k)]^{-1} J(\underline{x}_k)^T\underline{f}(\underline{x}_k) \tag{A24}$$

where μ_k, α_k are positive scalars. Consider the approximation M to the Hessian matrix $B(\underline{x}_k)$ in Eq. (A24),

$$M = \mu_k I + D(\underline{x}_k) \tag{A25}$$

where

$$D(\underline{x}_k) = J^T(\underline{x}_k)\ J(\underline{x}_k) \tag{A26}$$

In Eq. (A25) one sees that the eigenvalues of M are $\mu_k + \lambda_j$, $j = 1,2,..,n$, so that choosing $\mu_k > -\min \lambda_j$ guarantees that the eigenvalues of M are positive and thus M is positive definite[51]. This then guarantees that for some $\alpha_k > 0$

$$\phi(\underline{x}_{k+1}) < \phi(\underline{x}_k) \tag{A27}$$

Note that the $\underline{p}_k$ in Eq. (A24) is somewhere between the Gauss-Newton direction ($\mu_k = 0$) and the gradient direction ($\mu_k = \infty$).

The numerical scheme that was employed in the computer program approximates $J(\underline{x}_k)$ by the corresponding matrix of difference quotients. This matrix of difference quotients is denoted by $\Delta F(\underline{x},h)$ whose m-th, n-th element is

$$\Delta F(\underline{x},h) = f_m(\underline{x} + h\underline{u}_n) - f_m(\underline{x}) \tag{A28}$$

where h is a scalar and $\underline{u}_n$ is the n-th unit vector. The finite difference analogue of the Levenberg-Marquardt algorithm (f.d.L.M.)[43] is

$$\underline{x}_{k+1} = \underline{x}_k - \alpha_k[\mu_k I + h_k^{-2}\Delta F^T(\underline{x}_k,h_k)\Delta F(\underline{x}_k,h_k)]^{-1} h_k^{-1}\Delta F^T(\underline{x}_k,h_k)\underline{f}(\underline{x}_k) \tag{A29}$$

$$= \underline{x}_k - \alpha_k h_k[h_k^2\mu_k I + \Delta F^T(\underline{x}_k,h_k)\Delta F(\underline{x}_k,h_k)]^{-1}\Delta F^T(\underline{x}_k,h_k)\underline{f}(\underline{x}_k) \tag{A30}$$

If $\mu_k = 0$ then the finite difference analogue of the Gauss-Newton method is obtained. The convergence of the f.d.L.M. algorithm to a local minimum point for sufficiently small h is proven in reference 43.

Appendix B
Transfer Matrices

Since the system of ordinary differential equations represented by Eq. (2.61) is linear its solution can be determined by a linear combination of N linear independent solutions. With this fact, the general solution can be written as

$$A(x) = C_1 A^{(1)}(x) + C_2 A^{(2)}(x) + \ldots + C_N A^{(N)}(x) \tag{B1}$$

where the column vectors $A^{(1)}, \ldots, A^{(N)}$ are the linearly independent solutions whose numerical determination is described in the text and the C's are arbitrary constants. The right-running modes are the first N_R components of the A's and the remaining N_L components are the left-running modes.

Equation (B1) leads to the following:

$$B(x) = C_1 T^{(1)}(x) + \ldots + C_N T^{(N)}(x) \tag{B2}$$

where

$$T^{(k)}(x) = \begin{bmatrix} A_1{}^{(k)} e^{i\int k_1 dx} \\ \cdot \\ \cdot \\ \cdot \\ \cdot \\ A_N{}^{(k)} e^{i\int k_N dx} \end{bmatrix}, \quad k = 1, 2, \ldots, N \tag{B3}$$

and

$$B(x) = \begin{bmatrix} A_1 e^{i\int k_1 dx} \\ \cdot \\ \cdot \\ \cdot \\ \cdot \\ A_N e^{i\int k_N dx} \end{bmatrix} \tag{B4}$$

At $x = 0$, Eq. (B2) reduces to

$$B(0) = C_1 \begin{bmatrix} 1 \\ 0 \\ \cdot \\ \cdot \\ 0 \end{bmatrix} + \ldots + C_N \begin{bmatrix} 0 \\ 0 \\ \cdot \\ \cdot \\ 1 \end{bmatrix}$$

$$\begin{bmatrix} A_1(0) \\ A_2(0) \\ \cdot \\ \cdot \\ \cdot \\ A_N(0) \end{bmatrix} = \begin{bmatrix} C_1 \\ C_2 \\ \cdot \\ \cdot \\ \cdot \\ C_N \end{bmatrix} \tag{B5}$$

so that the constants in Eq. (B2) are equal to the mode amplitudes at $x = 0$. Following the notation already introduced in the text Eq. (B5) can be rewritten as

$$\begin{bmatrix} C_1 \\ C_2 \\ \cdot \\ \cdot \\ C_N \end{bmatrix} = \begin{bmatrix} B^+(0) \\ \hline B^-(0) \end{bmatrix} \tag{B6}$$

Also, Eq. (B2) can be expressed in matrix form as

$$B(x) = \begin{bmatrix} T_1^{(1)} & T_1^{(2)} & ---- & T_1^{(N)} \\ T_2^{(1)} & T_2^{(2)} & & T_2^{(N)} \\ \cdot & \cdot & & \cdot \\ \cdot & \cdot & & \cdot \\ \cdot & \cdot & & \cdot \\ \cdot & \cdot & & \cdot \\ T_N^{(1)} & T_N^{(2)} & & T_N^{(N)} \end{bmatrix} \begin{bmatrix} C_1 \\ C_2 \\ \cdot \\ \cdot \\ \cdot \\ \cdot \\ C_N \end{bmatrix} \tag{B7}$$

The above equation will now be written in partitioned form as

$$\begin{bmatrix} B^+(x) \\ \hline B^-(x) \end{bmatrix} = \left[\begin{array}{c|c} TR_1 & TR_2 \\ \hline TR_3 & TR_4 \end{array}\right] \begin{bmatrix} B^+(0) \\ \hline B^-(0) \end{bmatrix} \tag{B8}$$

so that we arrive at Eqs. (2.62) and (2.63)

$$B^+(x) = TR_1(x)B^+(0) + TR_2(x)B^-(0) \tag{B9}$$

$$B^-(x) = TR_3(x)B^+(0) + TR_4(x)B^-(0) \tag{B10}$$

With Eqs. (B9) and (B10) transmission and reflection matrices can be determined in terms of the transfer matrices. The transmission and reflection matrices obey

$$B^+(L) = T^{L,0}B^+(0) + R^{L,L}B^-(L) \tag{B11}$$

$$B^-(0) = T^{0,L}B^-(L) + R^{0,0}B^+(0) \tag{B12}$$

Solving for $B^-(0)$ in Eq. (B10) and then substituting the result into Eq. (B9) yields

$$B^+(L) = [TR_1 - TR_2TR_4^{-1}TR_3]B^+(0) + TR_2TR_4^{-1}B^-(L) \tag{B13}$$

where x = L. Comparing Eq. (B13) with Eq. (B11) implies that

$$T^{L,0} = TR_1 - TR_2TR_4^{-1}TR_3 \tag{B14}$$

$$R^{L,L} = TR_2TR_4^{-1} \tag{B15}$$

Also, by directly comparing Eqs. (B10) and (B12) yields

$$T^{0,L} = TR_4^{-1} \tag{B16}$$

$$R^{0,0} = -TR_4^{-1}TR_3 \tag{B17}$$

Appendix C

The Nonlinear Differential Equation

If y is the column vector of the unknowns $\bar{u}_{1N},\ldots, u_{1N}, \bar{\rho}_{1N},\ldots, \rho_{1N}, \bar{T}_{1N},\ldots T_{1N}$ the coefficients of Eq. (3.60) take the following forms:

$$A(x,y) = \begin{bmatrix} \alpha_{11} & \alpha_{12} & \alpha_{13} \\ \alpha_{21} & \alpha_{22} & \alpha_{23} \\ \alpha_{31} & \alpha_{32} & \alpha_{33} \end{bmatrix}$$

where α_{ij} are $(2N + 1) \times (2N + 1)$ submatrices defined as

$$\alpha_{nm} = \begin{bmatrix} E_{nm}(0) & \bar{E}_{nm}(1) & \bar{E}_{nm}(2) & \cdots \\ E_{nm}(1) & E_{nm}(0) & \bar{E}_{nm}(1) & \cdots \\ E_{nm}(2) & E_{nm}(1) & E_{nm}(0) & \cdots \\ \vdots & \vdots & \vdots & \end{bmatrix}$$

where

$$E_{11}(0) = \rho_{10},\ E_{12}(0) = u_{10},\ E_{13}(0) = 0,$$

$$E_{11}(n) = \rho_{1n},\ E_{12}(n) = u_{1n},\ E_{13}(n) = 0,$$

$$E_{21}(0) = F_1(0), \qquad E_{22}(0) = \frac{T_{10}}{\gamma},$$

$$E_{23}(0) = \frac{\rho_{10}}{\gamma}, \qquad E_{21}(n) = F_1(n),$$

$$E_{22}(n) = \frac{T_{1n}}{\gamma}, \qquad E_{23}(n) = \frac{\rho_{1n}}{\gamma},$$

$$E_{31}(0) = 0, \quad E_{32}(0) = (1-\gamma)[F_2(0)],$$

$$E_{33}(0) = E_{21}(0), \quad E_{31}(n) = 0,$$

$$E_{32}(n) = (1-\gamma)(F_2(n)), \quad E_{33}(n) = E_{21}(n).$$

$$F_1(0) = \sum_{j=-N}^{N} u_{1j}\bar{\rho}_{1j}, \text{ where } ()_{1,-n} \equiv (\bar{\ })_{1,n}$$

$$F_1(1) = \sum_{j=-N}^{N-1} \bar{\rho}_{1j}u_{1j+1}$$

$$F_1(2) = \rho_{11}u_{11} + \sum_{j=-N}^{N-2} \bar{\rho}_{1j}u_{1j+2}$$

$F_2(n)$ has the same form as $F_1(n)$ but with ρ being replaced by T.

$$B = \begin{bmatrix} B_1(n) \\ B_2(n) \\ B_3(n) \end{bmatrix} \qquad , \; n = -N,\ldots,0,\ldots,N$$

where

$$B_1(n) = -\ [in\omega\rho_{1n} + F_1(n)A_s]$$

$$B_2(n) = -\ F_5(n)$$

$$B_3(n) = -[F_3(n) + (1 - \gamma)F_4(n)]$$

$$A_s = \frac{1}{A}\frac{dA}{dx}$$

$$F_3(0) = \sum_{j=-N}^{N} \bar{\rho}_{1j} i\omega j T_{1j}$$

$$F_3(1) = \sum_{j=-N}^{N-1} \bar{\rho}_{1j} i\omega(j + 1)T_{1j+1}$$

etc.

.

.

$F_4(n)$ has the same form as $F_3(n)$ but with ρ, T being replaced by T, ρ respectively.

$F_5(n)$ has the same form as $F_3(n)$ with T being replaced by u.

Appendix D

The Singular Value Decomposition

If the elements in a set of vectors cannot be expressed as a linear combination of the other elements then the vectors are said to be independent. In the following we shall develop a quantitative approach to the idea of linear independence. For example the vectors,

$$\begin{bmatrix}1\\0\\0\end{bmatrix}, \begin{bmatrix}0\\1\\0\end{bmatrix}, \quad \text{and} \quad \begin{bmatrix}0\\0\\1\end{bmatrix}$$

are very independent while the vectors

$$\begin{bmatrix}1.01\\1.00\\1.00\end{bmatrix}, \begin{bmatrix}1.00\\1.01\\1.00\end{bmatrix}, \quad \text{and} \quad \begin{bmatrix}1.00\\1.00\\1.01\end{bmatrix}$$

are almost dependent. It will be shown that a numerical value can be associated with the concept of independence[48].

Two vectors are dependent if they are parallel and are very independent if they are orthogonal. Two vectors u and v are orthogonal if their inner product is zero, $u^T v = 0$.

Also, if

$$u^T u = 1$$

the vector u is said to have length 1. An orthogonal matrix is defined to be a square matrix whose columns are mutually orthogonal vectors each of length 1. Therefore a matrix U is orthogonal if

$$U^T U = I$$

Since $U^{-1} = U^T$ an orthogonal matrix will always be nonsingular. In what follows the concept that an orthogonal matrix is very nonsingular and that its columns are very independent will become apparent.

The length of a vector and the angle between two vectors are invariant under multiplication by orthogonal matrices. Since they do not magnify errors, orthogonal matrices are quite useful in computational analysis.

The singular value decomposition of an $m \times n$ real matrix A is of the form

$$A = U\Sigma V^T$$

where U is an $m \times m$ orthogonal matrix, V is an $n \times n$ orthogonal matrix, and Σ is an $m \times n$ diagonal matrix where $\sigma_{ii} \equiv \sigma_i \geq 0$. The σ_i's are referred to as the singular values of A. It is shown in texts on linear algebra[52] that this decomposition is always possible for any matrix A. The columns of U and V are called the left and right singular vectors.

It is also shown in linear algebra[52] that the matrices AA^T and A^TA have the same nonzero eigenvalues and that the singular values of A are the positive square roots of these eigenvalues. Also, the left and right singular vectors can be constructed from the eigenvectors of AA^T and A^TA, respectively.

Two simple examples are presented now to illustrate the above procedure for determining the SVD.

EXAMPLE 1:

$$A = \begin{bmatrix} 1 & 1 \\ 1 & 2 \end{bmatrix}$$

First compute A^TA and determine its eigenvalues,

$$A^TA = \begin{bmatrix} 2 & 3 \\ 3 & 5 \end{bmatrix}$$

The eigenvalues of A^TA are

$$\lambda_{1,2} = 6.854,\ .146.$$

Now using the following equations compute the eigenvectors

$$(2-\lambda)\ V_1 + 3V_2 = 0$$

$$V_1^2 + V_2^2 = 1$$

So that,

$$V = \begin{bmatrix} .526 & .851 \\ .851 & -.526 \end{bmatrix}$$

where the first column of V is the eigenvector corresponding to λ_1 and the second column is the eigenvector of λ_2. In this example U = V since A is symmetric. The singular values are 2.618 and .382 so that

$$\sum = \begin{bmatrix} \sqrt{\lambda_1} & 0 \\ 0 & \sqrt{\lambda_2} \end{bmatrix} = \begin{bmatrix} 2.618 & 0 \\ 0 & .382 \end{bmatrix}$$

EXAMPLE 2:

Consider the singular matrix

$$A = \begin{bmatrix} 1 & 1 \\ 2 & 2 \end{bmatrix}$$

As before, form

$$A^TA = \begin{bmatrix} 5 & 5 \\ 5 & 5 \end{bmatrix}$$

whose eigenvalues are

$$\lambda_{1,2} = 10,\ 0$$

Determining the eigenvectors give us

$$V = \begin{bmatrix} \frac{1}{\sqrt{2}} & \frac{1}{\sqrt{2}} \\ \frac{1}{\sqrt{2}} & -\frac{1}{\sqrt{2}} \end{bmatrix}$$

Now then

$$AA^T = \begin{bmatrix} 2 & 4 \\ 4 & 8 \end{bmatrix}$$, whose eigenvalues are $\lambda_{1,2}$=10,0 as expected.

Evaluating the eigenvectors of AA^T determines U as

$$U = \begin{bmatrix} \frac{1}{\sqrt{5}} & -\frac{2}{\sqrt{5}} \\ \frac{2}{\sqrt{5}} & \frac{1}{\sqrt{5}} \end{bmatrix}$$

Finally the singular values are $\sqrt{10}$ and 0 so that

$$\Sigma = \begin{bmatrix} \sqrt{10} & 0 \\ 0 & 0 \end{bmatrix}$$

We see that one of the singular values is zero which is to be expected since A is singular.

The rank of a matrix is another basic concept of linear algebra. This is defined as the maximal number of independent columns or the order of the maximal nonzero subdeterminant in the matrix. For a particular matrix it can be quite difficult to determine its rank using this definition. If a matrix is diagonal it is simple to determine its rank since it is the number of nonzero elements in the matrix. The set resulting from the multiplication of a set of independent vectors by an orthogonal matrix is still independent. Therefore the rank of a general matrix A is equal to the rank of the diagonal matrix Σ in its SVD. Hence the rank of a matrix can be determined by the number of nonzero singular values that it has.

Now let k represent the rank and consider an $m \times n$ matrix with $m \geq n$. The matrix is called full rank if $k = n$ or rank deficient if $k < n$. In the case of a square matrix nonsingular and singular are used instead of full rank and rank deficient, respectively. In computing the SVD of a rank-deficient matrix all of its singular values can turn out to be nonzero due to roundoff errors, indicating a matrix of full rank. Usually in determining the SVD, an effective rank is used, which is the number of singular values greater than some prescribed tolerance so that the significance of single numbers, the small singular values, and not sets of vectors can be used to determine the rank of a matrix.

A numerical value can now be associated with the idea of linear independence. Suppose σ_{max} and σ_{min} are the largest and smallest singular values of a matrix A of full rank, then the condition number of A is defined to be

$$\operatorname{cond}(A) = \frac{\sigma_{max}}{\sigma_{min}} .$$

Cond(A) is said to be infinite if A is rank deficient ($\sigma_{min} = 0$). From this definition it is apparent that cond(A) ≥ 1. The columns of A are very independent if cond(A) is close to 1. The columns of A are nearly dependent if cond(A) is large. We can say far from singular or nearly singular if A is square. If cond(A) > cond(B), then A is considered to be more singular than B. For an orthogonal matrix A, cond(A) = 1 and its columns are as independent as possible. Also, if A is an arbitrary matrix and cond(A) = 1 then A must be a scalar multiple of an orthogonal matrix.

The advantage in using the SVD to solve a system of equations is now presented. To begin with suppose we want to solve the following system,

$$Ax = b$$

where A is an $m \times n$ matrix ($m \geq n$) and b is a given m vector. The n vector x is the solution vector to be determined. Note that A can be square and possibly singular. There are some fundamental properties of the system that must be examined. Questions about the consistency of the equations, existence of solutions, uniqueness and the possibility that $Ax = 0$ has nonzero solutions arise.

In theory there are a number of algorithms that can determine these properties. Considering the inexact data and the imprecise arithmetic involved in the numerical solution of the problem indicates that the only reliable numerical method is the SVD.

Now replacing A by its SVD implies that

$$U\Sigma V^T x = b$$

and

$$\Sigma z = d,$$

where $z = V^T x$ and $d = U^T b$. The above system ($\Sigma z = d$) is diagonal and depending on the dimensions m and n and the rank k, the number of nonzero singular values, it can be analyzed in three cases:

$$\sigma_j z_j = d_j, \text{ if } j \leq n \text{ and } \sigma_j \neq 0$$

$$0.z_j = d_j, \quad \text{if } j \leq n \text{ and } \sigma_j = 0$$

$$0 = d_j, \qquad \text{if } j > n.$$

If $k = n$, the second set of equations is empty. If $n = m$, the third set of equations is empty. The equations are consistent and a solution exists if and only if $d_j = 0$ whenever $\sigma_j = 0$ or $j > n$. If $k < n$, then the z_j associated with a zero σ_j can be given an arbitrary value and still yield a solution to the system.

So far nothing has been said about how the decomposition is actually performed in the computer routine. We will now consider the numerical procedure used by first looking at the following problem. Suppose we want to transform a real arbitrary vector $\underline{u}$ into a second real vector $\underline{v}$ of the same length by using the following transformation

$$\underline{v} = P\underline{u}$$

where P is a square matrix and is a function of $\underline{u}$ and $\underline{v}$ (refer to Fig. D.1).

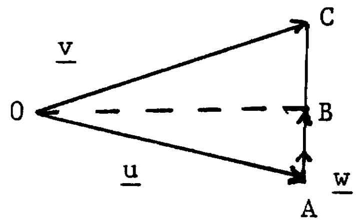

Fig. D.1

To implement this note that

$$\overrightarrow{0C} = \overrightarrow{0A} + 2\overrightarrow{AB}$$

where B is the midpoint of AC. Therefore 0B is perpendicular to AC and AB is minus the projection of 0A on AC. This equation can be rewritten as

$$\underline{v} = \underline{u} + 2\overrightarrow{AB}.$$

Let $\underline{w}$ be a unit vector along $\overrightarrow{AC}$ so that

$$\underline{w} = \frac{\underline{v} - \underline{u}}{||\underline{v}-\underline{u}||}$$

Since $\overrightarrow{AB}$ is minus the projection of $\underline{u}$ on $\overrightarrow{AC}$ then

$$\overrightarrow{AB} = -(\underline{w}^T\underline{u})\underline{w}.$$

Also

$$(\underline{w}^T\underline{u})\underline{w} = \underline{w}(\underline{w}^T\underline{u}) = \underline{w}\underline{w}^T\underline{u}$$

so that

$$\underline{v} = \underline{u} - 2\underline{w}\underline{w}^T\underline{u} = (I - 2\underline{w}\underline{w}^T)\underline{u}$$

Now we have the form of P, which is

$$P = I - 2\underline{w}\underline{w}^T, \quad ||\underline{w}|| = 1$$

and this is called a Householder transformation. One can substitute for P and algebraically verify that this is the correct form, that is

$$P\underline{u} = (I - 2\underline{w}\underline{w}^T)\underline{u} = \underline{u} - \frac{2(\underline{v}-\underline{u})(\underline{v}-\underline{u})^T}{||\underline{v}-\underline{u}||^2}\,\underline{u}$$

$$= \underline{u} - 2\,\frac{(\underline{v}-\underline{u})^T\underline{u}}{||\underline{v}-\underline{u}||^2}\,(\underline{v}-\underline{u})$$

But

$$||\underline{v}-\underline{u}||^2 = (\underline{v}-\underline{u})^T(\underline{v}-\underline{u}) = \underline{v}^T\underline{v} - \underline{u}^T\underline{v} - \underline{v}^T\underline{u} + \underline{u}^T\underline{u}$$

$$= 2\underline{u}^T\underline{u} - 2\underline{v}^T\underline{u}$$

$$= -2(\underline{v}-\underline{u})^T\underline{u}$$

so that

$$P\underline{u} = \underline{u} + (\underline{v}-\underline{u}) = \underline{v}$$

It is apparent that P depends only on $\underline{w}$, the direction of $\underline{v}-\underline{u}$. Therefore for any two vectors $\underline{u}'$ and $\underline{v}'$ for which $||\underline{u}'|| = ||\underline{v}'||$ and $\underline{v}'-\underline{u}'$ is in the same direction as $\underline{v}-\underline{u}$ the transformation $P\underline{u}' = \underline{v}'$ holds. The implication here is that P reflects each point u' through a plane that is perpendicular to $\underline{v}-\underline{u}$ and which contains the line through the origin and $\frac{1}{2}(\underline{u}+\underline{v})$. Since it appears that a Householder transformation is merely a reflection one would expect that lengths and angles will be preserved and hence it is an orthogonal transformation.

First note that,

$$P^T = I - 2(\underline{w}\underline{w}^T)^T = I - 2\underline{w}\underline{w}^T = P$$

so that P is symmetric. Moreover,

$$P^TP = (I - 2\underline{w}\underline{w}^T)^2 = I - 4\underline{w}\underline{w}^T + 4\underline{w}\underline{w}^T\underline{w}\underline{w}^T$$

$$= I - 4\underline{w}\underline{w}^T + 4\underline{w}\underline{w}^T$$

$$= I$$

Hence P is indeed an orthogonal matrix. Householder transformations are a fundamental part of the SVD routine.

The QR algorithm[53] is also associated with the SVD. In the QR algorithm a square matrix, say H_1, can be decomposed as follows:

$$H_1 = Q_1R_1$$

where Q_1 is an orthogonal matrix and R_1 is an upper triangular matrix. Interchanging the order of multiplication results in

$$H_2 = R_1Q_1 = Q_1^{-1}H_1Q_1 = Q_1^TH_1Q_1$$

and since Q_1 is orthogonal the eigenvalues of H_1 are preserved. For most matrices the QR algorithm is convergent and H_k, as $k \to \infty$, is block upper triangular (diagonal if the original matrix is symmetric). The eigenvalues of the original matrix will be the eigenvalues of the 2×2 blocks on the diagonal.

For computational efficiency a matrix is first reduced to upper Hessenberg form by using similarity transformations (which preserve the eigenvalues) before applying the QR algorithm. An upper Hessenberg form is a square matrix which consists of an upper triangular form with an additional band of elements adjacent to the main diagonal. The reduction of a matrix to upper Hessenberg form is accomplished by using Householder transformations. This is done successively until the upper Hessenberg form is obtained and can be represented mathematically as

$$Q^{(n)}\ldots Q^{(1)}H_1Q^{(1)T}\ldots Q^{(n)T} = \begin{bmatrix} \bar{h}_{11} & \bar{h}_{12} & - & - & - & - & \bar{h}_{1n} \\ h_{21} & \bar{h}_{22} & - & - & - & - & \bar{h}_{2n} \\ & \bar{h}_{32} & - & - & - & - & - \\ & & - & - & - & - & - \\ & & & - & - & - & - \\ & & & & - & - & - \\ & & & & & \bar{h}_{n,n-1} & \bar{h}_{nn} \end{bmatrix}$$

where the $Q^{(k)}$'s are Householder transformations.

The convergence of the QR method can be accelerated by employing shifts. Instead of decomposing H_k, the algorithm is modified so that the decomposition is now done on

$$H_k - \eta_k I = Q_k R_k$$

and the reverse multiplication is changed to

$$H_{k+1} = R_k Q_k + \eta_k I.$$

The value η_k is called the shift parameter. It has been shown[54] that an excellent choice of η_k is the eigenvalue of the 2×2 submatrix at the bottom right corner of (the upper Hessenberg) H_k which is closest to $h_{nn}^{(k)}$ (the last entry on the main diagonal).

The SVD computer program first uses Householder transformations to reduce the given matrix to a bidiagonal form and then a variant of the tridiagonal QR algorithm is used to find the singular values of the bidiagonal matrix.

Let A be an $m \times n$ matrix, with $m \geq n$, and let the SVD form

$$A = U\Sigma V^T$$

to be computed by the computer routine.

The reduction to bidiagonal form is accomplished by constructing two sequences of Householder transformations[47]

$$P^{(k)} = I - 2x^{(k)}x^{(k)T} \quad (k = 1, 2, \ldots, n)$$

and

$$Q^{(k)} = I - 2y^{(k)}y^{(k)T} \quad (k = 1, 2, \ldots, n-2)$$

$$(x^{(k)T}x^{(k)} = y^{(k)T}y^{(k)} = 1) \text{ such that}$$

$$P^{(n)} \dots P^{(1)} A Q^{(1)} \dots Q^{(n-2)} = \left[\begin{array}{cccccc} q_1 & e_2 & 0 & . & . & 0 \\ & q_2 & e_3 & 0 & & . \\ 0 & & & & & 0 \\ & & & & & e_n \\ & & & & & q_n \\ \hline & & & 0 & & \end{array}\right] \begin{array}{l} \\ \\ \\ \\ \\ \}\ (m-n)\times n \end{array} \equiv J^{(0)}$$

an upper bidiagonal matrix.

Let $A^{(1)} = A$ and define

$$A^{(k+1/2)} = P^{(k)} A^{(k)} \quad (k = 1, 2, \dots, n)$$

$$A^{(k+1)} = A^{(k+1/2)} Q^{(k)} \quad (k = 1, 2, \dots, n-2)$$

then $P^{(k)}$ is determined such that

$$a_{ik}^{(k+1/2)} = 0 \quad (i = k+1, \dots, m)$$

and $Q^{(k)}$ such that.

$$a_{kj}^{(k+1)} = 0 \quad (j = k+2, \dots, n)$$

A variant of the QR algorithm diagonalizes $J^{(0)}$. This is done iteratively so that

$$J^{(0)} \to J^{(1)} \to . \ . \ . \to \Sigma$$

where $J^{(i+1)} = S^{(i)T} J^{(i)} T^{(i)}$

and $S^{(i)}$, $T^{(i)}$ are orthogonal. The matrices $T^{(i)}$ are chosen so that the sequence $M^{(i)} = J^{(i)T} J^{(i)}$ converges to a diagonal matrix while the matrices $S^{(i)}$ are chosen so that $J^{(i)}$ is bidiagonal.

The following notation will now be adopted to explain the second phase of the SVD:

$$J \equiv J^{(i)},\ \bar{J} \equiv J^{(i+1)},\ S \equiv S^{(i)},\ T \equiv T^{(i)},$$

$$M = J^T J,\ \bar{M} = \bar{J}^T \bar{J}.$$

Givens rotations[53] are applied alternately from the right and the left to J to accomplish the transition $J \to \bar{J}$. Therefore

$$\bar{J} = \underbrace{S_n^T\, S_{(n-1)}^T \cdot \cdot \cdot\, S_2^T}_{S^T}\ J\ \underbrace{T_2 T_3 \cdot \cdot \cdot\, T_n}_{T}$$

where the Givens rotation S_k is

$$S_k = \begin{array}{cc} \begin{array}{ccccccc} & & (k-1) & (k) & & & \end{array} & \\ \begin{bmatrix} 1 & 0 & & & & & 0 \\ 0 & \ddots & & & & & \\ & & 1\ \cos\theta_k & -\sin\theta_k & & & \\ & & \sin\theta_k & \cos\theta_k & & & \\ & & & & 1 & & \\ & & & & & \ddots & \\ 0 & & & & & & 1 \end{bmatrix} & \begin{array}{c} \\ \\ (k-1) \\ (k) \\ \\ \\ \\ \end{array} \end{array}$$

and T_k is also a Givens rotation with ϕ_k instead of θ_k.

The angle ϕ_2 can be arbitrary but all the other angles are chosen such that $\bar{J}$ has the same form as J. So that,

T_2 annihilates nothing, generates an entry $\{J\}_{21}$

S_2^T annihilates $\{J\}_{21}$, generates an entry $\{J\}_{13}$

T_3 annihilates $\{J\}_{13}$, generates an entry $\{J\}_{32}$

.

.

.

until S_n^T annihilates $\{J\}_{n,n-1}$, and generates nothing. It is shown in reference 47 that ϕ_2 can be chosen so that the transition $M \to \bar{M}$ is a QR transformation with a given shift s. This is true if the first column of T_2 is constructed so that it is proportional to the first column of $M - sI$. The shift parameter s is set equal to the eigenvalue of the lower 2×2 submatrix of M that is closest to m_{nn}. These Givens rotations are applied iteratively until the super-diagonal elements converge to zero (computationally a numerical tolerance is preset in the program).

To demonstrate this algorithm let us apply it to the following example.

Example 3:

$$A = \begin{bmatrix} 1 & 1 & 2 \\ 1 & 2 & 2 \\ 1 & 2 & 3 \end{bmatrix}$$

Since n = 3 we need to apply two Householder transformations to the left of A and one to the right of A to reduce it to bidiagonal form. Let $A_1 = A$ and consider introducing zeros into $\underline{a}_1$, the first column of A_1. This is done by adding $||a_1||$ to the first component of $\underline{a}_1$. Therefore

$$\underline{u}_1 = \begin{bmatrix} 1 + \sqrt{3} \\ 1 \\ 1 \end{bmatrix} = \begin{bmatrix} 2.73205 \\ 1 \\ 1 \end{bmatrix}$$

and from this the Householder matrix can be evaluated which will be,

$$\beta_1 = \frac{||u_1||^2}{2} = \underline{u}_1^T \underline{a}_1 = 4.73205$$

$$U_1 = I - \beta_1^{-1}\underline{u}_1\underline{u}_1^T \qquad (\underline{w} = \underline{u}_1/||\underline{u}_1|| \text{ in the earlier notation})$$

The transformed matrix A_2 is actually computed column by column from

$$A_2 = U_1A_1$$

which implies that

$$U_1\underline{a}_1 = (I - \beta_1^{-1}\underline{u}_1\underline{u}_1^T)\underline{a}_1$$

$$= \underline{a}_1 - (\beta_1^{-1}\underline{u}_1^T\underline{a}_1)\underline{u}_1$$

$$= \underline{a}_1 - \underline{u}_1$$

$$= \begin{bmatrix} -1.73205 \\ 0 \\ 0 \end{bmatrix}$$

$$U_1\underline{a}_2 = \underline{a}_2 - \beta_1^{-1}(\underline{u}_1^T\underline{a}_2)\underline{u}_1$$

$$= \underline{a}_2 - (1.42265)\underline{u}_1$$

$$= \begin{bmatrix} -2.88675 \\ .57735 \\ .57735 \end{bmatrix}$$

$$U_1\underline{a}_3 = \underline{a}_3 - \beta_1^{-1}(\underline{u}_1^T\underline{a}_3)\underline{u}_1$$

$$= \begin{bmatrix} -4.04145 \\ -.21132 \\ .78868 \end{bmatrix}$$

Therefore,

$$A_2 = \begin{bmatrix} -1.73205 & -2.88675 & -4.04145 \\ 0 & .57735 & -.21132 \\ 0 & .57735 & .78868 \end{bmatrix}$$

The right Householder transformation, denoted by V_1, is derived from the first row of A_2. This is done by constructing the following vector

$$\nu_1 = 0$$

$$\nu_2 = -2.88675 - \sqrt{(2.88675)^2 + (-4.04145)^2}$$

$$\nu_3 = -4.04145$$

therefore

$$\underline{\nu}_1^T = [0 \quad -7.8533 \quad -4.04145]$$

so that

$$V_1 = I - 2\,\frac{\underline{\nu}_1 \underline{\nu}_1^T}{||\underline{\nu}_1||^2}$$

The transformed matrix A_3 is computed row by row, that is

$$A_3 = A_2 V_1$$

implies that

$$\underline{a}_1^T V_1 = \underline{a}_1^T - \underline{\nu}_1^T$$

$$= [-1.73205 \quad 4.96655 \quad 0]$$

$$\underline{a}_2^T V_1 = [0 \quad -.16362 \quad -.59264]$$

$$\underline{a}_3^T V_1 = [0 \quad -.97735 \quad -.01140]$$

Therefore

$$A_3 = \begin{bmatrix} -1.73205 & 4.96655 & 0 \\ 0 & -.16362 & -.59264 \\ 0 & -.97735 & -.01140 \end{bmatrix}$$

The final left Householder transformation is derived from the second column of A_3 according to

$$\underline{u}_2 = \begin{bmatrix} 0 \\ -1.15457 \\ -.97735 \end{bmatrix}$$

so that

$$U_2 = I - 2\,\frac{\underline{u}_2\underline{u}_2^T}{||\underline{u}_2||^2}$$

and the desired bidiagonal form

$$A_4 = U_2A_3 = \begin{bmatrix} -1.73205 & 4.96655 & 0 \\ 0 & .99095 & .10910 \\ 0 & 0 & .58262 \end{bmatrix}$$

To implement the Givens' rotations the matrix M is formed according to

$$M = A_4^TA_4 = \begin{bmatrix} 3 & -8.60231 & 0 \\ -8.60231 & 25.64860 & .10811 \\ 0 & .10811 & .35135 \end{bmatrix}$$

The eigenvalues of the lower 2×2 submatrix are:

$$\lambda_{1,2} = 25.64906,\ .35089$$

Since λ_2 is closer to m_{33}, it will be the value chosen for the shift parameter s.

The first right Givens' rotation is

$$T_2 = \begin{bmatrix} \cos\phi_2 & -\sin\phi_2 & 0 \\ \sin\phi_2 & \cos\phi_2 & 0 \\ 0 & 0 & 1 \end{bmatrix}$$

and the first column of T_2 is proportional to the first column of M-sI so that

$$\alpha\cos\phi_2 = 2.64911$$

$$\alpha\sin\phi_2 = -8.60231$$

which implies

$\cos \phi_2 = .29431$

$\sin \phi_2 = -.95571$

Post-multiplying A_4 by T_2 produces

$$A_5 = A_4T_2 = \begin{bmatrix} -5.25634 & -.19363 & 0 \\ -.94706 & .29165 & .1091 \\ 0 & 0 & .58262 \end{bmatrix}$$

Now the left Givens' rotation, S_2, is applied to annihilate $\{A_5\}_{21}$.

The matrix S_2,

$$S_2 = \begin{array}{c} \begin{array}{ccc} p = 1 & q = 2 & \end{array} \\ \begin{bmatrix} \cos \theta_2 & -\sin \theta_2 & 0 \\ \sin \theta_2 & \cos \theta_2 & 0 \\ 0 & 0 & 1 \end{bmatrix} \end{array}$$

is determined from the following equations:

$$\sin \theta_k = \alpha_k a_{qi}^{(k)}$$

$$\cos \theta_k = \alpha_k a_{pi}^{(k)}$$

where

$$\alpha_k = \{[a_{qi}^{(k)}]^2 + [a_{pi}^{(k)}]\}^{-\frac{1}{2}}$$

In this case p = 1, q = 2, and i = 1 (since $\{A_5\}_{21}$ is to be annihilated) and the a_{mn}'s are the elements of A_5.

Therefore

$\sin \theta_2 = -.17732$

$\cos \theta_2 = -.98415$

so that

$$A_6 = S_2^T A_5 = \begin{bmatrix} 5.34096 & .13885 & -.01935 \\ 0 & -.32136 & -.10737 \\ 0 & 0 & .58262 \end{bmatrix}$$

Continuing the process

$$\begin{array}{cccc} & & p = 2 & q = 3 \\ T_3 = & \begin{bmatrix} 1 & 0 & 0 \\ 0 & \cos\phi_3 & -\sin\phi_3 \\ 0 & \sin\phi_3 & \cos\phi_3 \end{bmatrix} \end{array}$$

where

$$\sin\phi_k = \alpha_k a_{iq}^{(k)}$$

$$\cos\phi_k = \alpha_k a_{ip}^{(k)}$$

$$\alpha_k = \{[a_{iq}]^2 + [a_{ip}]^2\}^{-\frac{1}{2}}$$

Here $p = 2$, $q = 3$, and $i = 1$ (since $\{A_6\}_{13}$ is to be annihilated) which implies that

$$\sin\phi_3 = \alpha_3 a_{13}^{(3)} = -.13803$$

$$\cos\phi_3 = \alpha_3 a_{12}^{(3)} = .99043$$

thus

$$A_7 = A_6 T_3 = \begin{bmatrix} 5.34096 & .14019 & 0 \\ 0 & -.30346 & -.15070 \\ 0 & -.08042 & .57704 \end{bmatrix}$$

The elements of S_3 are

$$\sin\theta_3 = \alpha_3 a_{32}^{(3)} = -.25617$$

$$\cos\theta_3 = \alpha_3 a_{22}^{(3)} = -.96663$$

which results in

$$A_8 = S_3^T A_7 = \begin{bmatrix} 5.34096 & .14019 & 0 \\ 0 & .31393 & -.00215 \\ 0 & 0 & -.59639 \end{bmatrix}$$

After one iteration it is seen that the off-diagonal terms have been reduced in magnitude (on each successive iteration they are always reduced in a least-squares sense). Following the above procedure, the off-diagonal terms will converge to zero with the singular values on the diagonal.

VITA

The author was born in Columbia, South Carolina, in July 1947. He attended public schools in Houston, Baltimore, Louisville and Gretna, Virginia from 1954 until 1966. In June 1966 he enrolled at Virginia Polytechnic Institute where he received his B.Sc. degree in Mathematics in June 1970.

From June 1970 to August 1976 he was employed at the Naval Surface Weapons Center at Dahlgren, Virginia. In September 1976 he enrolled in the Engineering Science and Mechanics Department of Virginia Polytechnic Institute and State University where he received his M.S. degree in June 1977 and has been working toward his Ph.D.

The author is a member of Phi Kappa Phi National Honor Society and Pi Mu Epsilon Honor Society.

Jeffrey Kelly

ACOUSTIC PROPAGATION IN NONUNIFORM CIRCULAR DUCTS

CARRYING NEAR SONIC MEAN FLOWS

Jeffrey J. Kelly

(ABSTRACT)

A linear model based on the wave-envelope technique is used to study the propagation of axisymmetric and spinning acoustic modes in hard-walled and lined nonuniform circular ducts carrying near sonic mean flows. This method is valid for large as well as small axial variations, as long as the mean flow does not separate.

The wave-envelope technique is based on solving for the envelopes of the quasiparallel acoustic modes that exist in the duct instead of solving for the actual wave, thereby reducing the computational time and the round-off error encountered in purely numerical techniques.

The influence of the throat Mach number, frequency, boundary-layer thickness and liner admittance on both upstream and downstream propagation of acoustic modes is considered.

A numerical procedure, which is stable for cases of strong interaction, for analysis of nonlinear acoustic propagation through nearly sonic mean flows is also developed. This procedure is a combination of the Adams-PECE integration scheme and the singular value decomposition scheme. It does not develop the numerical instability associated with the Runge-Kutta and matrix inversion methods for nearly sonic duct flows. The numerical results show that an impedance condition can be satisfied at the duct exit and a

corresponding solution obtained. The numerical results confirm that the nonlinearity intensifies the acoustic disturbance in the throat region, reduces the intensity of the fundamental frequency at the duct exit, and increases the reflections. This implies that the mode conversion properties of variable area ducts can reflect and focus the acoustic signal to the vicinity of the throat in high subsonic flows. Also the numerical results indicate that a shock develops if certain limits on the input parameters are exceeded.